Theses and Dissertations   1. Thesis and Dissertation Collection, all items

1982

A combustion and heat transfer model for porpous media.

Vatikiotis, Costa S.

Monterey, California. Naval Postgraduate School

http://hdl.handle.net/10945/20095

NAVAL POSTGRADUATE SCHOOL
Monterey, California

THESIS

A COMBUSTION AND HEAT TRANSFER MODEL
FOR POROUS MEDIA

by

Costa S. Vatikiotis

June   1982

Dissertation Advisor: D. Salinas

Approved for public release; distribution unlimited.

T204928

REPORT DOCUMENTATION PAGE		READ INSTRUCTIONS BEFORE COMPLETING FORM
1. REPORT NUMBER	2. GOVT ACCESSION NO.	3. RECIPIENT'S CATALOG NUMBER
4. TITLE (and Subtitle) A Combustion and Heat Transfer Model for Porous Media		5. TYPE OF REPORT & PERIOD COVERED Doctor of Engineering June 1982
		6. PERFORMING ORG. REPORT NUMBER
7. AUTHOR(s) Costa S. Vatikiotis		8. CONTRACT OR GRANT NUMBER(s)
9. PERFORMING ORGANIZATION NAME AND ADDRESS Naval Postgraduate School Monterey, California 93940		10. PROGRAM ELEMENT, PROJECT, TASK AREA & WORK UNIT NUMBERS
11. CONTROLLING OFFICE NAME AND ADDRESS Naval Postgraduate School Monterey, California 93940		12. REPORT DATE June 1982
		13. NUMBER OF PAGES 172
14. MONITORING AGENCY NAME & ADDRESS(If different from Controlling Office)		15. SECURITY CLASS. (of this report) Unclassified
		15a. DECLASSIFICATION/DOWNGRADING SCHEDULE

16. DISTRIBUTION STATEMENT (of this Report)

Approved for public release; distribution unlimited.

17. DISTRIBUTION STATEMENT (of the abstract entered in Block 20, If different from Report)

18. SUPPLEMENTARY NOTES

19. KEY WORDS (Continue on reverse side if necessary and identify by block number)

Combustion	Porous Media
Heat Transfer	Darcy Flow
Carbon	Semenov Model

20. ABSTRACT (Continue on reverse side if necessary and identify by block number)

A general combustion and heat transfer model for porous media subject to Darcy flow is formulated. The transient one dimensional model treats the combustion process in two phases. During the initial phase, combustion occurs within the porous medium. The second phase occurs when the exothermic reaction moves to the air inlet surface of the medium resulting in surface recession. The temperature dependency of the system parameters

DD $_{1\ JAN\ 73}^{FORM}$ 1473   EDITION OF 1 NOV 68 IS OBSOLETE
S/N 0102-014-6601 |

#20 - ABSTRACT - (CONTINUED)

and thermophysical properties is taken into account. An
analysis of combustion in a carbon porous medium is
presented, as well as an assessment of the accuracy of
the model.

A Combustion and Heat Transfer Model
for Porous Media

by

Costa S. Vatikiotis
Lieutenant, United States Navy
B.S., Florida State University, 1971
M.S., Naval Postgraduate School, 1980
Mechanical Engineer, Naval Postgraduate School, 1980

Submitted in partial fulfillment of the
requirements for the degree of

DOCTOR OF ENGINEERING

from the

NAVAL POSTGRADUATE SCHOOL
June, 1982

ABSTRACT

A general combustion and heat transfer model for porous media subject to Darcy flow is formulated. The transient one dimensional model treats the combustion process in two phases. During the initial phase, combustion occurs within the porous medium. The second phase occurs when the exothermic reaction moves to the air inlet surface of the medium resulting in surface recession. The temperature dependency of the system parameters and thermophysical properties is taken into account. An analysis of combustion in a carbon porous medium is presented, as well as an assessment of the accuracy of the model.

4

TABLE OF CONTENTS

5

LIST OF SYMBOLS

A   -   Arrhenius coefficient, wetted surface area

$\underset{\approx}{A}$ -   Stiffness matrix

$\underset{\sim}{B}$ -   Mass matrix

c   -   Specific heat

D   -   Unit cell dimension

$\mathcal{D}$ -   Mass diffusion coefficient

d   -   Particle diameter

E   -   Activation energy

e   -   Specific internal energy

F   -   Fraction

$\underset{\sim}{F}$ -   Excitation vector

f   -   Stoichiometric ratio

G   -   Pseudo mass velocity, global basis function

g   -   Local basis function

g_c -   Gravitational constant

ΔH -   Heat of combustion

h   -   Convection heat transfer coefficient

h -   Specific enthalpy

K   -   Constant

k   -   Thermal Conductivity

L   -   Thickness of porous medium

L -   Boundary layer length

ℓ -   Element length

M   -   Molecular weight

m	-	Specific permeability
n	-	Reaction order
P	-	Pressure
Pr	-	Prandtl number
p	-	Porosity
Q	-	Filter velocity
q	-	Heat generation or loss
q'	-	Heat flux
R	-	Reaction rate
R'	-	Rate per unit area
R	-	Gas constant
Re	-	Reynolds number
r	-	Residual function
S	-	Local stiffness ratio
s	-	Kozeny constant
T	-	Temperature
$\hat{T}$	-	Absolute temperature
t	-	Time
Δt	-	Time increment
U	-	Free stream velocity
u	-	Pore velocity
V	-	Void volume, molecular volume
x	-	Spatial coordinate
z	-	Specific internal area

Greek symbols

α	-	Thermal diffusity
δ	-	Pore diameter

δ^Δ — Dirac delta function

δ^K — Kronecker delta function

ε — Thermal emissivity

η — Nondimensional spatial coordinate

θ — Solution coefficient

Λ — Field operator

λ — Nondimensional parameter, real part of eigenvalue

μ — Dynamic viscosity

ξ — Local element coordinate

ρ — Mass density

σ — Stefan-Boltzman constant

τ — Tortuosity, stress

ϕ — Oxygen concentration

ψ — Particle shape factor, approximate solution

ω — Mean free path

Subscripts

a — Air

c — Carbon

CO — Carbon monoxide

CO_2 — Carbon dioxide

e — Effective

fm — Film

g — Heat generation

i — At the current time or step

ig — Ignition

ℓ — Heat loss

9

L   -   At x = L

O_2 - Oxygen

p   -   At constant pressure

r   -   Radiation

s   -   Solid

st -   Starting

u   -   Universal

w   -   Fluid

x   -   At the specific location

∞   -   Ambient conditions

ACKNOWLEDGMENTS

I. INTRODUCTION

Studies were conducted at the Naval Weapons Center, China
Lake, California to assess the survivability of the F-18
aircraft when exposed to open pool fires. A portion of the
F-18 aircraft is constructed of graphite-epoxy materials.
When this composite material is exposed to a severe thermal
environment, the epoxy burns off at a low temperature (about
400-500 degrees Fahrenheit) leaving behind a porous graphite
mat. Experiments were conducted by J. Fontenot [1] to evaluate
the combustion behavior of the porous graphite or carbon mat.
Due to the complex behavior of the combustion observed for the
carbon fibers, a mathematical model to simulate this behavior
was developed by Vatikiotis [2]. The model was formulated to
consider a porous medium composed of cylindrically shaped
fibers, typical of fiber reinforced composite materials. The
details of the initial effort were presented by Vatikiotis.
Significant improvements have been made to the initial combus-
tion model, and the model has been extended to consider
spherically shaped particles, typical of thermal flow reactors.
The initial work of Vatikiotis [2], where it applies to the
present investigation is included in the discussion for the
sake of completeness. Other analytical investigations taking
a similar approach, but concerned with other aspects of com-
bustion or thermally active porous media, have been performed
by Kordylewski [3], Sahota and Pagni [4], and Mehta, Sams and

12

Luss [5]. Kordylewski performed a numerical analysis of homogeneous combustion in a two dimensional reactor. The objective of Kordylewski's investigation was to show that the flow within the reactor influenced the conditions necessary for ignition. Sahota and Pagni considered the transient behavior of heat transfer in a porous medium when exposed to a fire. Their analysis was part of an overall investigation for determining the internal stresses in a structure caused by a fire. Combustion of the porous medium was not a consideration. Mehta, Sams, and Luss investigated the transient temperature response of a packed-bed reactor when the entering fluid temperature was decreased. Their model assumed that the temperatures of the porous solid and the fluid were the same.

Slattery [6], Yaron [7], and Kassoy [8] present three approaches for mathematically modelling a porous media. Slattery's and Yaron's approaches were similar in using integral methods in their development. Slattery considered only mass transfer whereas Yaron treated transport processes in general. Kassoy's approach was based on performing Taylor series expansions of energy transport processes with respect to a differential volume of a porous medium. An energy balance yielded two differential heat transfer equations, one for the porous solid and one for the fluid. A fundamental requirement of this approach is that the particle diameters remain small with respect to the thickness of the porous medium.

Although the above investigations were concerned with specific aspects of thermally active porous media, the present

combustion model was developed to treat a larger class of problems (i.e., combined mass transfer, heat transfer, and combustion). In contrast to other investigations, the present model takes into account the temperature dependency of all the thermophysical properties of the air and the geometric parameters of the porous medium. The physical parameters such as porosity, permeability, and thickness affect the magnitude and behavior of pressure-driven air flow within the porous medium. As discussed by Kordylewski [3], the air flow influences the conditions for ignition. Therefore, sensitivity analyses were performed using the combustion model showing the effects of these parameters on combustion. In addition, a functional relation between the internal pore velocity and an initial uniform temperature distribution needed to sustain combustion is presented. The initial work of Vatikiotis [2] showed that the initial conditions are important in determining whether or not sustained combustion will occur. An analysis is presented showing the dependence of combustion on the shape of the initial temperature. In addition, the effects of the boundary conditions are examined using the combustion model. Specifically, there is a change in the behavior of combustion when insulated boundaries on the porous solid are changed to permit heat transfer by radiation. The Semenov model is used to explain the behavior observed during the analyses discussed above. Although the Semenov model was originally proposed for homogeneous combustion, the

14

results show that the Semenov model can be applied to hetero-
geneous combustion in porous media.

II. DESCRIPTION OF THE PROBLEM

The problem under investigation is that of a porous slab, with a pressure differential across its thickness, in a severe thermal environment. The effect of the pressure differential is to induce air flow through the porous medium. This internal air flow produces two opposing effects, (1) internal convection heat transfer, and (2) a supply of oxygen for heat generation by combustion. Whether the porous medium moves towards sustained combustion or extinguishment depends on the interaction of these effects. A mathematical model was formulated to provide an understanding of this interaction and its effect on thermal behavior.

The mathematical model was formulated as follows. Energy balances on the porous solid and the convected air provide heat transfer equations for each. The heat transfer mechanisms included in the model are (1) conduction, (2) convection, and (3) radiation. In addition, nonvolatile combustion is included in the porous solid heat transfer equation as a heat generation term of Arrhenius type.

The conservation of species law was applied to the oxygen molecule concentration. The resulting mass transfer equation includes the transfer mechanisms of (1) molecular diffusion, and (2) species transport by convection. A term accounting for the consumption of oxygen due to combustion is included as well. Darcy's law was taken as the constitutive equation

16

for flow through the porous medium. The pressure gradient, needed to calculate pore velocity, is obtained by solving a combined Darcy's law and continuity equation.

As the behavior of the system occurs over a large temperature range, all thermophysical properties which depend upon temperature, such as conductivity, viscosity, and air density, are treated as temperature dependent properties. Moreover, as combustion consumes the porous solid, changes in porosity and permeability are accounted for in the transient analysis.

In order to provide a general model, a number of boundary conditions are included in the formulation of the model. A detailed discussion of boundary conditions is presented in Section III.H. The final system of equations to be solved are four transient, nonlinear, coupled partial differential equations. The three heat and mass transfer equations were solved by a Galerkin formulation of the finite element method. The remaining combined Darcy's law-continuity equation was solved by a shooting method. The details of the solution procedure are presented in Appendix C.

III. THEORY AND BACKGROUND

A. DESCRIPTION OF THE POROUS MEDIUM

For this investigation, a porous medium is defined as a solid containing interconnected pores (i.e., path for airflow). There are two classes of porous media, consolidated and unconsolidated. Consolidated porous media are those where the solid constituent or matrix remains rigid. Consolidated porous media may be comprised of either individual particles attached to one another (e.g., sintered metal), or a solid where a portion has been removed (e.g., charcoal). Unconsolidated porous media are comprised of discrete particles (e.g., granular beds). The properties of an unconsolidated porous medium can change if the porous medium is agitated or settling takes place. Both consolidated and unconsolidated porous media can have spatially varying properties.

The physical properties which characterize porous media (i.e., allow comparison of porous media without regard to class or form) are (1) porosity, (2) specific internal area, (3) pore size or diameter, and (4) tortuosity. These properties are common to both consolidated and unconsolidated porous media. Porosity, p, is defined as the ratio of void volume to total volume. The specific internal area, z, is the ratio of internal surface area to bulk volume. The dimension is the reciprocal of length. Pore diameter is used to describe the pore system of a porous medium. The actual shape and size of

a pore may be irregular and complex, and would be difficult
to describe geometrically. In practice, there are many con-
ventions used to define the pore diameter. For this inves-
tigation, a hydraulic diameter theory is used and is discussed
later in this section. The tortuosity of a porous medium is
defined as the ratio of the length of the flow path of a fluid
particle to the straight line distance. Originally, tortu-
osity was considered a kinematic property, but was subsequently
adopted for characterizing porous media. Tortuosity is also
discussed later in this section. Scheidegger [9] discusses
various methods used to measure properties of porous media.
Though most methods discussed are based on experimental tech-
niques, the above properties for this investigation are calcu-
lated based on an idealization of the geometry of a porous
medium.

The porous medium was modelled as shown in Figure III.1.
In Figure III.1, D is the distance between the fiber or parti-
cle centers, and d is the particle diameter. The geometry is
idealized since the actual porous medium may be irregular in
particle diameter and distribution. For cylindrical fibers,
the porosity, which was defined as the ratio of void per unit
volume is,

$$p \;=\; 1 - \frac{\pi}{4}(d/D)^2 \hspace{3cm} \text{(III.1)}$$

and for spherical particles,
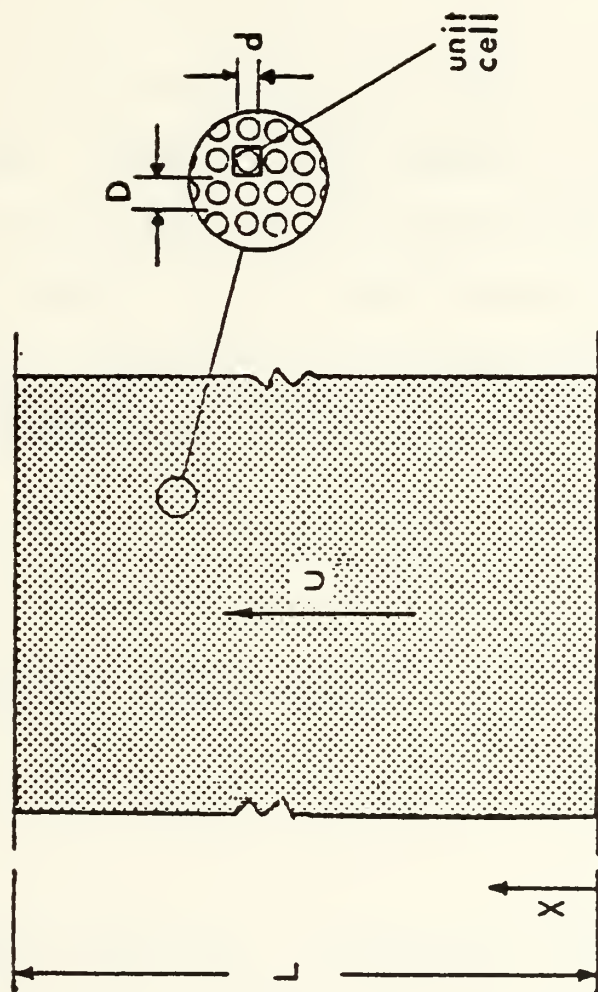
FIGURE III.1 --- Idealized geometry of a porous medium.

$$p = 1 - \frac{\pi}{6}(d/D)^3 \qquad \text{(III.2)}$$

The pore diameter is obtained by an expression proposed by Carman [10],

$$\delta = 4p/z \qquad \text{(III.3)}$$

where z is the specific internal area or the particle surface area per unit volume of porous medium. Expression III.3 is analogous to the more familiar form of mean hydraulic diameter, 4V/A, where V is the void volume and A is the wetted surface area. The specific internal area, z, based on the idealized geometry of Figure III.1 is calculated by,

$$z = \frac{1}{2}\pi \, d/D^2 \qquad \text{(III.4)}$$

for cylindrical fibers, and by,

$$z = \frac{1}{2}\pi \, d^2/D^3 \qquad \text{(III.5)}$$

for spherical particles. Expressions III.4 and III.5 assume one half the total internal surface area is effective for convection heat transfer. This fractional amount of total area was an estimate based on Fontenot's experimental results and does not apply to porous media in general. A more general approach, as presented by Scheidegger [9], is the Kozeny

equation given by,

$$z = (sp^3/m)^{1/2} \qquad\qquad (III.6)$$

In equation III.6, m is the specific permeability or hydraulic
conductivity (discussed in Section III.B), and s is the Kozeny
constant. The Kozeny constant is usually taken as .2 for
specific surface calculations. Advantages to using the Kozeny
equation are (1) the calculated values of specific internal
area are in fair agreement with the experimental values, and
(2) the calculation is independent of particle shape. A
disadvantage is that the Kozeny equation fails for highly
porous fibrous media. The tortuosity, τ, is the ratio of the
length of the flow path for a fluid particle to the straight
line distance. For the geometric configuration of Figure III.1,
the tortuosity depends on the ratio d/D. Carman [10] pre-
sents a table of measured tortuosity factors of various materials
and geometries, and points out the differences between the
analytical determinations of tortuosity. Here, we adopt his
recommended value of 1.4. Since particle size decreases as
the carbon is consumed, all geometric properties which depend
on fiber or particle diameter are functions of time and posi-
tion. The model assumes that the carbon matrix remains rigid
as the particle diameter decreases, and thus, porosity in-
creases with combustion. In his discussion on the packing
theory of spheres, Scheidegger [9] states the highest reported
porosity for spherical particles in a stable configuration is

22

.875. Carman [10] reports of investigations of fibrous porous media with porosities as high as .99. The change in particle diameter is accounted for, and will be discussed in the section on the Arrhenius expression (Section III.D) for carbon combustion.

B. DARCY'S LAW AND PORE VELOCITY

Reynolds number for porous media is defined by

$$Re = (\rho_a u d)/\mu \qquad \text{(III.7)}$$

where u is the local pore velocity, ρ_a is the mass density of air, and μ is the dynamic viscosity. Depending on the magnitude of the Reynolds number, the motion of the fluid may be dominated by molecular, viscous, or inertial effects. Most investigations of fluid flow in porous media have been in the range of Reynolds number where the flow is dominated by viscous and inertial effects. The Navier-Stokes equations are applicable in describing the fluid motion in this range of Reynolds number. However, because of the convoluted geometry and the necessary boundary conditions (i.e., u = 0 at a solid-fluid interface), solution of the Navier-Stokes equations are difficult for a porous medium. Extensive experimental work, as discussed by Scheidegger [9] has shown that fluid flow in porous media is governed by Darcy's law for the range of Reynolds number where viscous effects dominate. The upper limit (high velocity end) Reynolds number reported in the

23

experimental investigations varied from .1 to 75. As Reynolds

number increases, inertial effects increase. However, Boffa

[11] has shown that for a fixed Reynolds number, inertial

effects diminish with increasing air temperature. For the

problems covered in this investigation, the Reynolds number

did not exceed a value of 5.

Neglecting body forces, Darcy's law for one dimensional

flow is,

$$Q = - \frac{m}{\mu} \left(\frac{dP}{dx} \right) \qquad \qquad (III.8)$$

where Q is the filter velocity or the volumetric flow rate per

unit of cross-sectional area, and dP/dx is the pressure gradi-

ent. The specific permeability or the hydraulic conductivity

of the porous medium is defined by,

$$m = 96 \, p \, (\delta/\tau)^2 \qquad \qquad (III.9)$$

Expression III.9 is based on a capillaric-serial model given

by Scheidegger [9]. It should be noted that, in a physical

sense, permeability and porosity are not related. Porosity

is a quantifiable property of the porous medium. Whereas,

permeability is a constitutive property (i.e., a property

specified by a constitutive equation, Darcy's law). As in

the case of Fourier's law of heat transfer, Darcy's law is

not derived from first principles, but has been obtained

through exhaustive experimental analyses. The Dupuit-
Forcheimer assumption, presented by Carman [10], relates
the local pore velocity to the filter velocity by,

$$Q = p u \qquad (III.10)$$

The hypothesis of the Dupuit-Forcheimer assumption is that the
local pore velocity is greater than the filter velocity.
Noting that the actual velocity in a single pore is not a
constant, but rather a function of the location within the
pore, the Dupuit-Forcheimer assumption defines an "average"
velocity within the pore.

The continuity equation for one dimensional fluid flow in
porous media with nonconstant porosity distribution is,

$$\frac{D(p\rho_a)}{Dt} + p\rho_a \frac{\partial u}{\partial x} = 0 \qquad (III.11)$$

Substituting in the Dupuit-Forcheimer assumption and Darcy's
Law, the continuity equation becomes,

$$\frac{d^2 P}{dx^2} + \left(\frac{1}{\rho_a} \frac{\partial \rho_a}{\partial x} + \frac{1}{m} \frac{\partial m}{\partial x} - \frac{1}{\mu} \frac{\partial \mu}{\partial x} \right) \frac{dP}{dx} - \frac{\mu}{\rho_a m} \frac{\partial(p\rho_a)}{\partial t} = 0 \qquad (III.12)$$

Equation III.12 along with the boundary conditions can be
integrated to provide the pressure and the pressure gradient
distributions through the porous medium. The boundary condi-
tions are $P(0) = P_\infty$, the ambient pressure, and $P(L) = P_L$. The

pressure differential across the porous medium is $\Delta P = P_L - P_\infty$.

Knowing the pressure gradient distribution, the pore velocity distribution is obtained from Darcy's law and the Dupuit-Forcheimer assumption. Derivations of equation III.12 and the continuity equation are presented in Appendix A and B, respectively.

C. SEMENOV MODEL OF COMBUSTION

In this work we adopt the combustion model of N. N. Semenov as described in the texts of Frank-Kamenetskii [12] and Vulis [13]. A brief discussion of those features of the model which relate to the present investigation will be given. Fundamental to the model is the relation of reaction rate to temperature, and the interaction of heat generation and heat transfer. The reaction rate, R_c, is represented by the Arrhenius law for a simple n-th order reaction,

$$R_c = A \phi^n \exp\left(\frac{-E}{R_u \hat{T}}\right) \qquad (III.13)$$

where A^{-1} is the characteristic time of the chemical reaction, E is the activation energy, R_u is the universal gas constant, $\hat{T}$ is the absolute temperature, and ϕ is the oxygen concentration. A simple reaction is one in which the rate depends on the concentrations of the reactants and not on the products. The heat generated by the exothermal reaction is obtained by multiplying R_c by the heat of combustion.

26

In Figure III.2, heat generation R_g is plotted versus temperature. The resulting curve is referred to as the S-curve due to its sinuous shape. The S-curves are distinguished by two regions. In region I, the reaction rate and temperature are low and as a result, there is an excess supply of oxygen. In this region the reaction is controlled by the temperature, and is called the kinetic regime of combustion. In the kinetic regime, the reaction rate increases exponentially with increasing temperature. In region II, the higher reaction rates are only slightly affected by the higher temperatures, and the reaction is limited by the availability of oxygen. Region II is called the diffusion regime of combustion. It should be noted that S-curves are not obtained by plotting R_g versus temperature for a constant oxygen concentration. The flattening of the S-curve at the higher temperatures is due to decreasing oxygen concentration at those temperatures. The S-curve, which represents the behavior of an actual system, demonstrates the strong coupling between temperature and oxygen concentration.

In addition to the S-curves, Figure III.2 shows two convection heat transfer curves, $q_{\ell 1}$ and $q_{\ell 2}$, at air flow temperatures, T_1 and T_2, respectively. The equation for the heat transfer lines is of the form,

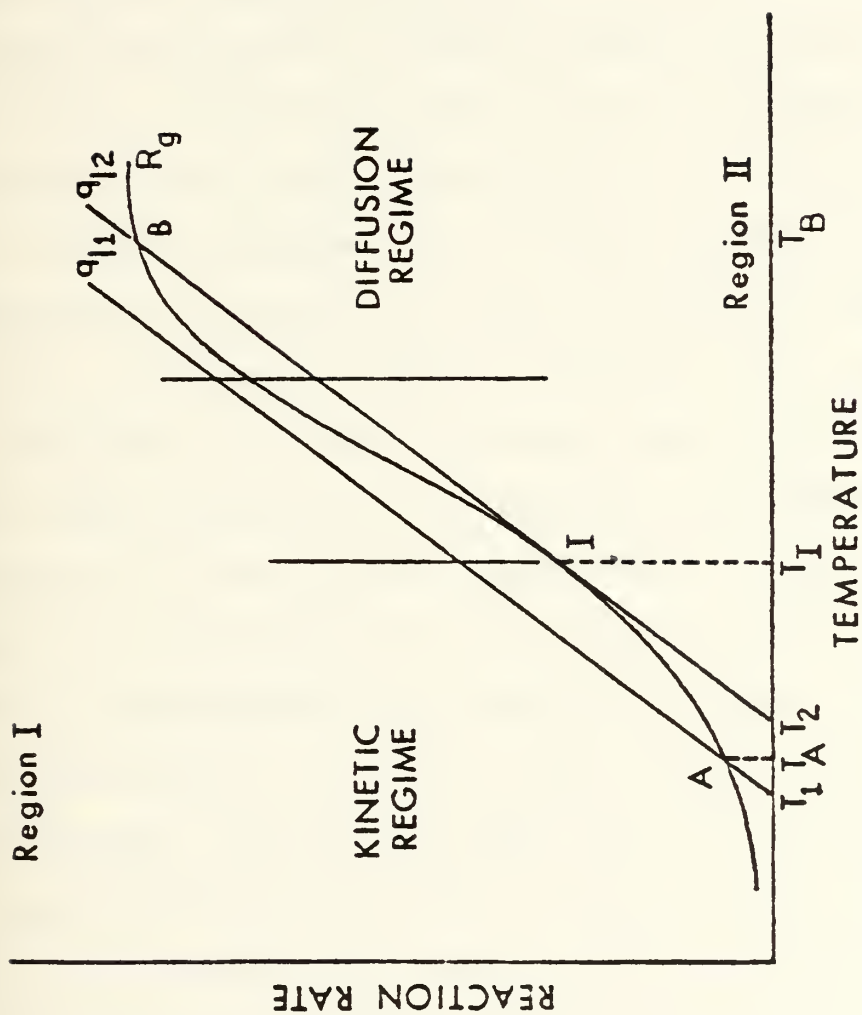$$q_\ell = h(T_s - T_a) \qquad\qquad (III.14)$$

FIGURE III.2 --- Semenov model of combustion.

28

where h is a convection heat transfer coefficient, and T_s and T_a are the solid surface and air temperatures, respectively. The intersection of the heat generation and heat transfer curves, $R_g = q_\ell$, defines the stable quasi-stationary point A. For a system in thermal equilibrium, the solid and air temperatures will remain at T_A and T_1, respectively. Perturbing the system from one equilibrium position to another causes the quasi-stationary point to adjust accordingly (e.g., raising the air flow temperature from T_1 to T_2 will cause the quasi-stationary point to move from T_A to T_I). At point I, the R_g and q_ℓ curves are tangent, and an infinitesimal increase in temperature will result in a jump in reaction temperature from T_I to T_B. At point I, which is defined as the "critical ignition condition", the reaction moves from the kinetic regime to the diffusion regime of combustion. Temperature T_I is referred to as the ignition temperature. Although the description of the process just presented is for a surface in which only heat transfer by convection occurs, the underlying ideas carry over for the total heat transfer at a point in the porous medium. The heat transfer can include contributions from conduction and radiation, as well as from convection.

In his original work, Semenov [14] developed his theory to explain reaction behavior within homoegenous gas mixtures. Frank-Kamenetskii [12] later adapted this theory to describe the behavior associated with heterogeneous mixtures (i.e., a solid surface and air). In their study of coal combustion,

Thomas, Stevenson, and Evans [15] state that a "temperature jump", as described by Frank-Kamenetskii, may or may not occur depending on the partial pressure of oxygen. This present investigation does not consider this aspect of the combustion theory. However, analyses were made using the present model to determine whether the reaction takes place in the kinetic regime or in the diffusion regime. Moreover, the Semenov model will be used to explain these results in Chapter V.

D. ARRHENIUS LAW OF REACTION RATE

For carbon reacting in air, Parker and Hottel [16] proposed the following Arrhenius expression for the reaction rate in units of kg-carbon/m^2-s,

$$\dot{R}_c = 9.55 \times 10^6 \frac{P_{O_2}}{\hat{T}_c^{1/2}} \exp\left(\frac{-44000}{R_u \hat{T}_c}\right) \qquad (III.15)$$

where P_{O_2} is the partial pressure of oxygen in atmosphere units, and R_u is the universal gas constant (1.986 cal/gmole-K). Equation III.15 assumes a simple first order reaction for the combustion of carbon in air. Frank-Kamenetskii [12] has shown that the experimental data of Parker and Hottel is better correlated by a fractional order reaction, where the reaction order, n, is between 1/3 and 2/3. Replotting Parker's and Hottel's data for n = 1/2, yields the reaction rate expression used in the present analysis,

$$R_c = 2.065 \times 10^6 (R_{O_2} \phi)^{1/2} \exp(\frac{-57240}{R_u \hat{T}_c}) \qquad \text{(III.16)}$$

In expression III.16, R_c is in units of lbm-carbon/ft^2-hr, R_{O_2} is the gas constant for oxygen (48.29 ft-lbf/lbm-R), ϕ is in lbm/ft^3, R_u is 1.986 Btu/lbmole-R, and $\hat{T}_c$ is in Rankines. The ideal gas law was used to replace the partial pressure, P_{O_2}. Figure III.3 and Table III.1 show the results of plotting Parker's and Hottel's data for values of n equal to 1, 2/3, 1/2, and 1/3. The values presented in Table III.1 are in S.I. units.

In order to determine the rate of heat generation and the rate of oxygen consumption, the chemical reaction for the combustion process must be considered. For nonvolatile combustion of carbon and oxygen, two reactions that describe the process are,

$$C + \frac{1}{2} O_2 \rightarrow CO \qquad \text{(III.17)}$$

$$C + O_2 \rightarrow CO_2 \qquad \text{(III.18)}$$
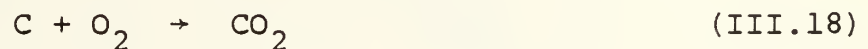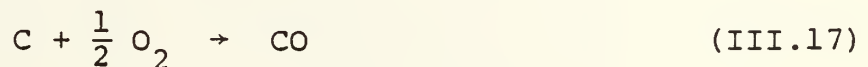
The ratio of the mass rates of carbon monoxide to carbon dioxide produced increases with increasing temperature. Arthur [17] presents an expression for the rate ratio as a function of temperature (in Kelvins).

$$CO/CO_2 = 2500 \exp(\frac{-6240}{\hat{T}_c}) \qquad \text{(III.19)}$$
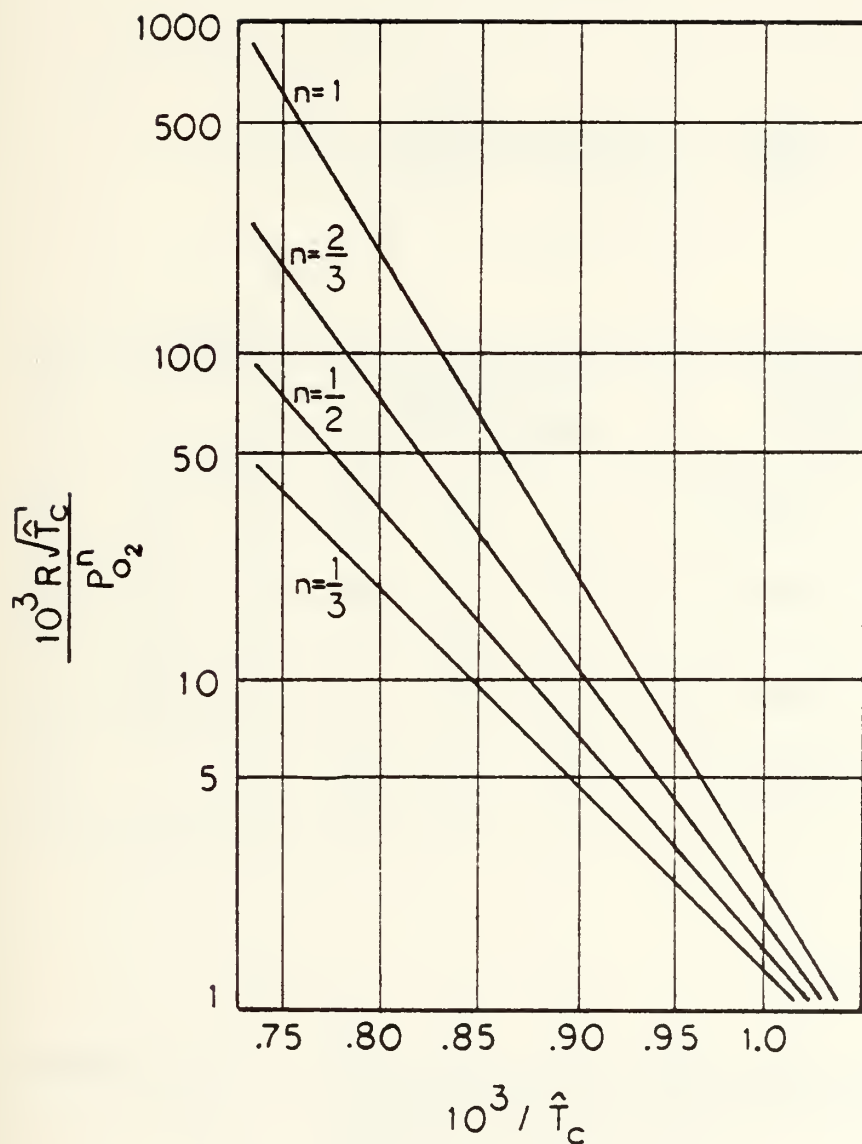
FIGURE III.3 --- Results of plotting reaction rate
data of Parker and Hottel [16] for
several values of n.

32

$$R_c = A \frac{P_{O_2}^n}{\sqrt{\hat{T}_c}} \exp\left(\frac{-E}{\mathcal{R}\,\hat{T}_c}\right) \quad \frac{gr\text{-}c}{cm^2 \cdot s}$$

n	$A \left[\dfrac{gr_c - K^{1/2}}{cm^2\text{-}atm^n\text{-}sec}\right]$	$E \left[\dfrac{gr\text{-}cal}{mole}\right]$
$\dfrac{1}{3}$	1.19×10^3	27500
$\dfrac{1}{2}$	1.29×10^4	31800
$\dfrac{2}{3}$	2.1×10^5	37100
1	9.55×10^6	44000

TABLE III.1 --- Results of plotting reaction rate
data of Parker and Hottel [16] for
several values of n.

33

As a result of this dependence on temperature, the stoichiometric ratio and the heat of reaction will also be functions of temperature. Defining the fraction of carbon monoxide being produced by,

$$F_{CO} = \frac{(CO/CO_2)}{1 + (CO/CO_2)} \qquad (III.20)$$

and the fraction of carbon dioxide as,

$$F_{CO_2} = \frac{1}{1 + (CO/CO_2)} \qquad (III.21)$$

the heat of combustion is then expressed as,

$$\Delta H_R = F_{CO} \Delta H_{CO} + F_{CO_2} \Delta H_{CO_2} \qquad (III.22)$$

Values for the heats of combustion, ΔH_{CO} and ΔH_{CO_2}, as functions of temperature were obtained from the JANAF (Joint Army, Navy, and Air Force) Tables [18]. The stoichiometric ratio (fuel to oxygen) of the overall reaction is,

$$f_R = f_{CO} f_{CO_2} / (f_{CO_2} F_{CO} + f_{CO} F_{CO_2}) \qquad (III.23)$$

where f_{CO} is the stoichiometric ratio for reaction III.17 and f_{CO_2} is the stoichiometric ratio for reaction III.18. The rate of heat generation, R_g, and the rate of oxygen consumption can now be expressed by,

34

$$R_g = \Delta H_R R_c \qquad \text{(III.24)}$$

$$R_{O_2} = f_R^{-1} R_c \qquad \text{(III.25)}$$

It should be pointed out that Parker's and Hottel's work [16] and Arthur's work [17] were accomplished using specific types of carbon. Smoot and Pratt [19] and Frank-Kamenetskii [12] list tables and references for many other rate expressions, depending on the particular type of carbon used. The present model was developed for any rate expression of Arrhenius type for carbon consumption. For this investigation, we will remain with Parker's and Hottel's expression III.16 as modified by Frank-Kamenetskii.

As previously stated, the particle diameter decreases as combustion progresses. The rate of decrease depends on the amount of carbon consumed at a point over time. Past observations have shown that the effect is significant when the reaction is concentrated in a small region of the porous medium. To take this into account, expressions for the time rate of change of the diameter as a function of reaction rate were derived. The equation for cylindrical fibers is,

$$\dot{d} = -2 R_c z D^2 / (\pi \rho_c d) \qquad \text{(III.26)}$$

and for spherical particles,

$$\dot{d} = -2 R_c z D^3 / (\pi \rho_c d^2) \qquad \text{(III.27)}$$

where ρ_c is the bulk mass density of carbon. The diameter
and the reaction rate are functions of both time and position.

E. HEAT TRANSFER EQUATIONS FOR POROUS MEDIA

In a previous investigation of porous media, Green and
Perry [20] developed heat transfer equations for the solid
and fluid phases. The model included the three basic mechan-
isms, (1) physical movement of the fluid with its own heat
content, (2) conduction of heat through the solid and fluid
phases, and (3) convective heat transfer between the solid
and the fluid phases. Radiation heat transfer was assumed
to be negligible, and combustion was not a consideration.
The differential equations for the solid and the fluid phases,
obtained from energy considerations,

$$\rho_s c_s (1-p)\frac{\partial T_s}{\partial t} = k_s (1-p)\frac{\partial^2 T_s}{\partial x^2} + hz(T_w - T_s) \qquad \text{(III.28)}$$

$$\rho_w c_w p\frac{\partial T_w}{\partial t} = -p\rho_w c_w u\frac{\partial T_w}{\partial x} + k_w p\frac{\partial^2 T_w}{\partial x^2} - hz(T_w - T_s) \qquad \text{(III.29)}$$

and were solved numerically by Green and Perry using the
finite difference method. In equations III.28 and III.29,
c is specific heat, h is the internal convection heat trans-
fer coefficient, k is thermal conductivity, and z is the wetted
surface area per unit volume. The s and w subscripts refer
to solid and fluid properties, respectively. Their model does
not account for the temperature dependency of the properties.
Other investigators such as Sundaresan [21], Riaz [22],

36

Mendelsohn [23], and Schneider [24] have presented a single equation approach to describe heat transfer in porous media,

$$[(1-p)c_s\rho_s+pc_w\rho_w]\frac{\partial T}{\partial t} = -u\rho_w c_w p\frac{\partial T}{\partial x} + [(1-p)k_s+pk_w]\frac{\partial^2 T}{\partial x^2} \quad (III.30)$$

Equation III.30 can be derived from equations III.28 and III.29 by assuming the solid and fluid phase temperatures are equal. Green and Perry proposed that the equal temperature assumption was valid for systems satisfying the following condition,

$$\lambda = (\frac{hz}{k_w p})^{1/2}\frac{\alpha_w}{u} > .342 \quad (III.31)$$

where α_w is the thermal diffusivity of the fluid.

In the present investigation, the heat transfer equations are generalized to also include (1) radiation, (2) internal combustion, (3) temperature dependency of properties, and (4) compressibility effects of the air.

An energy balance on the carbon gives the heat transfer equation,

$$\frac{\partial}{\partial x}[(1-p)(k_e+k_r)\frac{\partial T_c}{\partial x}] - hz(T_c-T_a) + R_g z = (1-p)\rho_c c_c\frac{\partial T_c}{\partial t} \quad (III.32)$$

where k_r is a pseudo thermal conductivity to account for radiation between particles. The derivation of equation III.32 is presented in Appendix A. The effective conductivity, k_e, of the porous solid was proposed by Russel [25],

$$k_e = k_a \frac{p'^{2/3} + \frac{k_a}{k_c}(1 - p'^{2/3})}{p'^{2/3} - p' + \frac{k_a}{k_c}(1 - p'^{2/3} + p')} \qquad \text{(III.33)}$$

where k_c and k_a are the bulk thermal conductivities of carbon and air, respectively, and $p' = (1-p)$. Russel's expression, based on an electrical resistance analogy, can be used for the full range of porosity, from 0 to 1.

The pseudo thermal conductivity due to radiation, k_r, is obtained as follows. Treating the idealized geometry of the porous medium as a series of closely spaced walls, the net radiation heat flux between two of the walls is,

$$q_r = \sigma \epsilon (\hat{T}_1^4 - \hat{T}_2^4)/(2-\epsilon) \qquad \text{(III.34)}$$

where ϵ is the emissivity, and σ is the Stefan-Boltzman constant. By expanding q_r in a Taylor series about $\hat{T}_2$, an analogy to Fourier's law of heat transfer by conduction yields the effective radiation conductivity as,

$$k_r = 4 \sigma \epsilon \delta \hat{T}_c^3/(2-\epsilon) \qquad \text{(III.35)}$$

Expression III.35 is then used for k_r in equation III.32. The details of the above derivation are presented in Appendix B. The application of expression III.35 to porous media is also proposed by Rohsenow and Hartnett [26]. In a more rigorous development, Whitaker [27] presents an alternative approach for treating radiation heat transfer in porous media.

Following the experimental work of Yoshida, Ramaswami, and Hougen [28], the internal convection heat transfer coefficient is given by the empirical correlation,

$$h = 0.91 \, \text{Re}'^{-0.51} [\psi \, c_a \, G (c_a \mu / k_a)_{fm}^{-2/3}] \qquad \text{(III.36)}$$

where ψ is equal to .91 for cylindrical fibers, and equal to 1 for spherical particles, G is a pseudo mass velocity given by $p\rho_a u$, and c_a is the specific heat of air at constant pressure. The fm subscript refers to the properties evaluated at film temperature. Re' is a pseudo Reynolds number defined by,

$$\text{Re}' = G/(z \, \mu \, \psi) \qquad \text{(III.37)}$$

The air properties vary with temperature, and h varies with temperature. Finally, the reaction rate for the heat generation term in equation III.32 is given by expression III.24.

An energy balance on the air within the porous medium provides the second heat transfer equation as,

$$\frac{\partial}{\partial x}(pk_a \frac{\partial T_a}{\partial x}) - p\rho_a c_a u \frac{\partial T_a}{\partial x} + hz(T_c - T_a) + u\frac{\partial (pP)}{\partial x} = p \, \rho_a \, c_a \frac{\partial T_a}{\partial t}$$

$$\text{(III.38)}$$

The density of air, ρ_a, is approximated in the model by the ideal gas law. The term, $\partial(pP)/\partial x$, is due to the compressibility of the air. The derivation of equation III.38 is

39

presented in Appendix A. All properties in equation III.38
vary with temperature. The properties of standard air were
used in the analysis. During combustion, oxygen in the air
is replaced by carbon monoxide and carbon dioxide. Calcula-
tions showed that the gas mixture would have thermophysical
properties slightly different from those of standard air.
In a "worst case" situation, the average difference between
the thermophysical properties of air and a mixture of .79 N_2
and .21 CO_2 is 7 percent. This mixture assumes that the oxy-
gen is totally consumed. Viscosity had the largest difference
of 13 percent, and specific heat the smallest at 1.5 percent.
The properties of a .79 N_2 and a .21 CO mixture are approxi-
mately those of air (different by less than 2 percent). At
typically observed temperatures (greater than 1200 deg-F), the
combustion gas will be mostly carbon monoxide, and the error
introduced by assuming the properties of standard air is mini-
mum. A small difference in the properties is acceptable since
an additional molecule mass transfer equation for either carbon
monoxide or carbon dioxide would be necessary to calculate
the effective properties of the gas mixture. The methods used
to obtain the thermophysical properties of the gas mixtures
above were those of Mason and Saxena [29], and Reynolds and
Perkins [30]. The polynomial expressions used to calculate
the thermophysical properties of air are derived in Appendix B.

F. OXYGEN DIFFUSION EQUATION FOR POROUS MEDIA

As a result of combustion, the heat transfer equations
include four response variables, the carbon and air temperatures,

T_c and T_a, the concentration of oxygen, ϕ, and the total internal pressure, P. The fourth field equation necessary to complete the system is obtained from species conservation considerations. The oxygen molecule transport mechanisms included in the model are (1) molecular diffusion resulting from concentration gradients (Fick's Law), (2) convective mass flow, and (3) oxygen consumption due to combustion. Diffusion resulting from pressure and temperature gradients was considered negligible. An example cited by Bird, Stewart, and Lightfoot [21] where pressure diffusion is important is the centrifuge separator; and for thermal diffusion, the Clusius-Dickel column, where very steep temperature gradients are used to separate complex mixtures of organic molecules. Thus, the oxygen molecule transfer equation for a porous medium is,

$$\frac{\partial}{\partial x}(p \, \mathcal{D}_e \frac{\partial \phi}{\partial x}) - \frac{\partial}{\partial x}(p \, u \, \phi) - R_{O_2} z = p \frac{\partial \phi}{\partial t} \qquad (III.39)$$

The derivation of equation III.39 is presented in Appendix A. The second order term in equation III.39 results from Fick's law of diffusion. The effective diffusivity of the porous medium, $\mathcal{D}_e$, is a function of pressure, temperature, and pore geometry of the medium. Scheidegger [9] presents several models for $\mathcal{D}_e$ which have been proposed by a number of investigators. Briefly, there are two limiting cases of diffusion, (1) diffusion associated with the collision between gas molecules, and (2) diffusion associated with the collision of

41

gas molecules with the pore walls of the medium. This second phenomenon is discussed by Bennett and Myers [32], and is referred to as Knudsen diffusion. The former case occurs when the mean free path of the molecules is smaller than the pore diameter. The expression for mean free path, ω, given by Treybal [33] is,

$$\omega = \frac{3.2\mu}{P}(R_u \hat{T}/2 \pi g_c M)^{1/2} \tag{III.40}$$

where g_c is the gravitational constant and M is the molecular weight. From equation III.40, a value of $\omega = \delta/100$ is obtained for oxygen for the geometry of typical porous media encountered in the analysis. Thus, collision between molecules is the governing diffusion mechanism. A semi-empirical expression, proposed by Gilliland [34], is used to obtain the diffusion coefficient of oxygen into air. Gilliland's expression is given by,

$$\mathcal{D} = 435.7 \hat{T}_a^{2/3} (M_a^{-1} + M_{O_2}^{-1}) / [P (V_a^{1/3} + V_{O_2}^{1/3})] \tag{III.41}$$

where $\mathcal{D}$ is in units of cm^2/sec, P is the total pressure in Pa, V_a and V_{O_2} are the molecular volumes of air and oxygen, respectively. M_a and M_{O_2} are the molecular weights of air and oxygen. The values of V_a and V_{O_2} were obtained from Holman [35] as 29.9 and 7.4, respectively. The effective diffusivity proposed by Denbigh and Turner [36] for a porous medium is,

$$\mathcal{D}_e = \mathcal{D}/\tau \qquad\qquad (III.42)$$

Expression III.42 accounts for the tortuous path the oxygen molecules follow through the porous medium. Lastly, the oxygen consumption term in equation III.39 is given by expression III.25.

G. THE SURFACE RECESSION PROBLEM

The previous system of equations describes the combustion process occurring within the porous medium. As combustion progresses, the oxygen concentration goes to zero, and as a result, the reaction moves to the air inlet surface of the porous medium. Thereafter, the carbon consumption takes place at the surface. During the surface recession phase, the thickness of the porous medium decreases with time, i.e., surface recession. This suggests partitioning the problem into two parts, (1) initial combustion within the porous medium, and (2) combustion at the air inlet surface. The second phase of the problem is formulated as a moving boundary problem. The governing equations for the moving boundary problem are those developed previously with the exception of the oxygen molecule mass transfer equation. With combustion occurring at the surface, oxygen is totally consumed in a shallow region near the surface. Experimentation by Koizumi [37] has shown this penetration of the oxygen to be 1 to 2 particle diameters. As a result, the oxygen molecule mass transfer equation is not needed for this phase of the problem, and the heat generation can be treated as a planar source.

The carbon heat transfer equation with the modified heat generation term is,

$$L^{-2}\frac{\partial}{\partial \eta}[(1-p)(k_e+k_r)\frac{\partial T_c}{\partial \eta}]-hz(T_c-T_a)+R'_g z\delta^{\Delta}(\eta = 0)$$

$$= (1-p)\rho_c c_c[\frac{\eta}{L}\frac{\partial T_c}{\partial \eta}\dot{L} + \frac{\partial T_c}{\partial t}] \qquad (III.43)$$

where η is equal to x/L. The first term on the right side of equation III.43 arises from the x coordinate becoming a function of time during surface recession. A similar term appears in the air temperature and combined Darcy's law-continuity equations as well. Transformation of the field equations from a fixed coordinate to a moving coordinate system is presented in Appendix A. As was observed (see Figure V.2), the temperature gradient through the porous medium during surface recession was small. As a result, the additional term may be omitted without affecting the results. The moving boundary problem formulation is based on Crank's [38] extension of a method proposed by Murray and Landis [39]. The thickness, L, is updated continuously by evaluating its time rate of change given by,

$$\dot{L} = -(p\,u\,f_R)_{x=0}\phi_\infty/[(1-p)_{x=0}\rho_c] \qquad (III.44)$$

Expression III.44 is obtained from a mass balance on the carbon (i.e., the time rate of change in carbon is equal to

44

the carbon consumption). Noting that all the oxygen entering

the plate is consumed in a small region near x = 0, the carbon

consumption can be represented in terms of the oxygen flow

and the stoichiometric ratio (i.e., $R_C' = -p u f_R \phi_\infty A$ where A

is area). The time rate of change for carbon is $(1-p)\rho_c A\dot{L}$.

The planar heat source, R_g'', in equation III.43, is determined

by the amount of oxygen entering the porous medium at x = 0.

This is converted to heat generation by using the stoichio-

metric ratio, f_R, and the heat of combustion, ΔH_R. Thus in

equation III.42, the planar heat source becomes $p u f_R \Delta H_R \phi_\infty$.

Ozisik [40] presents a general discussion and references for

the moving heat source problem.

Transition from the internal combustion problem to the

surface recession problem occurs when the porosity at x = 0

nears a value of 1. The computer program, implementing the

analysis, was written so that the change from an internal

combustion problem to a surface recession problem occurs

automatically.

H. BOUNDARY CONDITIONS

Three sets of boundary conditions may be used for equations

III.32, III.38, and II.39. Each set of boundary conditions

approximates a physical situation (e.g., thermal flow reactor

or Fontenot's experiments [1]). The boundary conditions

were the nearest approximations that could be made and remain

within the limitations of a one dimensional model. The first

and second set of boundary conditions are typical of thermal

flow reactors with and without radiation from the boundary
surfaces. These are

$$\frac{\partial T_c}{\partial x} = 0 \qquad\qquad x = 0 \qquad \text{(III.45)}$$

$$\frac{\partial T_c}{\partial x} = 0 \qquad\qquad x = L \qquad \text{(III.46)}$$

$$k_a \frac{\partial T_a}{\partial x} = \rho_a c_a u (T_a - T_\infty) \qquad\qquad x = 0 \qquad \text{(III.47)}$$

$$\frac{\partial T_a}{\partial x} = 0 \qquad\qquad x = L \qquad \text{(III.48)}$$

$$\mathcal{D}_e \frac{\partial \phi}{\partial x} = u(\phi - \phi_\infty) \qquad\qquad x = 0 \qquad \text{(III.49)}$$

$$\frac{\partial \phi}{\partial x} = 0 \qquad\qquad x = L \qquad \text{(III.50)}$$

and with radiation,

$$(k_e + k_r) \frac{\partial T_c}{\partial x} = \sigma \varepsilon (\hat{T}_c^4 - \hat{T}_\infty^4) \qquad\qquad x = 0 \qquad \text{(III.51)}$$

$$(k_e + k_r) \frac{\partial T_c}{\partial x} = -\sigma \varepsilon (\hat{T}_c^4 - \hat{T}_\infty^4) \qquad\qquad x = L \qquad \text{(III.52)}$$

$$k_a \frac{\partial T_a}{\partial x} = \rho_a c_a u (T_a - T_\infty) \qquad\qquad x = 0 \qquad \text{(III.53)}$$

$$\frac{\partial T_a}{\partial x} = 0 \qquad\qquad x = L \qquad \text{(III.54)}$$

$$\mathcal{D}_e \frac{\partial \phi}{\partial x} = u(\phi - \phi_\infty) \qquad\qquad x = 0 \qquad \text{(III.55)}$$

46

$$\frac{\partial \phi}{\partial x} \; = \; 0 \qquad\qquad\qquad x = L \qquad (III.56)$$

Expressions III.45 and III.46 represent insulated boundaries on the porous solid (i.e., no heat loss from the porous solid to the environment). Expressions III.51 and III.52 provide for radiation heat transfer from the porous solid boundaries to the environment. The boundary conditions for the air temperature and oxygen concentration, expressions III.47 through III.49 and III.52 through III.55, are the Danckwerts' boundary conditions for flow reactors. A convincing discussion of the Danckwerts' boundary conditions applied to mass diffusion equations for porous media is given by Bischoff [41]. A brief summary of the discussion was presented by Vatikiotis [2]. An analogy to Bischoff's approach for the air heat transfer equation is presented in Appendix B.

The third set of boundary conditions approximates the situation for Fontenot's experiments [1]. In the experiments, plate specimens were mounted into the wall of a wind tunnel. The interior surface of the plate (i.e., at x = L) was exposed to the wind tunnel air flow, and the external plate surface (i.e., at x = 0) was exposed to the outside environment. The expression for calculating the pressure differential across the porous medium as a result of the external flow over the surface at x = L is formulated in Appendix B. It must be emphasized that the purpose for modelling Fontenot's experiments was to analyze the combustion behavior within the plate specimens using the one dimensional model. However, the external flow

47

and plate surfaces involved convection heat transfer requiring two dimensional analysis. Noting this, the following approach was adopted to provide for convection heat transfer at the boundaries of the one dimensional model in a qualitative sense. The boundary conditions are,

$$(k_e + k_r) \frac{\partial T_c}{\partial x} = h_1 (T_c - T_\infty) + \sigma \epsilon (\hat{T}_c^4 - \hat{T}_\infty^4) \qquad x = 0 \qquad \text{(III.57)}$$

$$(k_e + k_r) \frac{\partial T_c}{\partial x} = -h_2 (T_c - T_\infty) - \sigma \epsilon (\hat{T}_c^4 - \hat{T}_\infty^4) \qquad x = L \qquad \text{(III.58)}$$

$$T_a = T_\infty \qquad x = 0 \qquad \text{(III.59)}$$

$$\frac{\partial T_a}{\partial x} = 0 \qquad x = L \qquad \text{(III.60)}$$

$$\phi = . \phi_\infty \qquad x = 0 \qquad \text{(III.61)}$$

$$\frac{\partial \phi}{\partial x} = 0 \qquad x = L \qquad \text{(III.62)}$$

As stated above, the values of h_1 and h_2 in the convection terms of expressions III.57 and III.58 are difficult to interpret for a one dimensional model. The difficulty arises from considering the boundary layers on the external surfaces of the porous medium (e.g., considering the porous medium as a flat porous plate, the boundary layer resulting from natural convection on the $x = 0$ surface increases in thickness in the vertical direction, and for forced convection at the $x = L$ surface, the boundary layer thickness increases in the flow

48

direction). For this investigation, h_1 was approximated by,

$$h_1 = \left(\frac{k_a \, u \, \rho_a}{\mu}\right)_{x=0} \tag{III.63}$$

This expression is based on the analytical results presented by Merkin [42]. Expression III.63 is obtained by considering natural convection heat transfer from a vertical flat plate with "suction". From Merkin's results, the boundary layer thickness becomes constant at some distance in the vertical direction, and thus, the convection heat transfer may also be considered constant. The magnitude of the convection heat transfer coefficient, h_2, varies in a direction parallel to the external flow, U_∞ at the x = L surface. In addition, h_2 depends on the efflux of the gas at the surface. To simplify the analysis, h_2 was approximated by the relations for a smooth flat plate given by Holman [35] as,

$$h_2 = .664 \, \frac{k_a}{L} \, Pr^{1/3} \, Re^{1/2} \tag{III.64}$$

for laminar flow, where L is the distance from the boundary layer initiation, and,

$$h_2 = \frac{k_a}{L} \, Pr^{1/3} (.037 \, Re^{.8} - 850) \tag{III.65}$$

for turbulent flow, where Pr is the Prandtl number. The Reynolds number here is based on the external flow velocity

over the surface at x = L. Kays [43] provides an alternate
scheme for treating boundary layers with "blowing and suction".
The air temperature and oxygen concentration boundary condi-
tions, III.59 through III.62 were also selected because of
the difficulties in treating external surface boundary layers
in a one dimensional model. Alternatives to the essential
boundary conditions of the air and oxygen are the Danckwerts'
conditions. However, using the Danckwerts' conditions with
convection boundary conditions poses the problem of approxi-
mating a reasonable value for u at x = 0 and x = L (i.e.,
boundary layers affect the component of velocity, u, normal
to an external surface). To overcome these difficulties, it
seemed prudent not to have pore velocity and the convection
heat transfer coefficients, h_1 and h_2, appear in the same set
of boundary conditions. However, the difficulty still re-
mains of specifying a distance from the origin of the boundary
layer for expressions III.64 and III.65. In the initial work
by Vatikiotis [2], an arbitrary distance of 1 foot was used
to compare results.

I. INITIAL CONDITIONS

To initiate combustion, the porous medium must be brought
to a temperature at which the heat generation rate is suffi-
ciently high. Experimentally, there are many techniques for
doing this. However, it is difficult to measure the actual
temperature and oxygen concentration during the experiments.
This difficulty is carried over to identifying a reasonable

set of initial conditions. Noting this, the model was de-
veloped so a problem can be started at ambient conditions
with a heat flux applied to the carbon at a boundary. The
heat flux is mathematically treated as,

$$(1-p)(k_e + k_r) \frac{\partial T_c}{\partial x} = -q_{st} \qquad (III.66)$$

This approach of starting the problem simplifies the task of
determining a reasonable set of initial conditions. In addi-
tion, any arbitrary set of initial conditions can be specified.

IV. IMPLEMENTATION OF NUMERICAL METHODS

A. SOLUTION ALGORITHM

The field equations and auxiliary equations which define the problem were presented in the previous sections. The following is the scheme used to solve for the dependent variables T_c, T_a, ϕ, u, P, L, and ρ_a:

1. Starting with the Dupuit-Forcheimer expression III.10, the filter velocity, Q, is represented as a function of the pore velocity, u.

2. Substitute for Q from the previous step into Darcy's law, equation A.1.

3. The expression formed in step 2 is solved for the pore velocity, u, as a function of dP/dx. This procedure yields equation A.2.

4. Equation A.2 is substituted into the continuity equation A.3 resulting in the 2nd order partial differential equation A.4 with the pressure, P, and the air density, ρ_a, as the dependent variables.

5. Expanding equation A.4 yields equation A.5. Equation A.5 is one of 4 equations which were integrated to produce the problem solution. By taking the air density, ρ_a, as a constant over a time step of integration, equation A.5 becomes an ordinary differential equation with respect to x. For equation A.5, the shooting method (with Euler's formula for the integration algorithm)

52

was used to solve for the pressure, $P(x)$, and the pressure gradient, $dP(x)/dx$ at each time step. The air density, ρ_a, was updated at each time step using the ideal gas law, equation B.41. The rate of change of the air density was neglected during the first two time steps of integration. Reasons for neglecting the time rate of change of the air density are given in Appendix C.2.

6. Having solved equation A.5 for the pressure gradient, dP/dx, the pore velocity can be obtained from equation A.2.

7. In solving the air heat transfer equation III.38 and the oxygen molecule transfer equation III.39, the pore velocity, u, and the air density, ρ_a, are obtained from equations A.2 and B.41, respectively. Equation III.38 and III.39, along with the carbon particle equation III.32, were transformed to ordinary differential equations in time by a Galerkin FEM formulation.

8. The ordinary differential equations from step 7 are given by equations C.17 through C.19. The time integration was performed by a version of Gear's method developed by Franke [44].

9. All thermophysical properties (i.e., k_e, k_r, k_a, c_a, c_c, μ) being functions of temperature are continuously updated during the transient analysis.

10. As carbon is consumed during combustion, the porous medium properties (i.e., p, m, δ, d) change with time and are updated continuously as well.

53

12. No attempt was made to match the orders of convergence
     of the integration algorithms.

Implementing the above solution algorithm resulted in a
computer program for the solution of the problem. Several
options were incorporated in the computer program allowing
the user flexibility in the analysis. Boundary conditions
simulating fixed air inlet temperature, and convection and
radiation heat transfer from the exterior surfaces can be se-
lected. The problem can be initiated in two ways; an arbitrary
set of initial conditions can be specified, or a heat flux,
shown by expression III.66, can be specified with the porous
medium at ambient conditions. In addition, the porosity at
$x = 0$ causing transition to the surface recession phase can
be specified. Other options permit investigating materials
other than carbon (e.g., boron), studying the effects of non-
constant distributions of porous media properties.

The computer program includes a main program and 24 sub-
routines (7 of the subroutines comprise Franke's [44] inte-
gration routine). The function and description of each of
the subroutines are found in the computer program listing.
Figure IV.1 shows the flow of the program, and briefly des-
cribes the process at each step. Each block represents a
subroutine. The configuration of the blocks (i.e., blocks
within blocks) in Figure IV.1 show the six levels of the
computer program. In addition, other processes associated
with the integration routine occur inside the block shown by

54

FIGURE IV.1 - Flow of computer program.

The flowchart contains the following elements:

Main program.

Read in parameters, initialize flags and counters; Calculate initial properties and pore velocity.

Construct FEM nodal point/element correspondence array.

Print current response variables and properties.

Check for transition to surface recession. — TRUE → Reset flags, counters delete ϕ (called once).

FALSE

Call integration routine for T_c, T_a, ϕ, (ϕ deleted during surface recession).

Construct O.D.E.'s.

Calculate properties.

Test for oxygen instabiltiy.

If surface recession, update thickness, L.

Calculate pore velocity and pressure gradient.

If surface recession, transform reaction rate expression to surface flux.

Set flag for surface recession if $p(n=1) = pmax$.

Zero-out system matrices.

Generate FEM operators.

Form mass and system matrices.

Adjust matrices for boundary conditions.

Adjust matrices for oxygen instability.

Perform integration.

FALSE — Test flags for program termination.

TRUE

Print last values of response variables and properties.

STOP

55

the dashed line. These processes are discussed in detail in Franke's report.

B. STIFFNESS CONSIDERATIONS

Initially, the ordinary differential equations resulting from the finite element formulation were integrated explicitly using a sixth order Runge-Kutta method (IMSL subroutine DVERK). The largest obtainable time step was approximately 10^{-4} seconds. A larger time step caused the integration to become unstable. Gear [45] described this behavior as typical of "stiff" differential equations, and suggested that implicit integration methods be used to improve the efficiency of the integration. Gear's method, presented by Brown and Gear [46] and modified by Franke [44], was adopted as the integration method. As a result, time steps of several seconds were obtained for some problems (i.e., for surface recession and when extinction occurred). In addition, moving the exponential reaction rate from the excitation vector to the stiffness matrix (discussed in Appendix C.1) improved the integration efficiency. The improved efficiency was attributed to a better approximation of the Jacobian matrix in Gear's method.

Bui [47] and Burka [48] discuss the difficulties of solving differential equations exhibiting "stiffness" and propose alternatives to Gear's method. For a system exhibiting "stiffness", small time steps are needed for the rapidly responding terms while the integration must be continued for a long period to account for the slowly responding terms. A measure of

"stiffness" for a system of differential equations is the
ratio of the real part of the maximum eigenvalue of the Jacob-
ian matrix to the real part of the minimum eigenvalue. This
is called the "local stiffness ratio", and is represented
by,

$$S = \frac{\underset{i=1,\ldots,n}{\text{Max}} |\lambda_i|}{\underset{i=1,\ldots,n}{\text{Min}} |\lambda_i|} \qquad (IV.1)$$

where n is the number of equations. A system of equations can
be considered "stiff" if S has a value greater than 10, and
the real parts of the eigenvalues are negative.

Lastly, most numerical integration methods are bound by
a maximum time step for which the solution remains stable.
This is defined by,

$$|\Delta t \cdot \lambda_i| < K \qquad (IV.2)$$

where Δt is the time step, λ_i is the real part of the maximum
eigenvalue of the Jacogian matrix, and K is a constant depend-
ing on the integration method (usually $1 < K < 10$). For
example, Bui [47] states that Euler's method requires
$|\Delta t \lambda_i| < 1$. Therefore, for a maximum Jacobian matrix eigen-
value (representing fastest response) of 50 $(seconds)^{-1}$, the
largest timestep for the integration is .02 seconds. Exceed-
ing this value results in the integration becoming unstable.
This explains the maximum timestep of 10^{-4} seconds for the
sixth order Runge-Kutta method as previously discussed.

C. TREATMENT OF NUMERICAL DIFFICULTIES ASSOCIATED WITH OXYGEN CONCENTRATION

In problems of combustion or kinetics, where dependent variables go to zero, numerical difficulties arise. In his discussion, Frank-Kamenetskii [12] points out that for fractional order reactions (expression III.16), both the oxygen concentration and concentration gradient can become equal to zero within the porous medium. This requirement is difficult to satisfy with approximate solution methods. In the initial effort (Vatikiotis [2]), run time errors resulted when the oxygen concentration became slightly negative. This was caused by attempting to take the logarithm of a negative concentration in the fractional order term in expression III.16. One approach for correcting this problem was to use the absolute value of the oxygen concentration in the reaction rate term. This resulted in the concentration becoming increasingly negative. Another approach was to check the values of oxygen concentration at each integration interval and setting the concentration to zero for the negative values. At the next integration, the reaction rate was zero at the locations of zero concentration. Without consumption the oxygen concentration at the nodal point previously set to zero becomes positive and the oscillation repeats itself. It was observed that decreasing the integration time step and the length of the elements (i.e., increasing the number of nodal points) minimized the oscillations. Since CPU time increased for a given problem, the approach was not totally satisfactory. However, this

method was adopted for obtaining the results presented by Vatikiotis [2].

An attempt to resolve the above numerical difficulty for the present model was by implementing the Moving Finite Element method of Gelinas, Doss, and Miller [49]. In the method, the nodal points defining the elements converge to regions where they are needed to minimize the error in the numerical solution. As a result, the size of the elements in a region of large reaction rate become small, and move with this region in time. The motivation for implementing the Moving Finite Element method was Frank-Kamenetskii's [12] discussion of fractional order reactions as stated above. Also, it was observed that the oxygen concentration approached zero in a small interval within the porous medium. This behavior resulted in steep concentration gradients. It was thought that a number of small elements in this region would improve the accuracy of the solution. The results obtained from the Moving Finite Elements showed the method was not effective in resolving the numerical difficulties discussed above. The method was subsequently abandoned because of the additional expense associated with solving the differential equation governing the nodal point locations.

The method adopted in the present model for minimizing the difficulties with the oxygen concentration is as follows. The time derivative of the oxygen concentration at a nodal point is set to zero when the concentration reaches a specified positive minimum value (less than 10^{-6} lbm/ft^3). At

the next integration interval, the time derivative remains zero if the concentration at the adjacent nodal point in the negative direction (i.e., upstream) has decreased. If the concentration at the adjacent nodal point has increased, then the time derivative is released. This method, in conjunction with Franke's [44] integration routine, appears to act in an iterative manner continually improving the solution. The values of concentration in the regions where the oxygen has been totally consumed are typically on the order of 10^{-15} lbm/ft^3. Although they do not give the details, Scheisser and Stein [50] have used the above method in their work of simulating coal conversion.

D.   AN ALTERNATE SOLUTION STRATEGY

The experience and difficulties of implementing the numerical methods, as discussed above, have provided insight for an alternate strategy for solving the combustion and heat transfer problem. The alternate strategy consists of formulating the problem with two moving boundaries. One moving boundary, as in the present formulation, would account for surface recession (i.e., the porous medium thickness changing with time). The second moving boundary would account for the oxygen concentration going to zero within the porous medium. This second boundary would be located where the concentration becomes zero, between $x = 0$ and the first moving boundary. The advantages of the alternate solution strategy are (1) eliminating the numerical difficulties associated with the

oxygen concentration (discussed in the previous section),
(2) relaxing the planar heat source assumption for the surface
recession phase (discussed in Section III.G), and (3) possibly
improving the numerical "stiffness" characteristics of the
integration (discussed in Section IV.B).

V. RESULTS AND OBSERVATIONS

A. BASIS FOR THE RESULTS

The results presented in the following sections are based on the idealized porous medium described in Section III.A and Figure III.1. For the idealized porous medium, porosity and permeability were explicit functions of pore diameter and unit cell thickness. Other porous media will have different geometric relationships for describing the properties. In addition, for naturally occurring porous media, experimental methods would be employed to determine the geometric properties. Noting this, the results of this investigation are intended to describe, in a qualitative sense, the behavior of a carbon porous medium during combustion. As will be shown, the temperatures observed during combustion are highly dependent on the geometric properties and the pore velocity. Although, the temperatures are typical of those reported for carbon combustion experiments, it would not be reasonable to perform a quantitative comparison between the results obtained by the model and those obtained experimentally unless the porous medium properties were the same for both. This point will be demonstrated in the next section.

B. COMPARISON OF COMBUSTION MODEL RESULTS TO EXPERIMENTAL RESULTS

The behavior of the temperature and oxygen concentration of the combustion and heat transfer model is in fair agreement

with the behavior reported in the experimental investigations of Vulis [13], Koizumi [37], Fontenot [51], Spalding [52], and Kolodstev [53]. A quantitative comparison of the results can not be made for two reasons. First, there have been few experimental investigations which present data for transient behavior of combustion in porous media. Most of the analyses present quasi-steady data (quasi in the sense that for some period of time, there is little change in the response varia- bles). When transient behavior is reported, it is usually presented in a narrative form. Secondly, the reported des- criptions of the porous media used in the experiments are not sufficient. The properties of the carbon used (e.g., thermal conductivity, density, Arrhenius rate law, etc.) and the porosity and permeability relationships are needed to accurately simulate the experiment. The profiles of the quasi-steady temperatures obtained by the combustion model and those ob- tained by Kolodstev's experiments will be shown together. The purpose of this is to demonstrate that although Kolodstev's porous medium could only be roughly approximated, the tempera- ture profile obtained by the combustion model was similar in shape and magnitude to that obtained experimentally.

In the experimental investigations of Vulis [13], Fontenot [51], and Spalding [52], it was observed that for a given temperature, sustained combustion occurred for a specific range of velocities. Velocities outside the range, either greater or lower, would cause the combustion to extinguish and the

porous medium to cool to ambient temperature. This phenomenon was also observed for the combustion model. The explanation of this behavior, discussed in Section V.G, is summarized as follows. As pore velocity increases, convection heat transfer and oxygen supply for combustion both increase. Similarly, a decrease in pore velocity will cause a decrease in convection heat transfer and oxygen supply. For a given set of conditions, pore velocities above the range will result in the heat transfer or heat loss overcoming the heat generation. Also, for pore velocities below the range, the oxygen supply for combustion is decreased to the extent that the heat generation is overcome by the heat loss. In other words, the higher pore velocities tend to "blowout" the reaction (e.g., blowing out a candle), and the lower pore velocities tend to "starve" the reaction (e.g., placing a container over a candle). Important at lower pore velocities are the effects of heat transfer from the external surface of the porous solid (i.e., at the boundaries). The experiments performed by Vulis [13], Fontenot [51], and Spalding [52] allowed heat transfer from the surfaces by either convection or radiation. The effects of heat transfer at the boundaries on combustion are discussed in Section V.G.

Kolodstev [53] investigated combustion gas dynamics in a porous medium comprised of spherically shaped carbon particles. This is the same type of carbon used by Parker and Hottel [16]. In his results, Kolodstev presents the quasi-steady air temperature as a function of the depth of the porous medium (particle

temperature was not reported). Figure V.1 shows Kolodstev's results plotted with the results obtained by the combustion model. Kolodstev's experiment could not be simulated accurately. As stated previously, the description of Kolodstev's porous medium was not sufficient. The description of the porous medium and the ambient conditions used to simulate the experiment is shown in Table V.1. Also shown are the known parameters given by Kolodstev. In Figure V.1, the temperature for the first inch of the 7.5 inches of the porous medium are shown (temperatures at greater depths were not reported). As can be seen, there is fair agreement in the shapes of the profiles. In addition, the magnitude of the temperatures produced by the combustion model are similar to those obtained in the experiment.

The combustion model results showed that once the reaction moved to the air inlet surface of the porous medium, the oxygen concentration penetrated the porous medium by 1 or 2 particle diameters. This observation was also reported in the experimental results of Koizumi [37] and Kolodstev [53]. The response of the oxygen concentration, in general, will be discussed in the next section.

C. EXAMPLE RESULTS

The intent here is simply to demonstrate the operation of the computer program. The behavior of a single porous medium subjected to several initial conditions is presented. The description of the porous medium and the ambient conditions
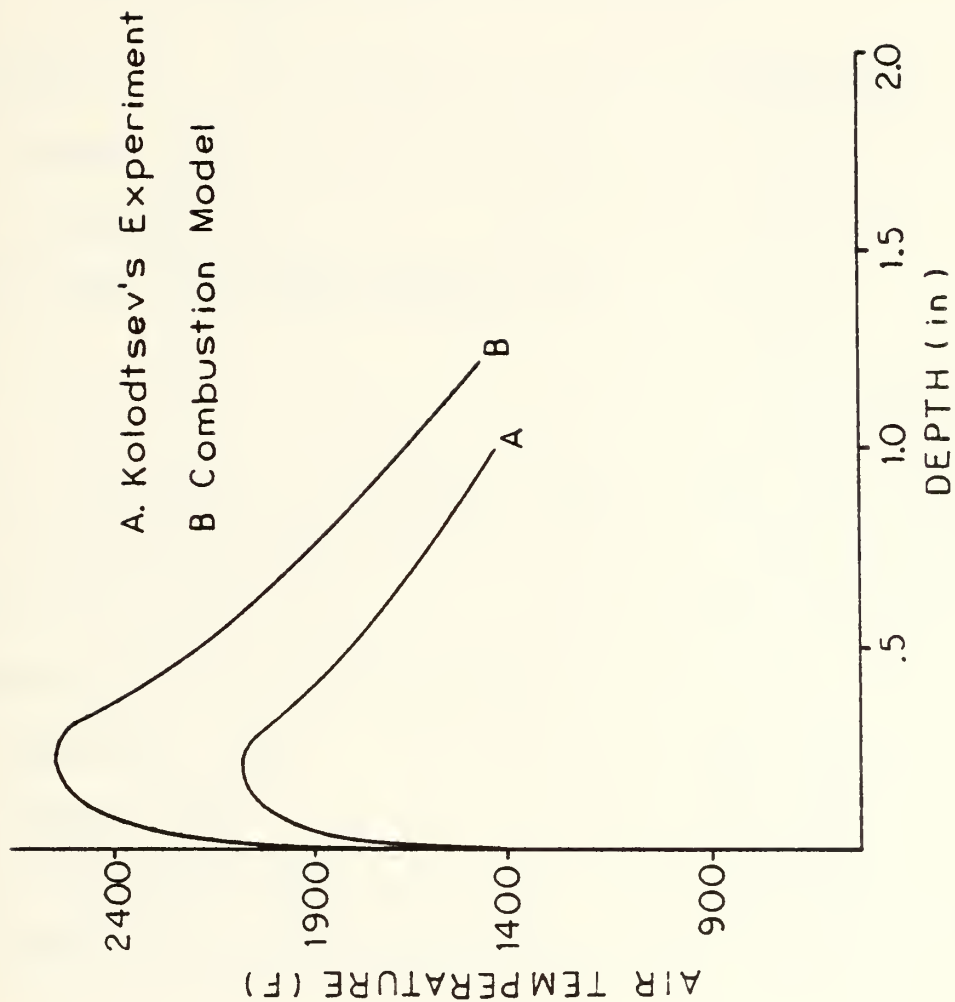
FIGURE V.1 --- Air temperature from combustion model shown with that obtained from Kolodstev's [53] experiment.

TABLE V.1 --- Geometry of porous medium and ambient conditions
           for simulating Kolodstev's [53] experiment.

● Particle Shape: spherical

● Particle Diameter (d):   .126 in

  Unit Cell Thickness (D):   .126 in

● Spatial Thickness of Porous Medium (L):   7.5 in

  Porosity (p)   .476

  Permeability (m) $.103 \times 10^{-6}$ ft^2

  Bulk Thermal Conductivity of Carbon (k_c):   86.0 Btu/ft-hr-F

  Bulk Specific Heat of Carbon (C_c):   .231 Btu/lbm-F

  Bulk Density of Carbon (ρ):   70.3 lbm/ft^3

  Thermal Emissivity of Particles (ϵ):   .9

  Ambient Temperature (T_∞):   80.0 deg-F

● Ambient Pressure (P_∞):   14.7 psi

● Pressure Differential (ΔP):   -.29 psi

● Ambient Oxygen Concentration (ϕ_∞):   .0172 lbm/ft^3

  ● Known parameter for Kolodstev's experiment.

67

used for the following problems are shown in Table V.2. The

boundary conditions for the examples in this section were

insulated boundaries on the porous solid temperature (ex-

pressions III.45 and III.46), and the Dankwerts conditions on

the air temperature and oxygen concentration (expressions

III.47 through III.50).

As the first example (referred to as example A), a heat

flux of 3.0×10^4 Btu/ft^2-hr was applied at x = 0 for 15 seconds.

The porous medium was initially at a constant temperature of

80 degrees Fahrenheit and a constant oxygen concentration of

.0172 lbm/ft^3 (ambient conditions). The results of this prob-

lem are shown in Figures V.2-V.4. Figure V.2 shows the tem-

perature increasing after the heat flux was removed. At 25

seconds, the porosity at x = 0 reached .95 and the problem

transitioned to the surface recession phase. The values of

thickness for the times shown in Figure V.2 are .25 inches to

25 seconds, .226 inches at 72 seconds, .133 inches at 357

seconds, and .0238 inches at 517 seconds. The computer pro-

gram was written such that the problem terminates when the

thickness becomes 10 percent or less of the initial value.

The air temperature shown by the dashed line in Figure V.2

follows the carbon temperature with the exception of the air

inlet region at x = 0. Figure V.3 shows the oxygen behavior

for this problem. At 25 seconds, the oxygen concentration at

x = 0 was 3.6×10^{-4} lbm/ft^3 and the penetration of the oxygen

was to x/L = .01. This supports the assumption of using a

planar source for the heat generation and deleting the oxygen

TABLE V.2 --- Geometry of porous medium and ambient conditions
              for the example problems in Section V.C.

Particle Shape: spherical

Particle Diameter (d):   .005 in

Unit Cell Thickness (D):   .005 in

Spatial Thickness of Porous Medium (L):   .25 in

Porosity (p)   .476

Permeability (m) $.162 \times 10^{-9}$ ft^2

Bulk Thermal Conductivity of Carbon (k_c):   86.0 Btu/ft-hr-F

Bulk Specific Heat of Carbon (C_c):   .231 Btu/lbm-F

Bulk Density of Carbon (ρ_c):   70.3 lbm/ft^3

Thermal Emissivity of Particles (ϵ):   .9

Ambient Temperature (T_∞):   80.0 deg-F

Ambient Pressure (P_∞):   14.7 psi

Pressure Differential (ΔP):   -.35 psi

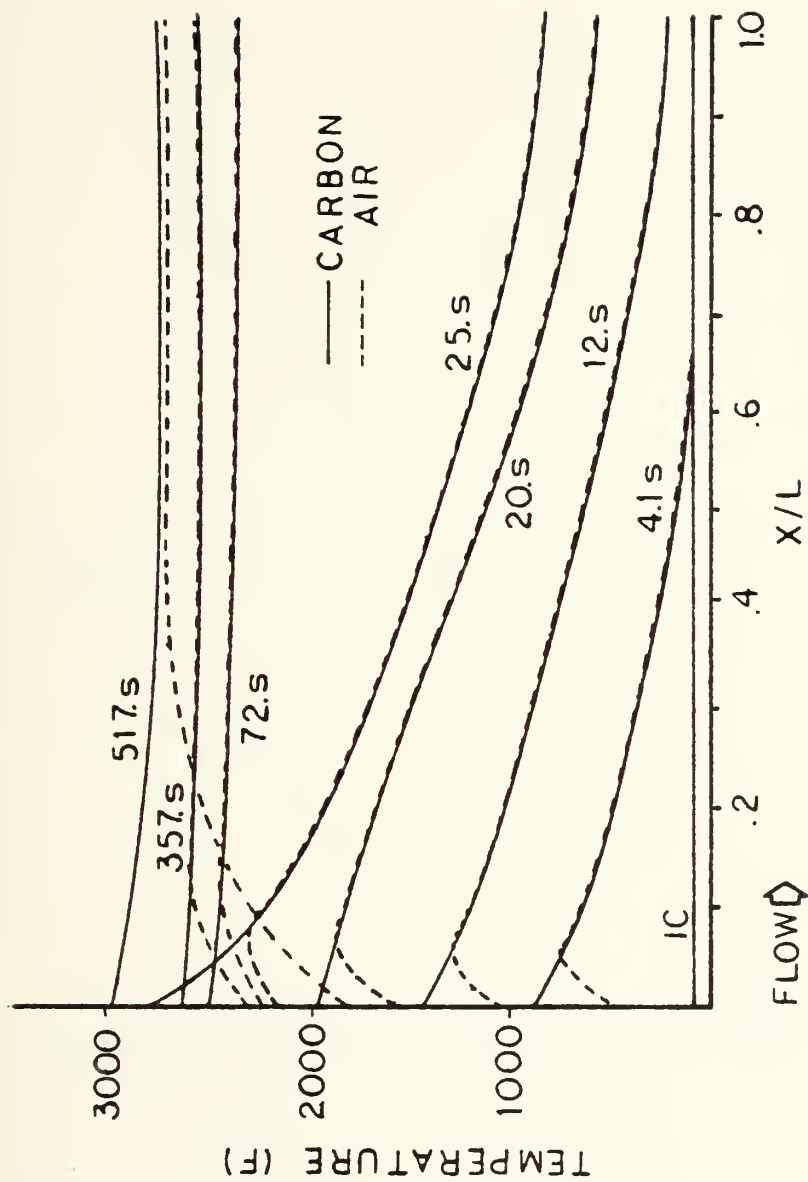Ambient Oxygen Concentration (ϕ_∞):   .0172 lbm/ft^3

FIGURE V.2 --- Sustained combustion resulting from a heat
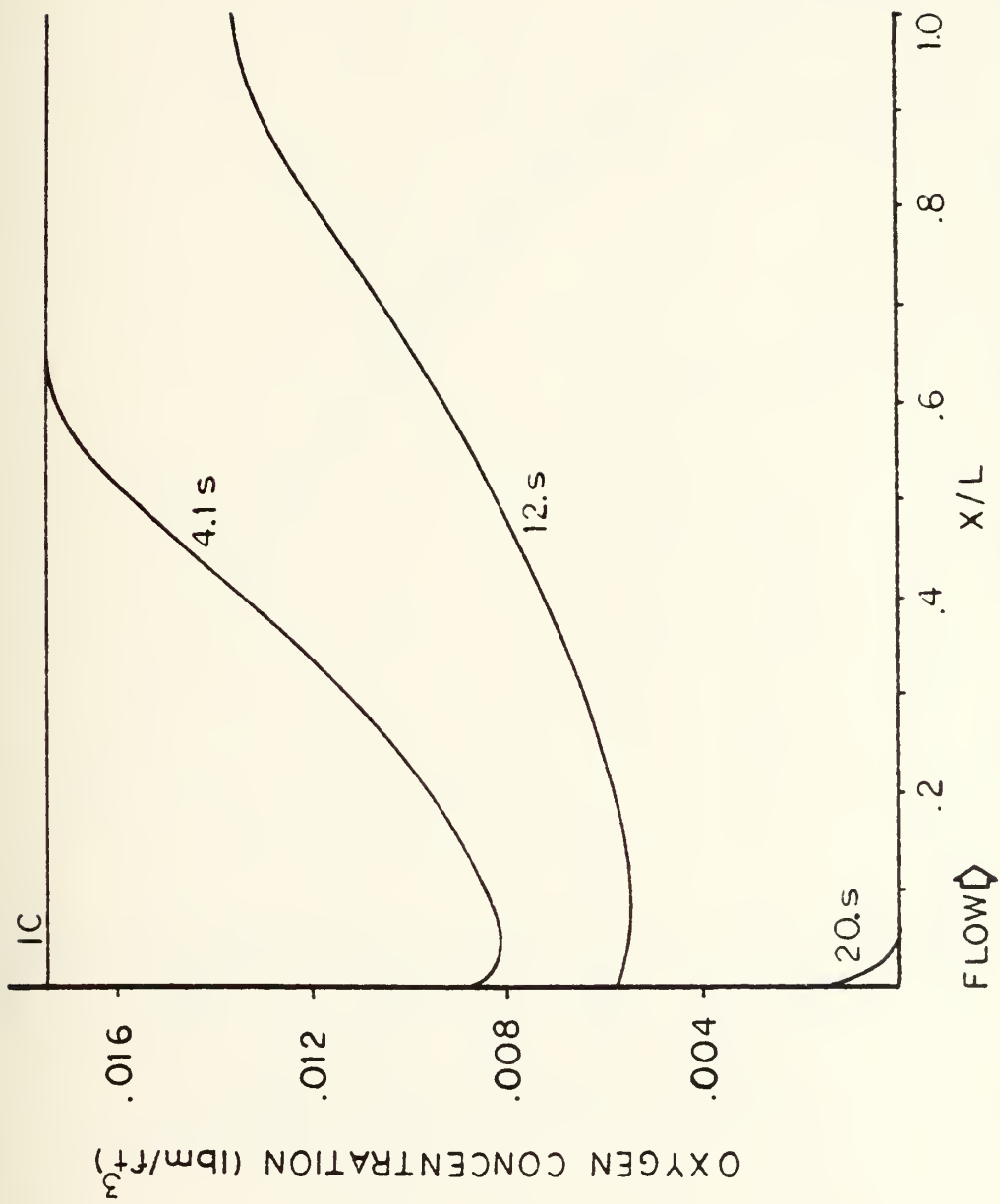flux at the x = 0 surface.

70

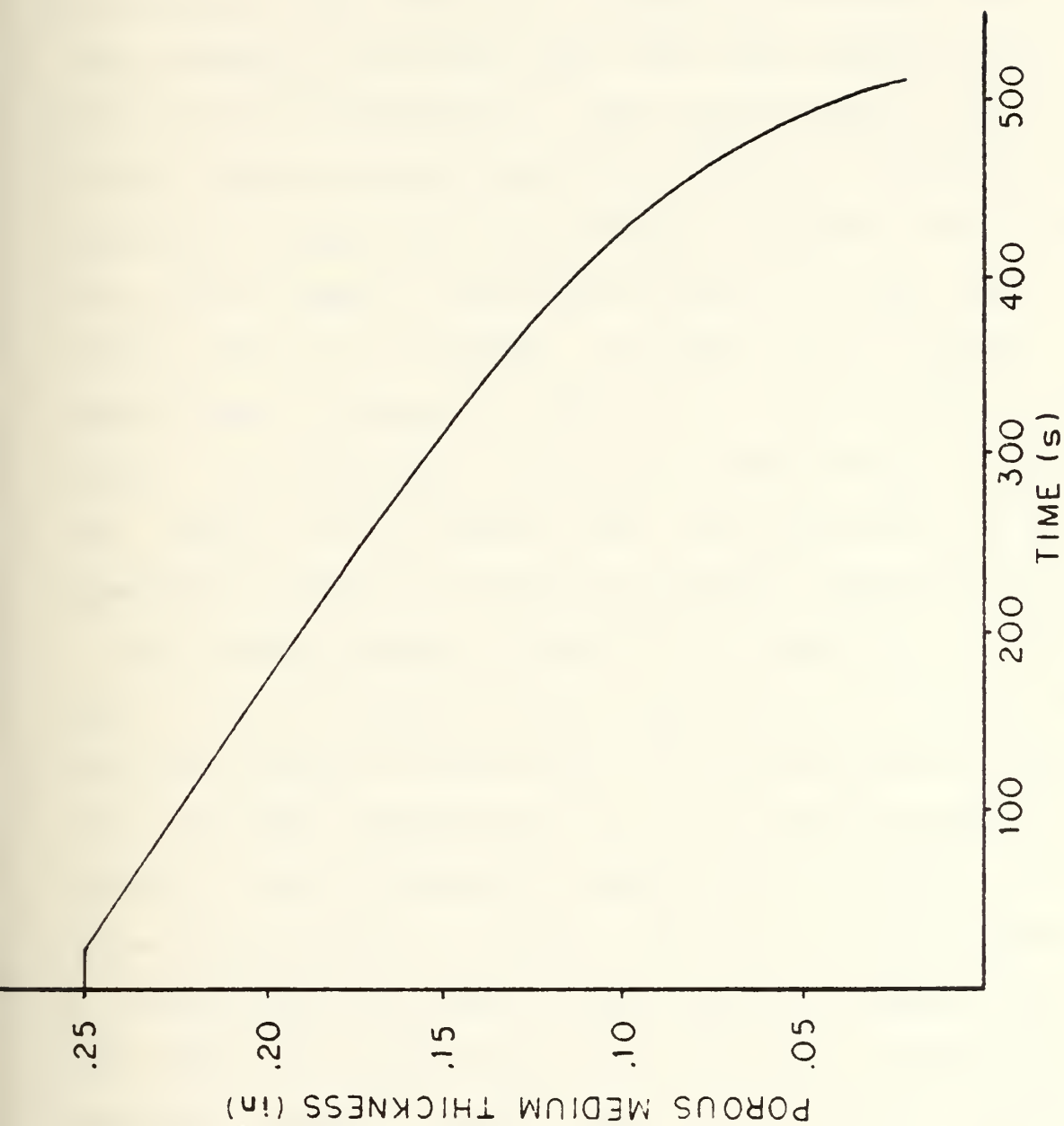FIGURE V.3 --- Oxygen response during sustained combustion.

71

FIGURE V.4 --- Change in thickness of porous medium during surface recession phase.

concentration equation during the surface recession phase.
Figure V.4 shows the decrease in the thickness of the porous
medium with time. The nondimensional parameter, λ, given by
expression III.31, had an average value of .63 at the start of
the problem. This value of λ is above the minimum value of
.342 proposed by Green and Perry [20] when assuming equal
carbon and air temperatures. This suggests that a single heat
transfer equation would have been sufficient to describe the
temperature response for this problem. However, this is not
valid for all cases. For example, when d, D, and L are
doubled, that is, .01 inches, .01 inches, and .5 inches,
respectively, λ equals .22, and for d, D, and L equal to .025
inches, .025 inches and 1.25 inches, respectively, λ equals
.056. Hence, for the general case, the carbon and the air
temperatures should be treated as separate response variables.

As a second example (referred to as example B), a heat
flux of 3.0×10^4 Btu/ft^2-hr was applied at x = 0 for 14 seconds.
The porous medium was initially at the same ambient tempera-
ture and oxygen concentration as in the previous example.
Figures V.5 and V.6 show the results of this problem. The
porous medium cooled to ambient conditions in approximately
41 seconds after the heat flux was removed. Applying the
heat flux for 14 seconds was not sufficient to produce the
conditions needed to sustain combustion. However, increasing
the duration of the heat flux for an additional second results
in sustained combustion. Figures V.5 and V.6 show the results
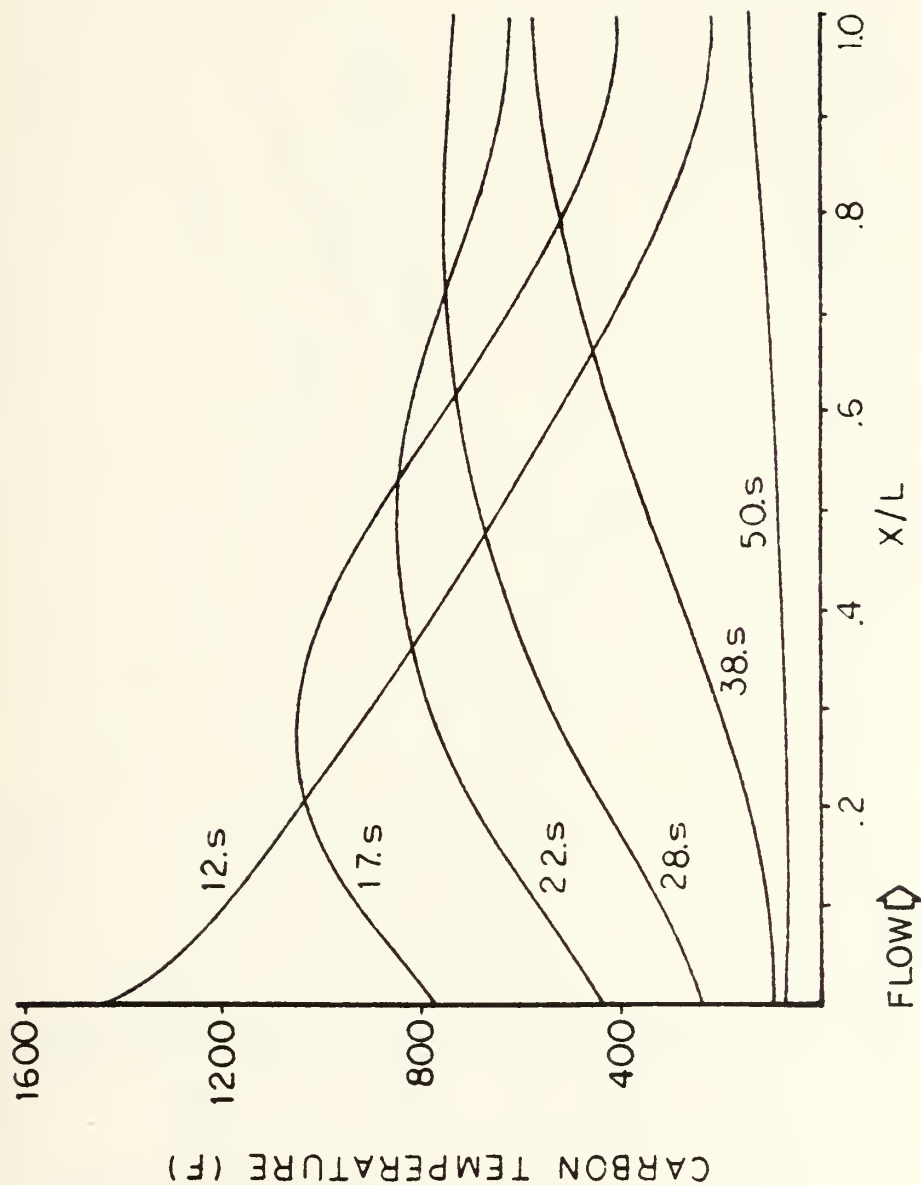starting at 12 seconds. The behavior of the system prior to

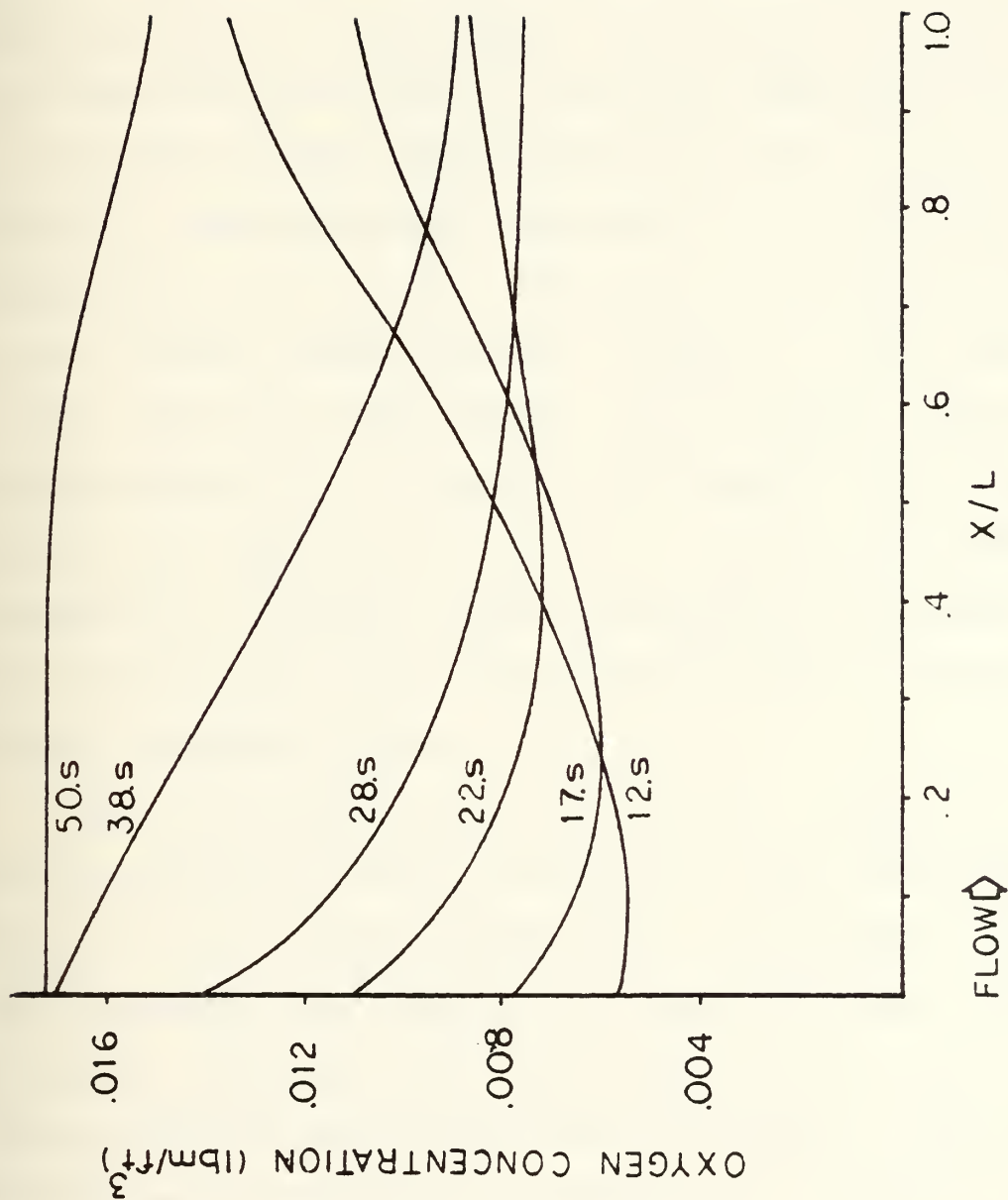FIGURE V.5 --- Response of temperature when heat flux at x = 0 insufficient to produce sustained combustion.

74

FIGURE V.6 --- Response of oxygen as porous medium cools to ambient temperature.

75

12 seconds is the same as in Figures V.2 and V.3 of the previous problem.

As the last example (referred to as example C), the problem was started with the porous medium at constant temperature and oxygen concentration of 1100 degrees Fahrenheit and .006 lbm/ft^3, respectively. Figure V.7 shows the large cooling effect of the air entering the porous medium at x = 0 during the early part of the problem. As a result of this cooling, the heat generation began to raise the temperature interior to the porous medium before moving as a wave to the air inlet surface. The problem was terminated at 49 seconds with a porosity at x = 0 of .96. This was at the point of transition to the surface recession phase. Figure V.8 shows the behavior of the oxygen for this problem. At 49 seconds, the oxygen concentration at x = 0 was 4.1×10^{-4} lbm/ft^3 and the penetration of the oxygen was to x/L = .01. This again supports the assumption of treating the heat generation as a planar source and deleting the oxygen concentration equation during the surface recession phase.

Other data generated by the model are spatial distributions of the following internal properties: particle diameter (d), porosity (p), specific permeability (m), pressure (P), pressure gradient, pore velocity (u), Reynolds number (Re), heat transfer coefficient (h), and surface area per unit volume (z). As previously stated in the model development, these system properties are functions of temperature, and hence, change
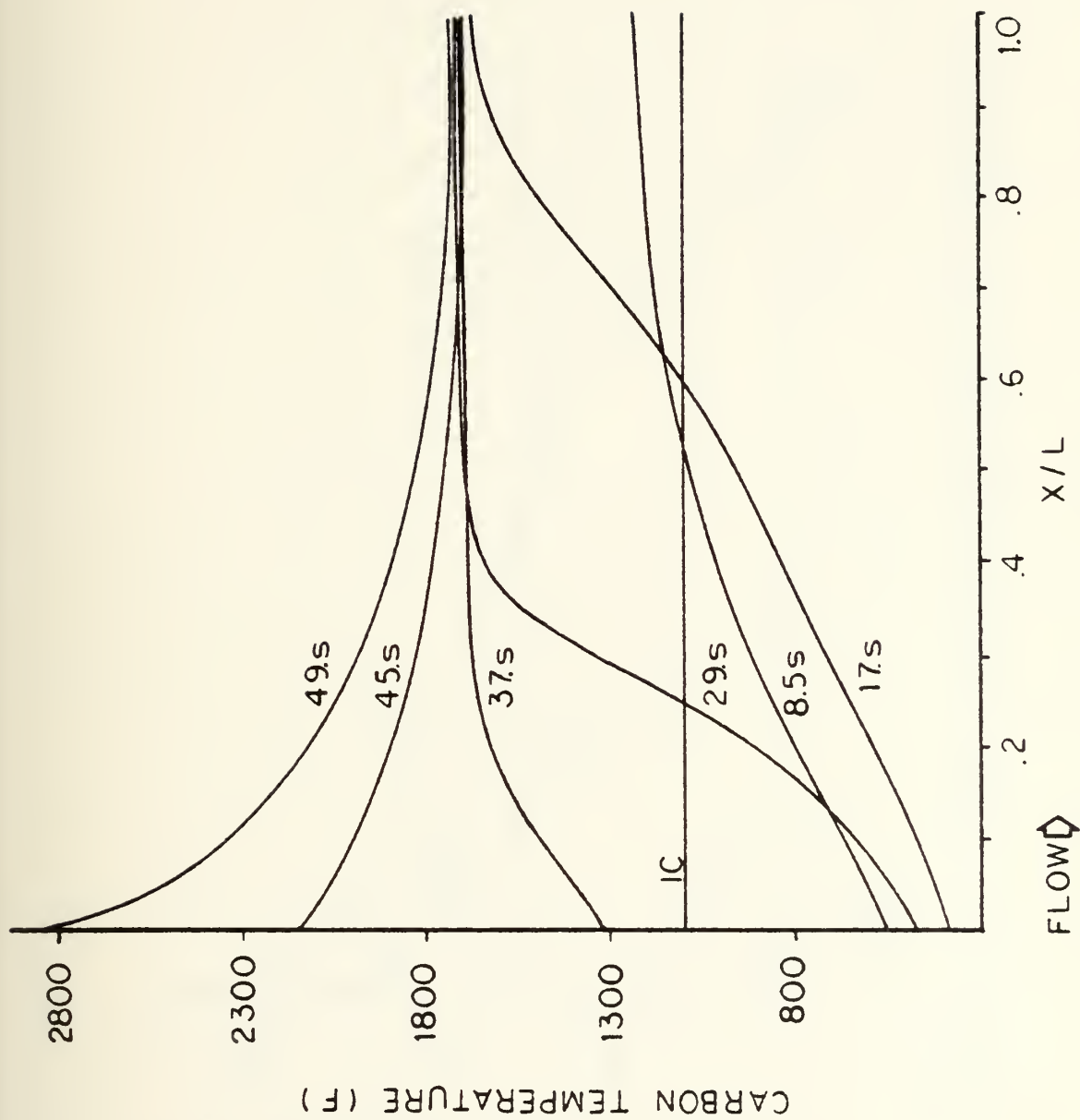
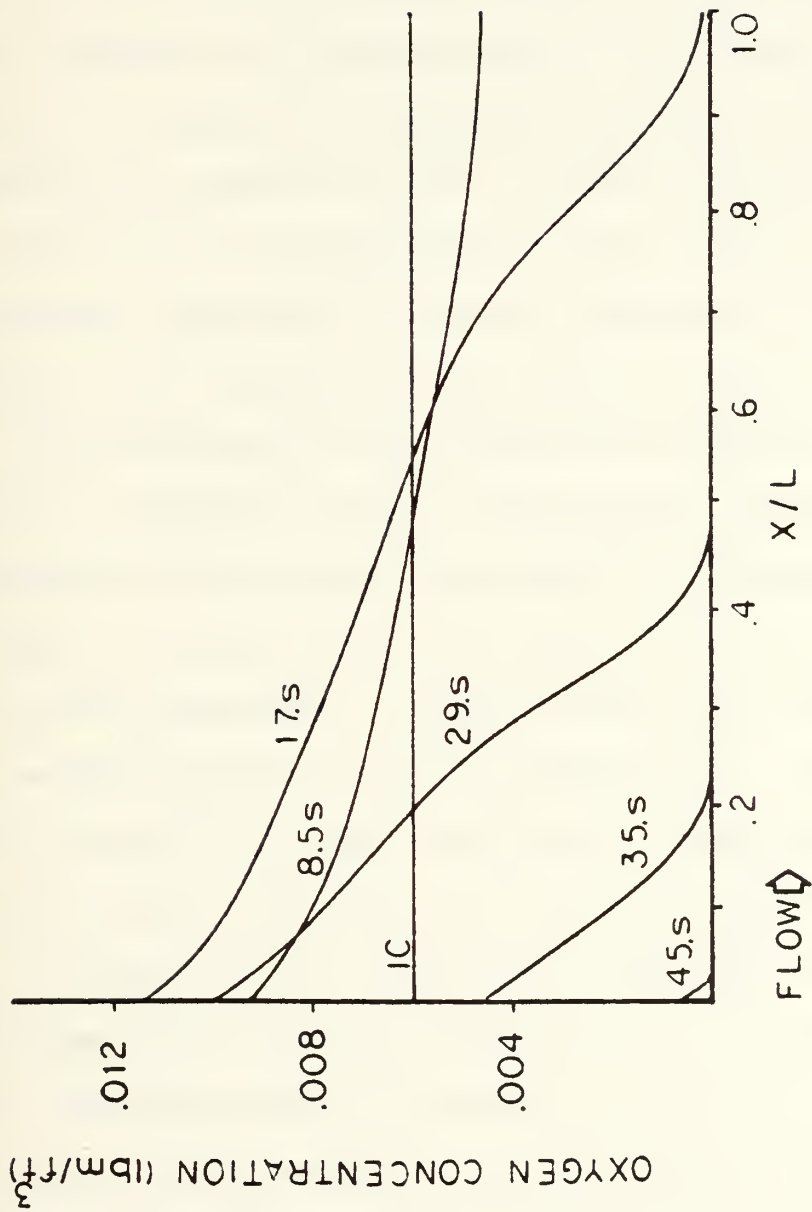FIGURE V.7 --- Sustained combustion produced by a high initial temperature.

77

FIGURE V.8 --- Oxygen response during sustained combustion.

78

with time. In addition, since surface recession may occur, the spatial thickness (L) of the porous medium is provided as output data.

D. EFFECT OF GEOMETRIC PARAMETERS

In the initial effort by Vatikiotis [2], it was observed that, for a given set of boundary and initial conditions, the internal geometry of a porous medium significantly influenced combustion. Results were reported describing the dependence of combustion on particle size, and the thickness of the porous medium. As a refinement of that initial work, results are presented below which show the influence of the geometric parameters (i.e., permeability, porosity, porous medium thickness) on the minimum initial temperature needed to sustain combustion. "Minimum initial temperature" is defined here as the minimum constant-value temperature distribution (i.e., slope equal to zero) that will sustain combustion when used as an initial condition. A lower temperature will cause the porous medium to cool to ambient temperature. As will be shown in Section V.E, both the shape and magnitude of the temperature initial conditions influences the combustion process. In order to form a basis for comparison, the analysis was performed with uniform distributions for the initial conditions (the carbon and air having the same initial temperature). The initial condition for the oxygen concentration (also uniform) was taken as the concentration found in air at the initial condition temperature and ambient pressure. However, any oxygen concentration distribution, as an initial condition,

would not have changed the results. The boundary conditions used in the analyses were the insulated boundaries, expressions III.45 and III.46, for the carbon temperature, and the Danck- werts conditions, expressions III.47 through III.50, for the air temperature and oxygen concentration. The results of the analysis were obtained by varying the initial conditions until the "minimum initial temperature" for sustaining combustion was obtained. A geometric parameter was then changed to a new value while all other parameters remained the same. A "mini- mum initial temperature" for this problem was obtained. This procedure was repeated for several values of the same geometric parameter while keeping all other parameters fixed. The re- sults obtained showed the "minimum initial temperature" which sustained combustion as a function of the respective parameter. The results for each geometric parameter are discussed individually.

1. Effects of Permeability

Figure V.9 shows the dependence of the "minimum initial temperature" (defined previously in this section) on permea- bility. The description of the porous medium and the ambient conditions used in the following analysis is given in Table V.3. The range of permeability was determined by the magni- tude of the Reynolds number. The largest permeability ($m = .4 \times 10^{-8}$ ft^2), at a pressure differential of 1.5 p.s.i., resulted in an average Reynolds number through the porous medium of approximately 5. It was felt that extending the
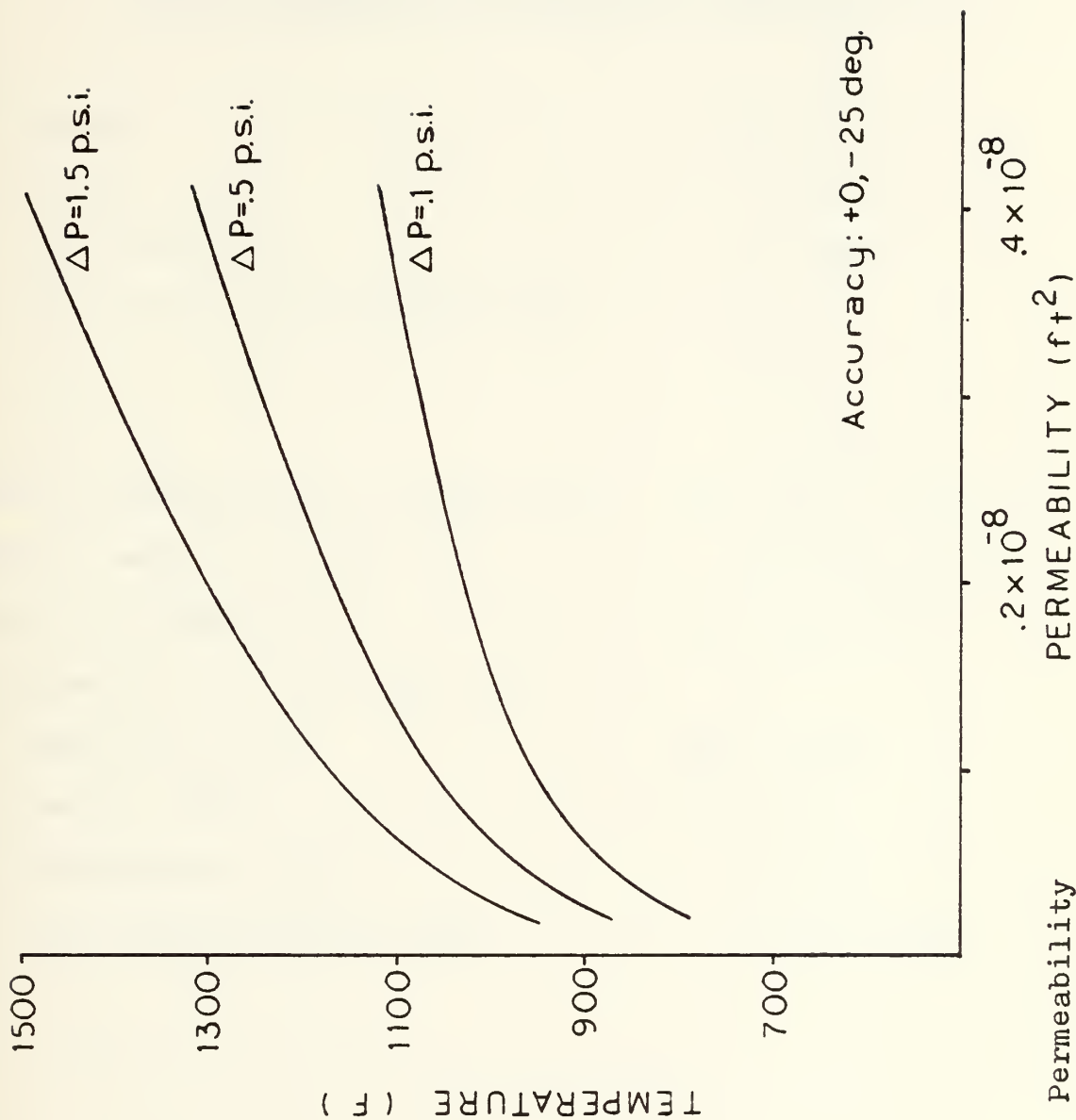
FIGURE V.9 --- Permeability analysis.

TABLE V.3 --- Geometry of porous medium and ambient conditions
for the permeability analysis in Section V.D.

Particle Shape: spherical

Particle Diameter (d):   (various)

Unit Cell Thickness (D):   (various)

Spatial Thickness of Porous Medium (L):   1.0 in

Porosity (p)   .476

Permeability (m)   (various)

Bulk Thermal Conductivity of Carbon (k_c):   86.0 Btu/ft-hr-F

Bulk Specific Heat of Carbon (C_c):   .231 Btu/lbm-F

Bulk Density of Carbon (ρ_c):   70.3 lbm/ft^3

Thermal Emissivity of Particles (ϵ):   .9

Ambient Temperature (T_∞):   80.0 deg-F

Ambient Pressure (P_∞):   14.7 psi

Pressure Differential (ΔP):   (various)

Ambient Oxygen Concentration (ϕ_∞):   .0172 lbm/ft^3

analysis to larger values of Reynolds number would exceed the limitations of the combustion model. Specifically, the assumption that Darcy's law governs the internal flow for Reynolds numbers greater than 5 would be questionable. Similarly, the smallest permeability ($m = .162 \times 10^{-9}$ ft^2), at a pressure differential of .1 p.s.i., gave an average Reynolds number of approximately .005. The lower limit Reynolds number for which Darcy's law remains valid is not known. There is little information in the literature that addresses a lower limit Reynolds number. Although lower Reynolds numbers may be valid, the analysis was restricted to a minimum Reynolds number of .005. As can be seen in Figure V.9, the "minimum initial temperature" for sustaining combustion is a monotonically increasing function of decreasing slope of permeability. In other words, as permeability increases, the temperature needed for sustained combustion also increases. Important to the results are that pore velocity also increases with increasing permeability. As stated previously, insulated boundaries were imposed on the porous solid. As will be shown in Section V.E, the results change when heat transfer occurs at the surfaces of the porous solid.

   2. Effects of Porosity

        Figure V.10 shows the dependence of the "minimum initial temperature" for sustaining combustion on porosity. The description of the porous medium and the ambient conditions used in the following analysis is shown in Table V.4. The
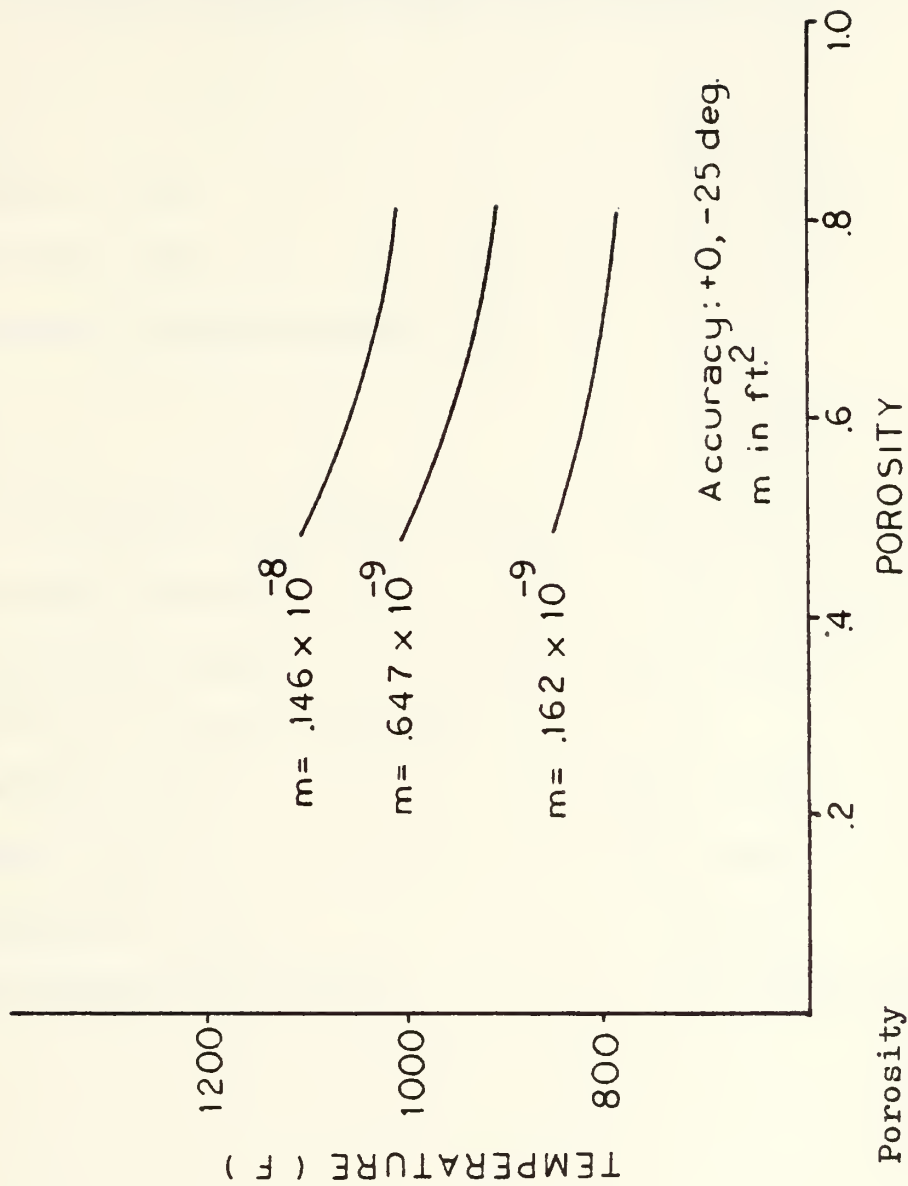
FIGURE V.10 --- Porosity analysis.

84

TABLE V.4 --- Geometry of porous medium and ambient conditions
           for the porosity analysis in Section V.D.

Particle Shape: spherical

Particle Diameter (d):   (various)

Unit Cell Thickness (D):   (various)

Spatial Thickness of Porous Medium (L):   1.0 in

Porosity (p)   (various)

Permeability (m)   (various)

Bulk Thermal Conductivity of Carbon (k_c): 86.0 Btu/ft-hr-F

Bulk Specific Heat of Carbon (C_c):   .231 Btu/lbm-F

Bulk Density of Carbon (ρ_c):   70.3 lbm/ft^3

Thermal Emissivity of Particles (ϵ):   .9

Ambient Temperature (T_∞):   80.0 deg-F

Ambient Pressure (P_∞):   14.7 psi

Pressure Differential (ΔP):   -.5 psi

Ambient Oxygen Concentration (ϕ_∞): .0172 lbm/ft^3

results show that as porosity increases, the temperature needed for sustaining combustion decreases monotonically. This behavior is opposite, but less pronounced than that observed for the permeability. In addition, pore velocity decreases as porosity increases. It seems reasonable that an increase in porosity provides more oxygen per volume of porous medium for combustion. The lowest value of porosity in the analysis (p = .48) was restricted by the idealized geometry shown in Figure III.1. For the idealized geometry, the lowest porosity occurs for the ratio of particle diameter to unit cell thickness, d/D, equal to 1. The maximum value of porosity in the analysis was limited by the highest porosity reported for spherical particles in a stable configuration. As stated by Scheidegger [9], this value is .875.

3. Effects of Porous Medium Thickness

Figure V.11 shows the dependence of the "minimum initial temperature" for sustaining combustion on the porous medium thickness. The description of the porous medium and ambient conditions used in the analysis is shown in Table V.5. The range of thicknesses (.25"-4.0") investigated was limited (as in the case of permeability) by the Reynolds number. As seen in Figure V.11, the "minimum initial temperature" is a monotonically decreasing function with decreasing negative slope of porous medium thickness. In other words, as the porous medium thickness decreases, the temperature needed to sustain combustion increases. In addition, the pore velocity
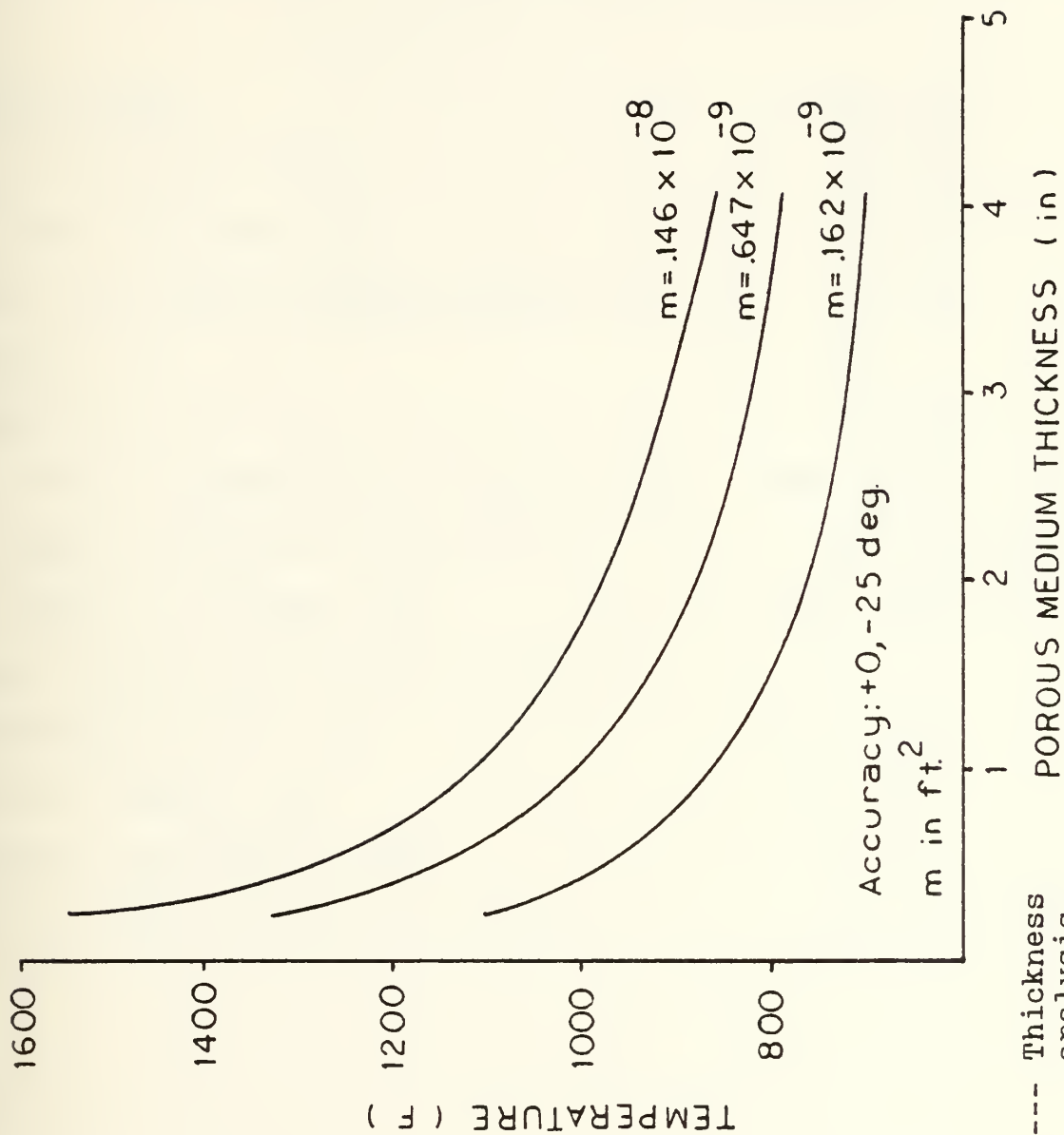
86

FIGURE V.11 --- Thickness
analysis.

87

TABLE V.5 --- Geometry of porous medium and ambient conditions
           for the thickness analysis in Section V.D.

Particle Shape: spherical

Particle Diameter (d):   (various)

Unit Cell Thickness (D):   (various)

Spatial Thickness of Porous Medium (L):   (various)

Porosity (p)   .476

Permeability (m)   (various)

Bulk Thermal Conductivity of Carbon (k_c):   86.0 Btu/ft-hr-F

Bulk Specific Heat of Carbon (c_c):   .231 Btu/lbm-F

Bulk Density of Carbon (ρ_c):   70.3 lbm/ft^3

Thermal Emissivity of Particles (ϵ):   .9

Ambient Temperature (T_∞):   80.0 deg-F

Ambient Pressure (P_∞):   14.7 psi

Pressure Differential (ΔP):   -.5 psi

Ambient Oxygen Concentration (ϕ_∞):   .0172 lbm/ft^3

decreases as the thickness increases. As in the case of the permeability, the results showed a wide range of temperatures. The "minimum initial temperature" for sustaining combustion may vary as much as 700 degrees Fahrenheit over a range of thicknesses for a particular porous medium.

E. EFFECTS OF EXTERNAL PARAMETERS

A similar analysis, as discussed in the previous section, was performed for the pressure differential. The boundary conditions for the carbon particle temperature equation were then changed from the insulated boundaries, expressions III.45 and III.46, to the radiation heat transfer boundary conditions, expressions III.51 and III.52. This permitted heat transfer from the surfaces of the porous solid. The emissivity, ε, was assumed equal to .9. With the new boundary conditions, the effects of permeability and pressure differential on the "minimum initial temperature" for sustaining combustion were again analyzed.

1. Effects of Pressure Differential

Figure V.12 shows the effects of pressure differential on the "minimum initial temperature" for sustaining combustion. The description of the porous medium and the ambient conditions used in the following analysis is shown in Table V.6. The range of pressure differentials considered (.1-2.0 p.s.i.) was governed by the Reynolds number for which Darcy's law remains applicable. This point was discussed in Section V.D. In the initial work of Vatikiotis [2], the maximum pressure
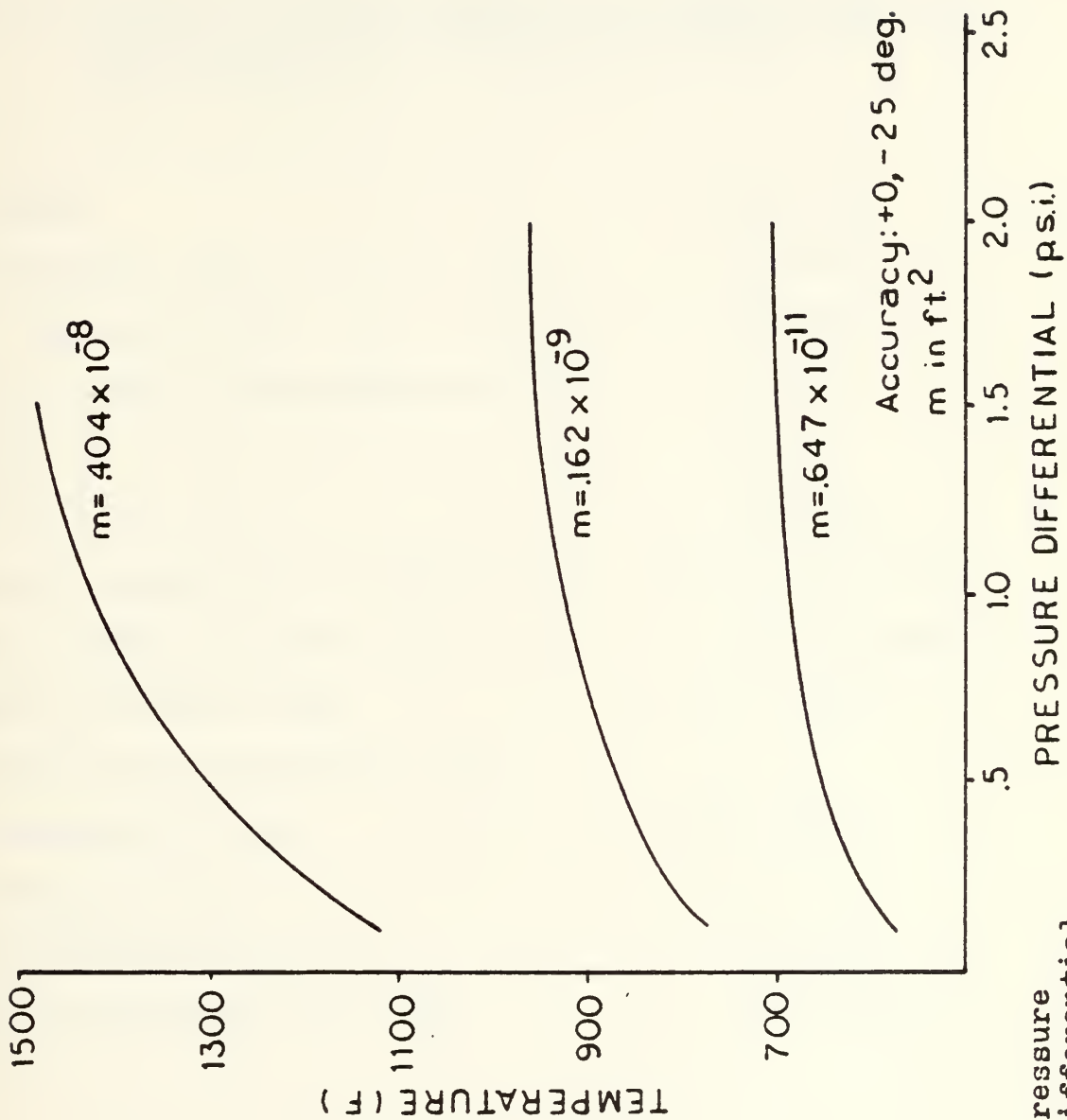
89

FIGURE V.12 --- Pressure differential analysis.

90

TABLE V.6 --- Geometry of porous medium and ambient conditions
for the pressure differential analysis in
Section V.E.

Particle Shape: spherical

Particle Diameter (d):   (various)

Unit Cell Thickness (D):   (various)

Spatial Thickness of Porous Medium (L):   1.0 in

Porosity (p)   .476

Permeability (m)   (various)

Bulk Thermal Conductivity of Carbon (k_c):   86.0 Btu/ft-hr-F

Bulk Specific Heat of Carbon (C_c):   .231 Btu/lbm-F

Bulk Density of Carbon (ρ_c):   70.3 lbm/ft^3

Thermal Emissivity of Particles (ϵ):   .9

Ambient Temperature (T_∞):   80.0 deg-F

Ambient Pressure (P_∞):   14.7 psi

Pressure Differential (ΔP):   (various)

Ambient Oxygen Concentration (ϕ_∞):   .0172 lbm/ft^3

differential considered was approximately .35 p.s.i. As seen in Figure V.12, the "minimum initial temperature" is a monotonically increasing function of pressure differential. The results show that, depending on pressure differential, the minimum temperature for sustaining combustion could vary as much as 400 degrees Fahrenheit for a particular porous medium. In addition, pore velocity increases as pressure differential increases.

   2. Effects of Boundary Conditions

        In this section, the results of allowing heat transfer at the boundaries of the porous solid will be compared to the results obtained with insulated boundaries. Figures V.13 and V.14 show the results of the permeability and the pressure differential analyses, with and without heat transfer from the surface of the porous solid. The description of the porous medium and ambient conditions for the permeability and pressure differential analyses are shown in Tables V.3 and V.6, respectively. As stated previously, the radiation heat transfer boundary conditions were those shown by expressions III.51 and III.52. As seen in Figures V.13 and V.14, heat transfer from the boundaries significantly affects the "minimum initial temperature" at the lower values of permeability and pressure differential (or at lower pore velocities). The results show that when heat transfer occurs from the boundaries, the "minimum initial temperature" is no longer a monotonic function of permeability and pressure differential. This behavior was
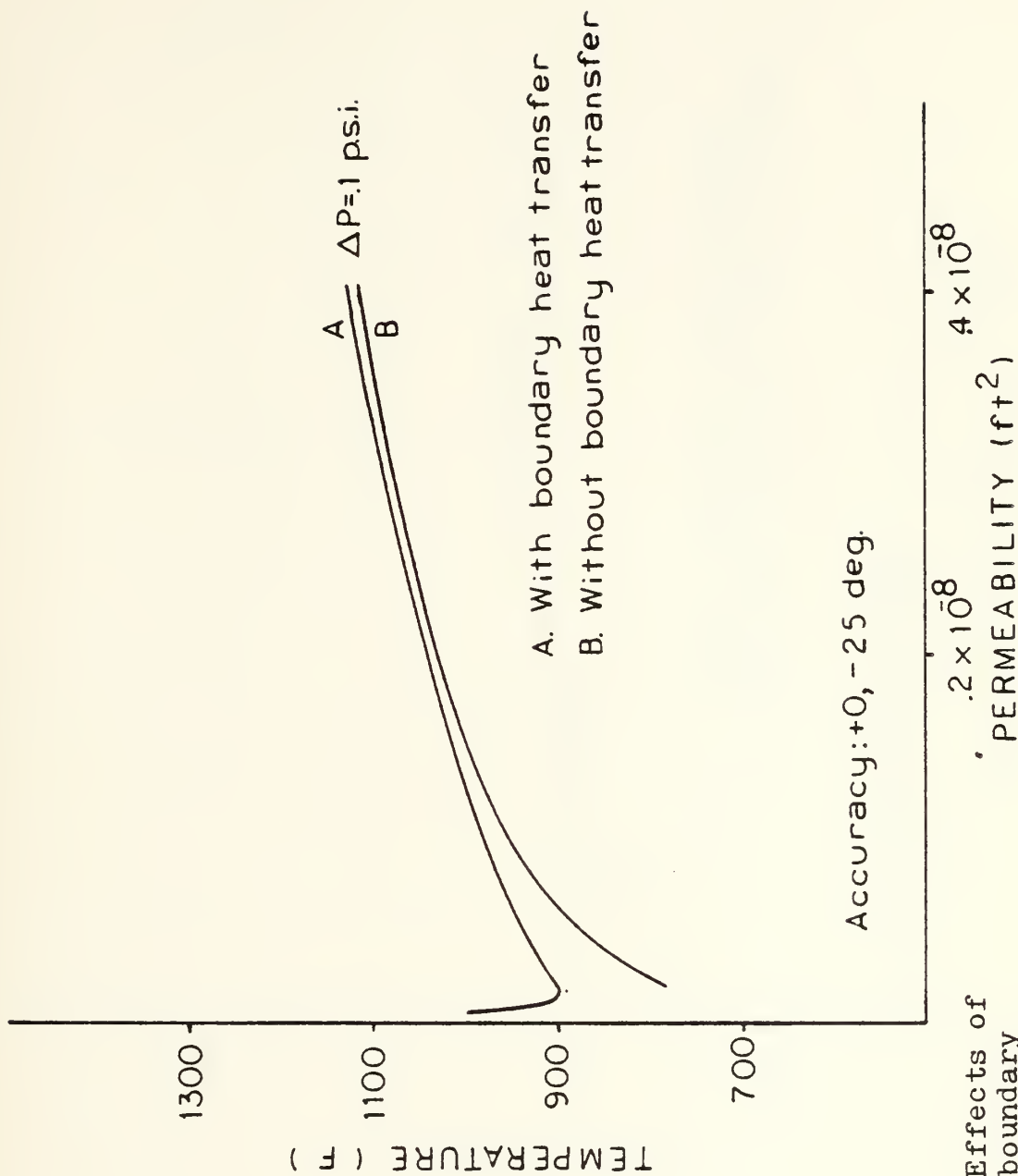
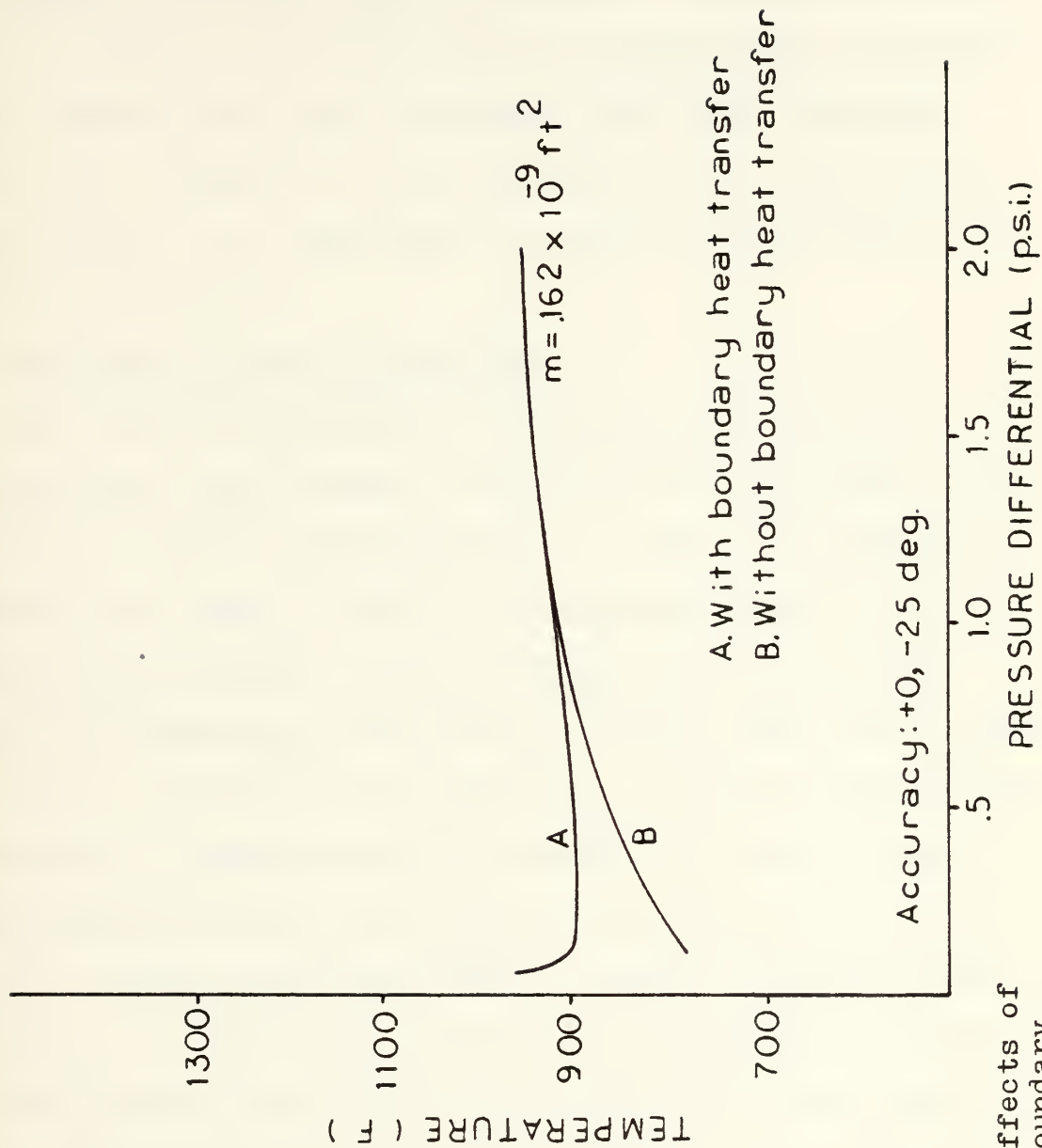FIGURE V.13 --- Effects of boundary conditions.

93

FIGURE V.14 --- Effects of boundary conditions.

94

suggested in the intial work of Varikiotis [2], where in addi-
tion to radiation heat transfer, convection heat transfer
was considered at the boundaries. The additional convection
heat transfer causes the effects produced by permitting radia-
tion heat transfer at the boundaries to become more pronounced.
Moreover, these results are consistent with those reported
by Vulis [13], Fontenot [51], and Spalding [52]. The reason
for this behavior was summarized in Section V.C and will be
explained in Section V.G.

3.   Effects of Initial Conditions

The previous analyses of determining the effects of
system parameters and boundary conditions were performed using
constant-value initial conditions (i.e., slope of temperature
distribution was equal to zero). The constant-value tempera-
ture defined the "minimum initial temperature" and was used
as a basis for comparing the results. To also show the effects
of the initial conditions on combustion, a single porous medium
was subjected to numerous initial conditions. The analysis
was performed as follows. The initial conditions of the car-
bon and air temperatures were given a constant slope as shown
in Figure V.15. With the slope fixed, the temperature distri-
bution was shifted (i.e., moved up or down) until the thres-
hold for sustained combustion was determined. That is, shift-
ing the initial temperature distribution slightly lower would
result in the porous medium cooling to ambient temperature.
This procedure was repeated for several initial conditions of
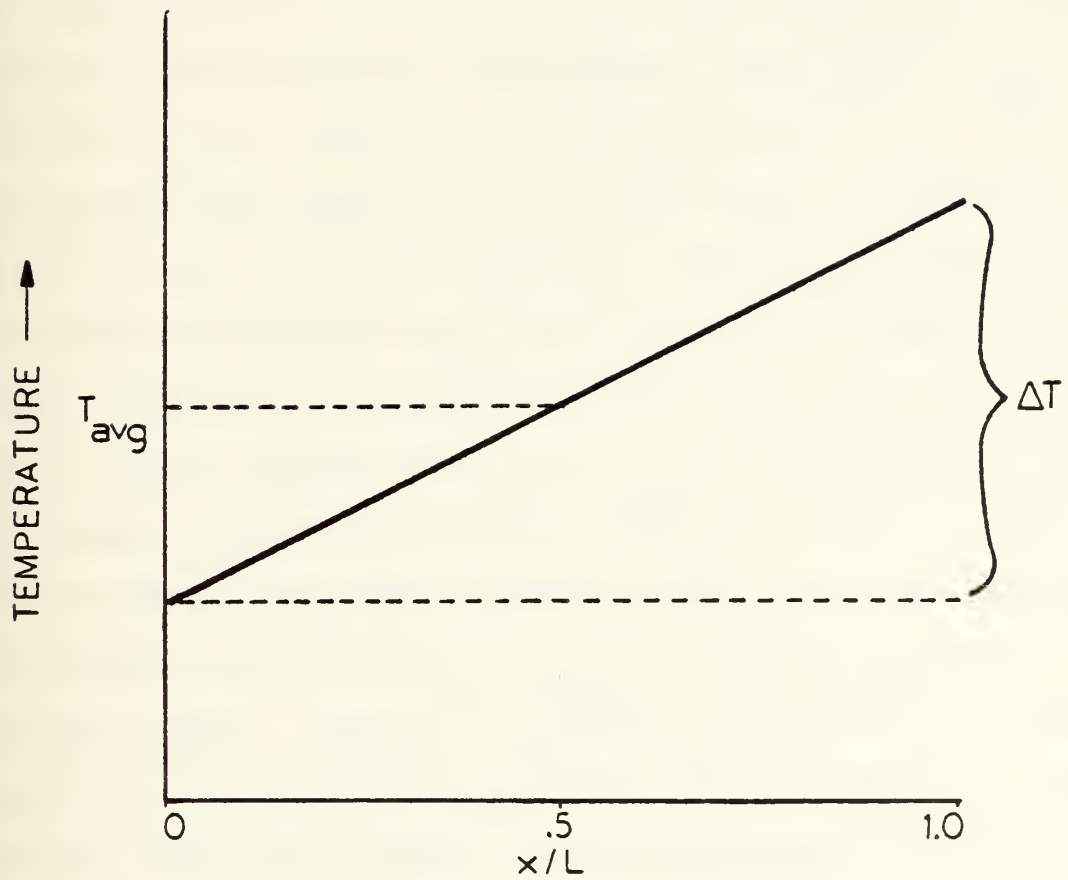temperature having different constant slopes (both negative

FIGURE V.15 --- Constant-slope initial condition.

and positive). The boundary conditions used in the analysis were the Danckwerts conditions, expressions III.47 through III.50, for the air temperature and oxygen concentration, and insulated boundaries, expressions III.45 and III.46, for the carbon temperature. The results of the analysis are shown in Figure V.16. In Figure V.16, the average temperature is plotted as a function of ΔT defined by $T(L) - T(0)$ for the particular temperature distribution. The average temperature, T_{avg}, is defined as $(T(L) + T(0))/2$. As seen in Figure V.16, the curve is not symmetrical about $\Delta T = 0$. This result is atributed to the direction of the pore velocity. The largest difference in temperature between the porous solid and the air (and greatest heat transfer) is at the air inlet region (i.e., $x = 0$). At the air exit region (i.e., $x = L$), the temperature difference between the porous solid and the air is small. The combined effect of high heat transfer at the air inlet region and low heat transfer at the air exit region produces the following result. There is a greater likelihood that sustained combustion will occur for a positive slope temperature distribution than for a negative slope temperature distribution having the same average temperature and ΔT as defined above. In other words, for a positive slope initial temperature distribution, sustained combustion occurs at a higher temperature.

F. EFFECTS OF PORE VELOCITY

The way the parameters (i.e., permeability, porosity, pressure differential, and porous medium thickness) affected
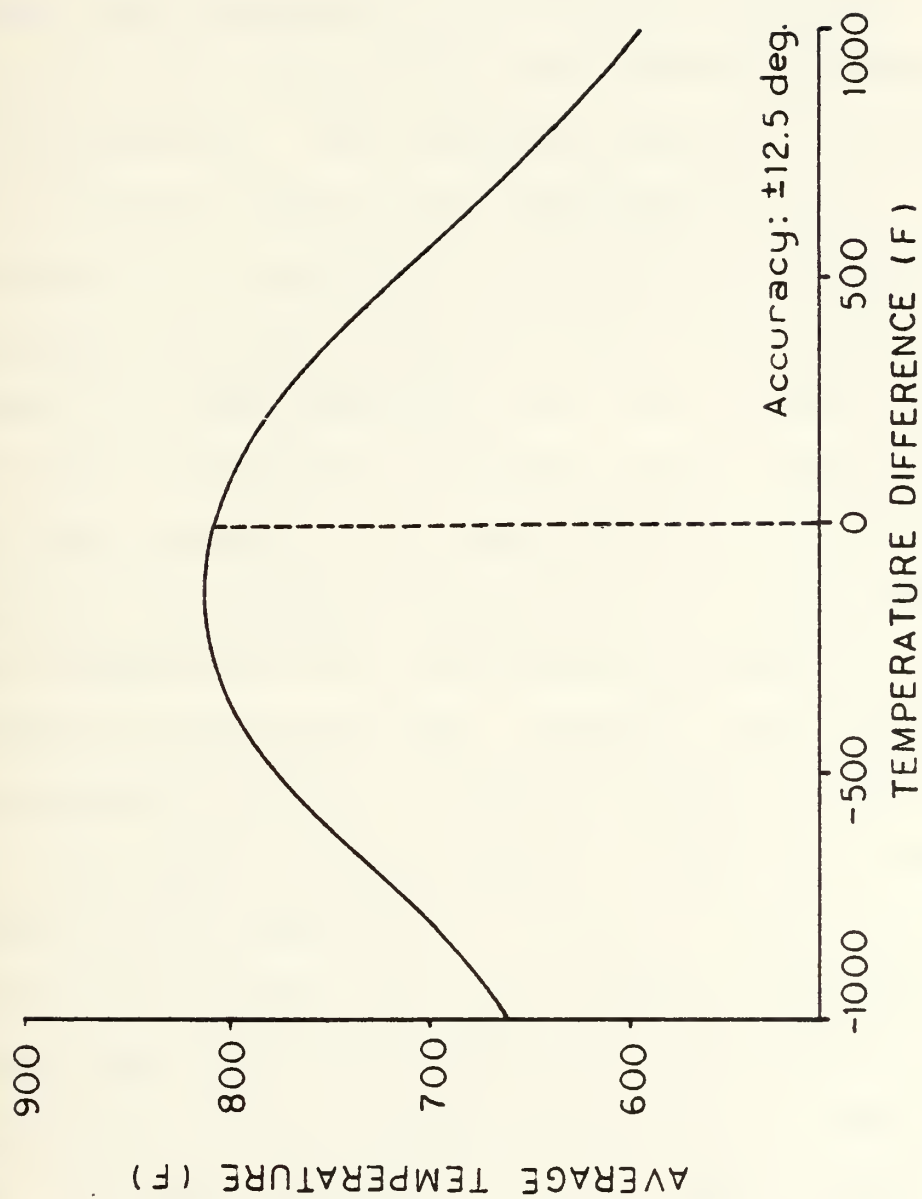
FIGURE V.16 --- Results of initial condition analysis.

combustion is in proportion to their effect on pore velocity. In other words, the results of the previous sections showed that pore velocity was affected by the parameters in the same manner as the "minimum initial temperature" for sustained combustion (i.e., minimum temperature increased as pore velocity increased, and decreased as pore velocity decreased). An exception to this occurred when heat transfer was permitted from the boundaries. This suggests that pore velocity is the dominant variable affecting the combustion process. Since pore velocity is a function of the parameters analyzed (i.e., permeability, porosity, pressure differential, porous medium thickness), it seems reasonable that the "minimum initial temperature" for sustained combustion may be posed as a function of pore velocity. With this approach, the "minimum initial temperature" for sustained combustion of a porous medium with unknown properties could be determined by specifying the magnitude of the pore velocity. Moreover, pore velocity can be represented by specific volumetric flowrate of filter velocity (i.e., V/A) which is easily measured. Figure V.17 shows the "minimum initial temperature", defined in Section V.D, as a function of the filter velocity at ambient temperature. The graph was made from the data obtained in the analyses of Sections V.D and V.E (for insulated boundaries on the porous solid). The data in Figure V.18 has a spread of approximately ±100 degrees Fahrenheit. The equation for the curve shown in Figure V.17 is,
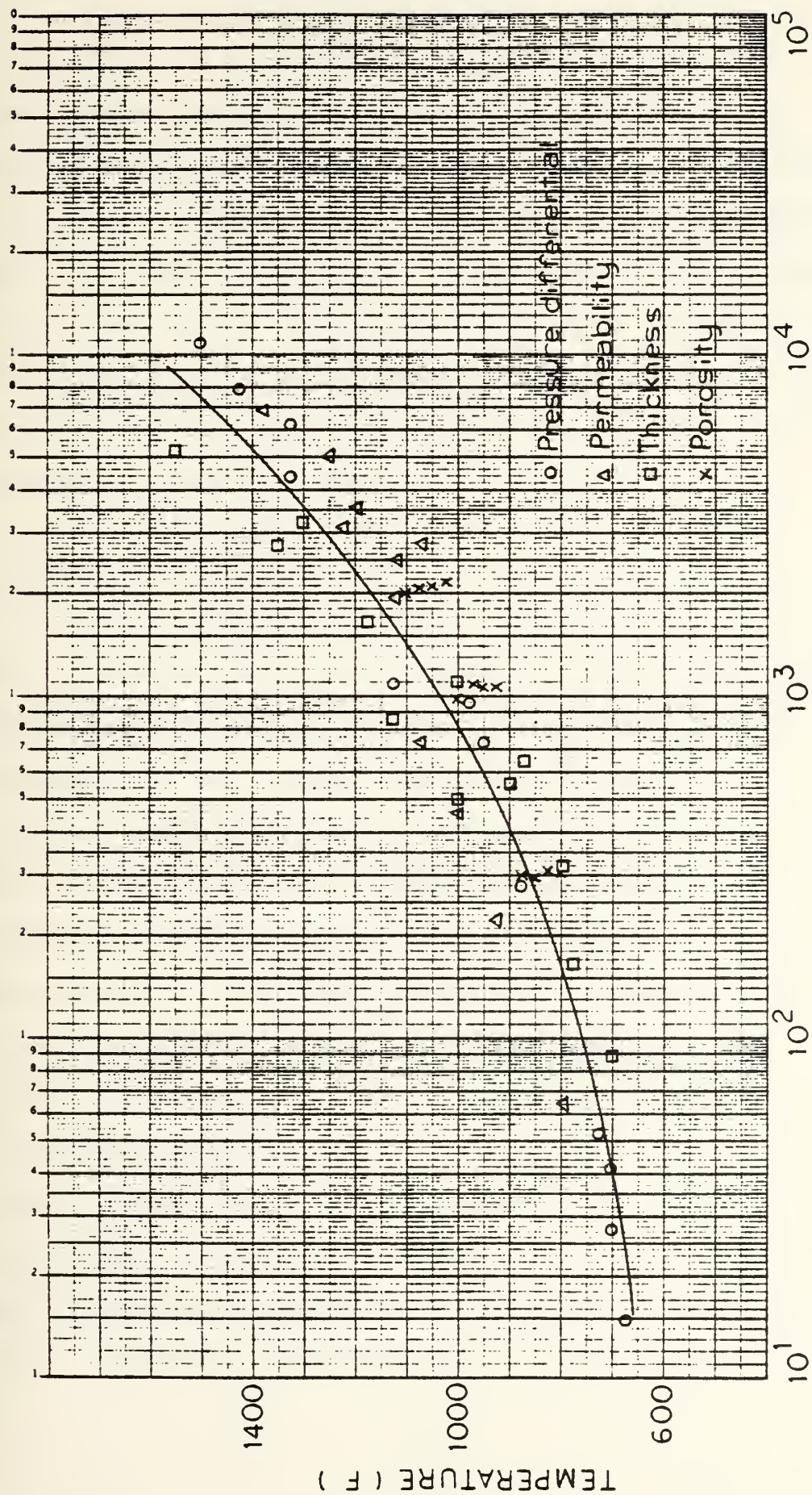
FIGURE V.17 --- "Minimum initial temperature" as a function of pore velocity.

100

$$T_{st} = 100 \ln^2(Q/10) + 650 \qquad (V.1)$$

where T_{st} represents the "minimum initial temperature" dis-
tribution in degrees Fahrenheit, and Q is the filter velocity
in ft/hr at an ambient temperature of 80 degrees Fahrenheit.
Figure V.17 shows promise as a simple method for determining
the "minimum initial temperature" for which sustained combus-
tion can be expected in a porous medium. Perhaps by refining
the formulation for calculating the pore velocity, there would
be a smaller spread in the data.

G. ANALYSIS OF RESULTS

The Semenov model, discussed in Section III.C and illus-
trated in Figure III.2, may be used to explain the results
reported in Sections V.B through V.F. Before continuing, cer-
tain aspects of the Semenov model must be emphasized. First,
the Semenov model does not govern combustion. It is an analy-
tical tool which is used to describe the behavior of combustion.
Secondly, the Semenov model as represented in Figure III.2
is for a point in the porous medium. A "Semenov surface"
would better explain combustion in the porous medium. This
will be illustrated below. It follows from the Semenov theory,
as discussed by Vulis [13], that "ignition" conditions (i.e.,
sustained combustion) are determined by all the conditions of
the combustion problem in a system. This is to say, that any
change in system parameters (e.g., pressure differential,
initial or boundary conditions) for a given porous medium

101

would result in a different Semenov surface. Lastly, the Semenov model is based on quasi-steady results. For example, the convection heat transfer, q_ℓ, and the heat generation, R_g, will be equal at their intersection (see Figure III.2). Conversely for the combustion model, at a particular point and time, q_ℓ may be smaller or larger than R_g depending on whether the temperatures are increasing or decreasing. However, if the rates of change in the temperatures are small, the Semenov model can be used to analyze the results of the combustion model.

Figure V.18 illustrates a "Semenov surface" generated from the results of the last example in Section V.C (Figures V.7 and V.8). In Figure V.18, R_g is a heat generation surface, and represents the particle temperature-heat generation relationship during the problem. The q_ℓ surface represents the convection heat transfer as a function of particle and air temperature (expression III.14). The particular heat transfer surface in Figure V.18 represents the instant the point at $x/L = 0$ transitioned from the kinetic regime to the diffusion regime of combustion. This can be seen by the tangent point, I, between the heat generation surface and the heat transfer surface. A difference between "classical" Semenov S-curves (Figure III.2) and those shown in the heat generation surface of Figure V.18 is the sudden drop in heat generation once a certain temperature has been reached. This is only observed in the region away from the air inlet ($x/L = 0$)
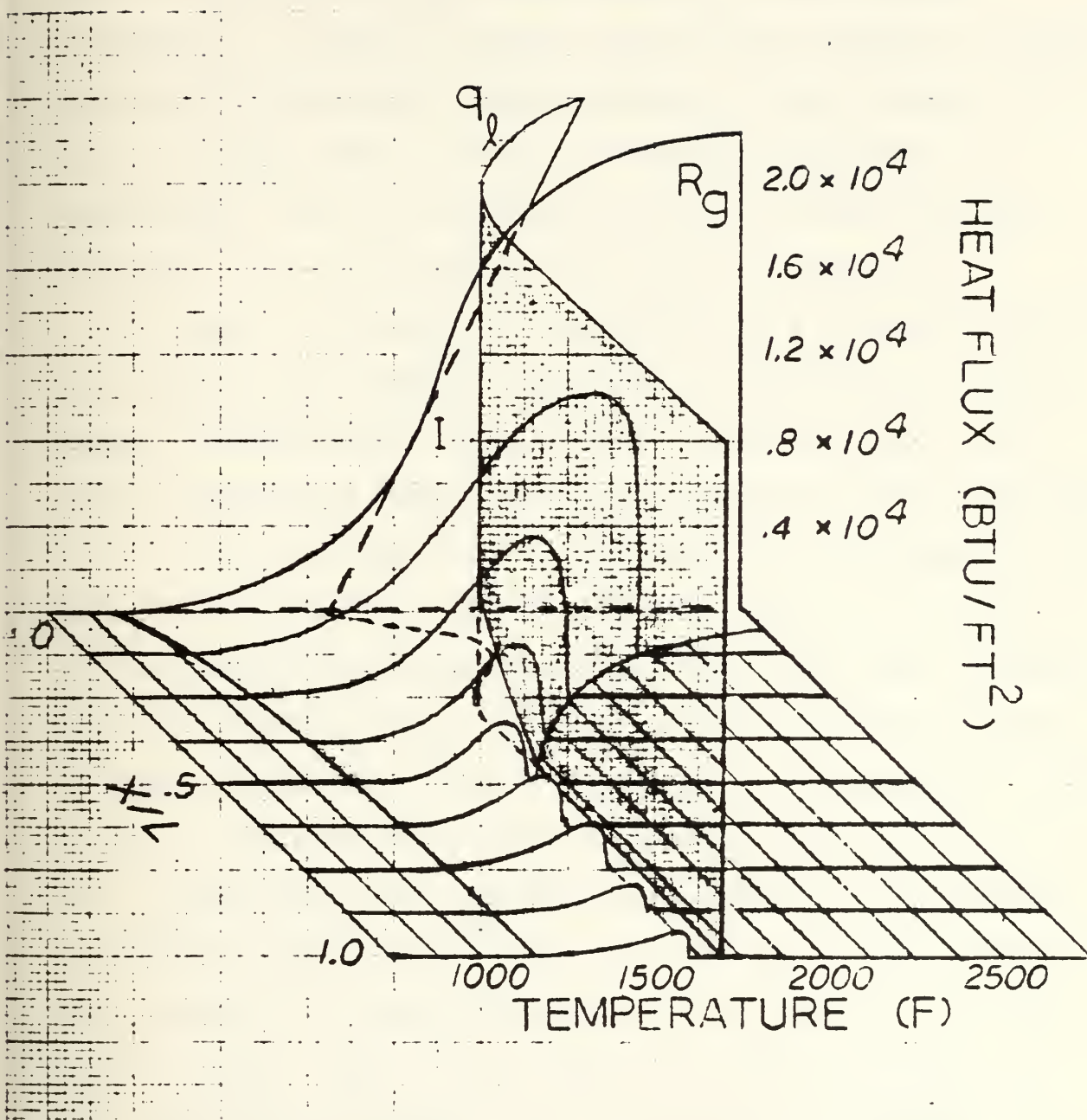
FIGURE V.18 --- Semenov surface.

103

and is attributed to the total depletion of oxygen in that region of the porous medium. One might say this is a weakness in the Semenov model when applied to porous media. Conversely, it might be argued that when the oxygen is totally depleted the combustion problem becomes a heat transfer problem (in a pure sense) of which the Semenov model has no application. Also in the region where the oxygen has been depleted, it is not necessary for q_ℓ to intersect R_g.

In order to visualize the results of the combustion model more clearly, the "Semenov surface" is abandoned for Semenov curves (illustrated in Figure III.2). Figures V.19, V.20, and V.21 show that Semenov model representations for locations $x/L = 0$, $x/L = .5$, and $x/L = 1$, respectively, of example C in Section V.C (transient results shown in Figures V.7 and V.8). The heat generation curves are shown along with heat transfer lines representing the film cooling at two different points in time. During this discussion, the term "film cooling" will be used to mean the heat transfer from the particle to the air. "Convection heat transfer" will refer to the transport of energy by the internal flow. In addition to film cooling, heat transfer by conduction and radiation occurs within the porous medium. This has an effect of slightly curving the heat transfer line upward (i.e., heat transfer becomes a non-linear vice a linear function of temperature). However in this problem, calculations showed that the ratio of film cooling to conduction and radiation was approximately 5, and
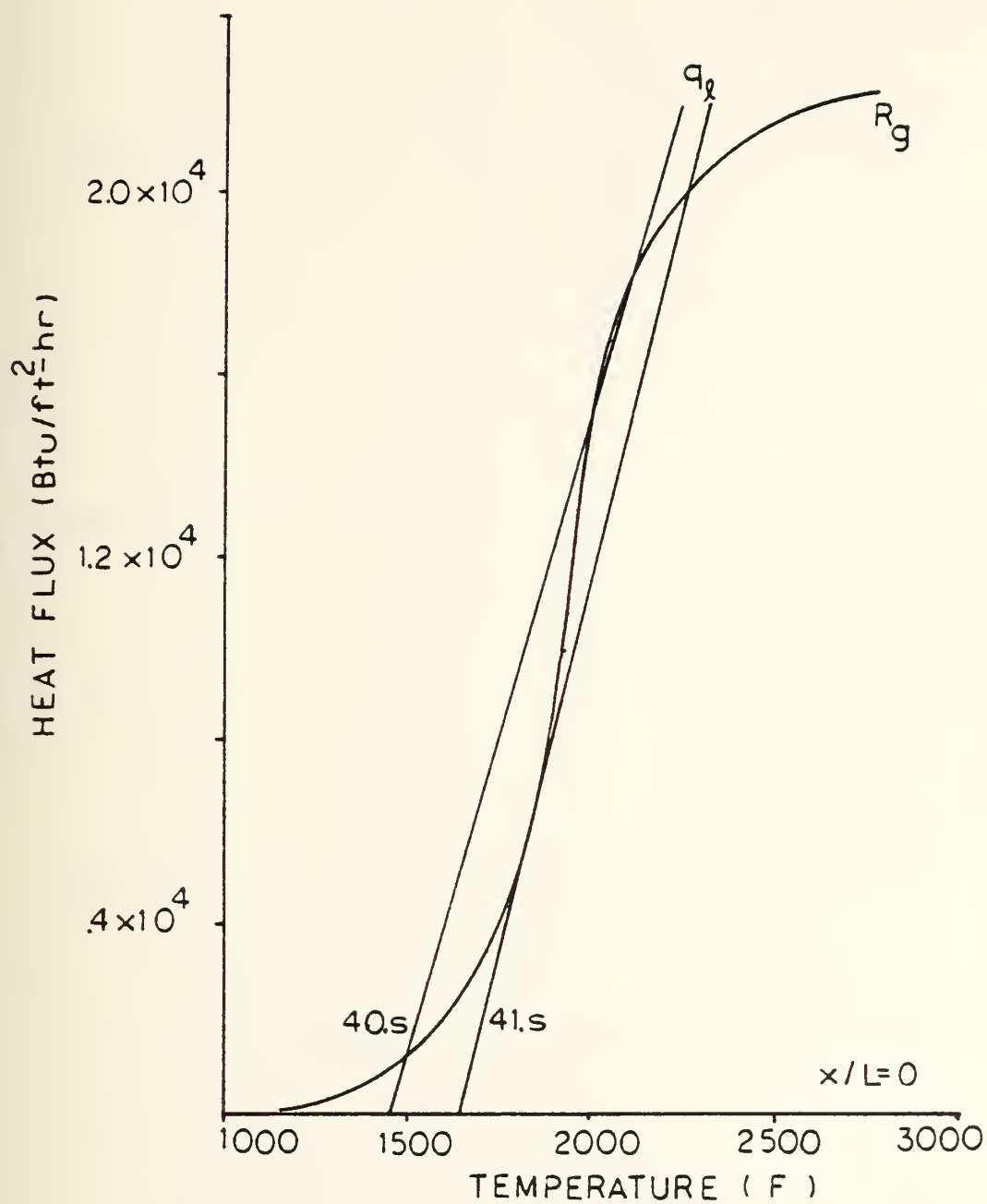
FIGURE V.19 --- S-curve at x/L = 0.

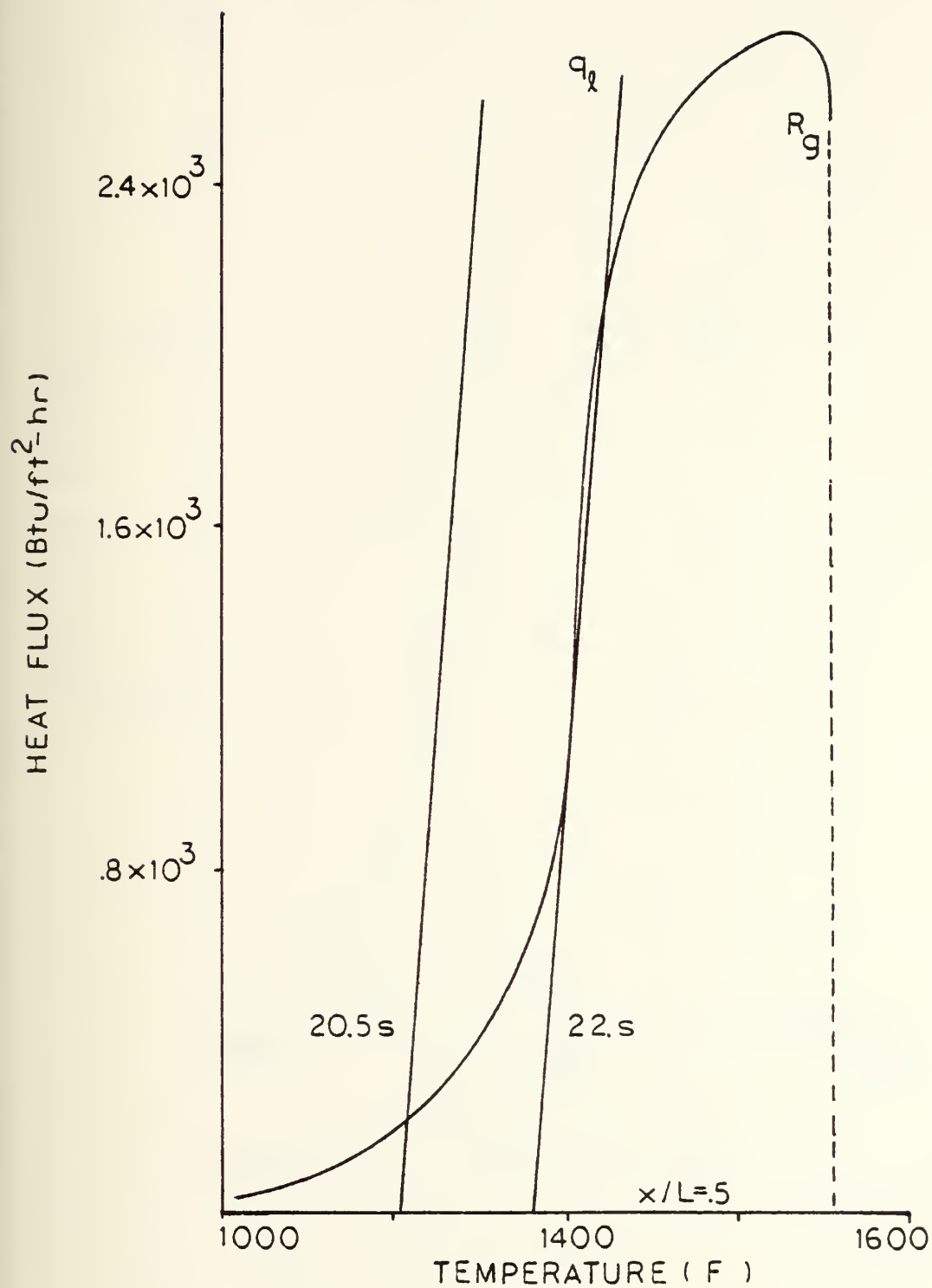105

FIGURE V.20 --- S-curve at x/L = .5
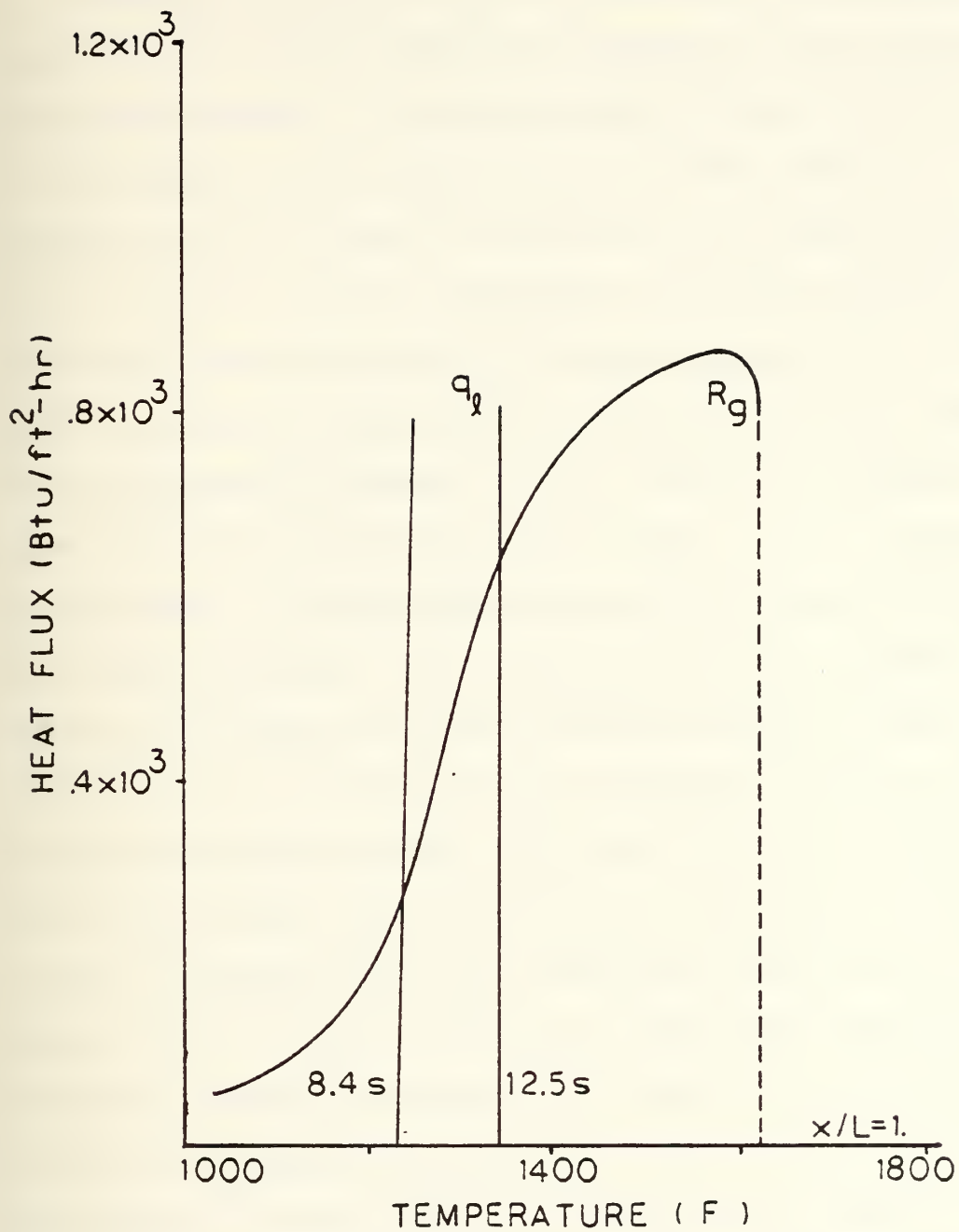
FIGURE V.21 --- S-curve at x/L = 1.

therefore, conduction and radiation will not be considered in order to simplify the graphical analysis.

Comparing Figures V.19-V.21 shows that the maximum heat generation rates are different depending on the location in the porous medium. It was mentioned in the general discussion of the Semenov model (Section III.C) that implicit in the shapes of the S-curves are the effects of oxygen concentration. In other words, decreasing the oxygen supply will cause the S-curves to peak at lower temperatures. Since it is more difficult for the oxygen to penetrate as the depth of the porous medium increase (i.e., oxygen is consumed as the flow passes through the porous medium), it is a reasonable outcome that the maximum heat generation rates decrease as the depth increases. The difficulty for the oxygen to penetrate as the depth increases produces another effect as seen in Figure V.21. Unlike those in Figures V.19 and V.20, the S-curve and heat transfer curve does not have a tangent point which defines the "critical ignition condition". This behavior is called noncritical combustion, and as discussed by Vulis [13], is characteristic of oxygen poor combustion. Moreover, these observations are supported by the experimental results of Thomas, Stevenson, and Evans [15]. In their experiments, it was shown by decreasing the ambient partial pressure of oxygen, that a critical combustion process (i.e., one in which a "temperature jump" occurs) transforms to a noncritical combustion process.

As seen in Figure V.7, the temperature first rises in a local region of the porous medium (in this case near x/L = 1) before moving as a wave toward the air inlet surface. The direction of movement was a characteristic of all the problems in which sustained combustion was observed. This behavior is explained as follows. Temperature rises in a region where the heat generation is greater than the heat transfer between the particles and the air. The region of higher temperature widens as heat is transferred by conduction and radiation. In addition, the increasing temperature simultaneously increases the reaction rate. At some moment, the oxygen entering through the upstream side of the high temperature region is totally consumed within that region. When this occurs, the simultaneous increase in temperature and reaction rate will occur only on the upstream side of the region of high temperature. As the increasing temperature moves towards the air inlet surface, the front of the region of depleted oxygen also moves nearer the air inlet surface. This results in the temperature response appearing to move in the form of a wave toward the air inlet surface. It is interesting to note, that the magnitude of heat transfer by conduction and radiation in the increasing temperature region was approximately twice that of the convection heat transfer at the outset of the example (Figures V.7 and V.8). It seems reasonable that by increasing the pore velocity to a sufficient magnitude, the region of increasing temperature would not propagate but blow

out (i.e., toward the x/L = 1 surface). In fact, this is observed for the problems in which the porous medium cools to ambient temperature.

Up to this point, the thermal response of the porous medium has been discussed in terms of "sustained combustion" or "cooling to ambient temperature". The Semenov curves generated from the results of the combustion model can be used to determine transition from kinetic to diffusion combustion. The kinetic and diffusion regimes of combustion are discussed in Section III.C. In a practical sense, the exothermic process occurring in the kinetic regime is synonymous with the term "oxidation". The process occurring in the diffusion regime is simply called "combustion". From everyday experience, one knows that oxidation can be a slow process, occurring at low reaction rates. Conversely, combustion can produce considerable heat, reflected by high temperatures and reaction rates. As will be shown, transition from oxidation to combustion occurs rapidly. In addition, the porous medium may be undergoing oxidation in one part, and combustion in the other. It is important to understand the behavior of the thermal process at this level. Especially, if there is a need to closely control the process.

Each point within the porous medium will transition from oxidation to combustion at different times. This can be seen in Figures V.19-V.21 which were obtained from the results of example C. The locations x/L = 1, x/L = .5, and x/L = 0

transitioned at 12.5 seconds, 22 seconds, and 41 seconds, respectively. Therefore at the start of the problem, the porous medium as a whole, was undergoing oxidation. Moreover, transition from oxidation to combustion started at x/L = 1 and moved to x/L = 0 with time. This is consistent with the behavior observed for the temperature response. As discussed by Vulis [13], the theoretical value for "critical ignition" temperature of the carbon can be calculated using the "N. N. Semenov equation" given by,

$$\hat{T}_I \;=\; \frac{E}{2R_u}[1 - (1 - 4R_u\hat{T}_a/E)^{1/2}] \qquad\qquad (V.2)$$

where E is the activation energy of the Arrhenius expression, R_u is the universal gas constant, and $\hat{T}_a$ is the absolute air temperature. This equation is derived by equating the Arrhenius expression III.16 to the convection heat transfer expression III.14, and requiring the slopes be equal. Note that the theoretical "critical ignition" temperature is a function of air temperature and activation energy only. Since the transition from oxidation to combustion at x/L = 1 shows a noncritical behavior, equation V.1 does not apply. The theoretical "critical ignition" temperatures for locations x/L = 0 and x/L = .5 are 1831 degrees Fahrenheit and 1492 degrees Fahrenheit, respectively. The values obtained by the combustion model (Figures V.19 and V.20) are approximately 1825 degrees Fahrenheit for x/L = 0, and 1440 degrees Fahrenheit for x/L = .5. Once the "critical ignition" temperature

111

was reached, the increase to the "combustion" temperature
occurred in less than 1 second for both cases. Examples A
and B in Section V.C (Figures V.2-V.6) were the same problem as
example C, discussed here, except combustion was initiated
differently. Example C was initiated with the porous medium
at a constant temperature known to sustain combustion. In
examples A and B, the porous medium was subjected to a heat
flux at the air inlet surface (x/L = 0) with the porous medium
at ambient temperature. The amount of time for which the heat
flux was applied determined if sustained combustion occurred.
Sustained combustion was observed for example A in Section
V.C. The amount of time the heat flux was applied in example
B was not sufficient for sustaining combustion and the porous
medium cooled to ambient temperature. It is interesting to
note that the temperature at x/L = 0 in example A reached the
"critical ignition" temperature of 1825 degrees Fahrenheit.
The maximum temperature obtained at x/L = 0 in example B was
approximately 1650 degrees Fahrenheit. There is good agreement
between the theoretical values of "critical ignition" tempera-
ture and those obtained by the combustion model.

The pore velocity significantly affects the combustion
process. This was discussed in Section V.F. Increasing pore
velocity has two effects. First, the internal heat transfer
coefficient, h, is increased, thereby, increasing the amount
of film cooling. Secondly, the supply of oxygen is made greater
(i.e., convection mass transfer of oxygen molecules increases).
The combined effect is that by increasing pore velocity, higher

local temperatures are needed for transition of the porous solid from oxidation to combustion. In other words, assume that transition occurs at a particular air temperature for a given pore velocity. Increasing the pore velocity without an increase in air temperature may not be sufficient for transition to occur. This is illustrated by Figure V.22. Increasing the pore velocity will increase the slope of the heat transfer line, and also change the shape of the heat generation curve as shown. It is apparent that an increase in air temperature is needed to make the steeper-sloped heat transfer line tangent to the heat generation curve. In addition, higher pore velocities produce higher combustion temperatures once transition occurs. In the general discussion of the Semenov model, it was pointed out that the temperature dominates the combustion process in the kinetic regime. Increasing the oxygen supply will have the greatest effect in the diffusion regime (i.e., increasing the combustion temperature). This behavior described by the Semenov model, combined with the effects produced by convection heat transfer (energy transport by internal flow) and to a lesser extent, heat transfer by conduction and radiation, will determine if the porous medium will undergo sustained combustion for an increase in pore velocity.

Figure V.23 shows the effects of decreasing the pore velocity. The slope of the heat transfer line becomes smaller, and the heat generation curve changes shape as shown. In
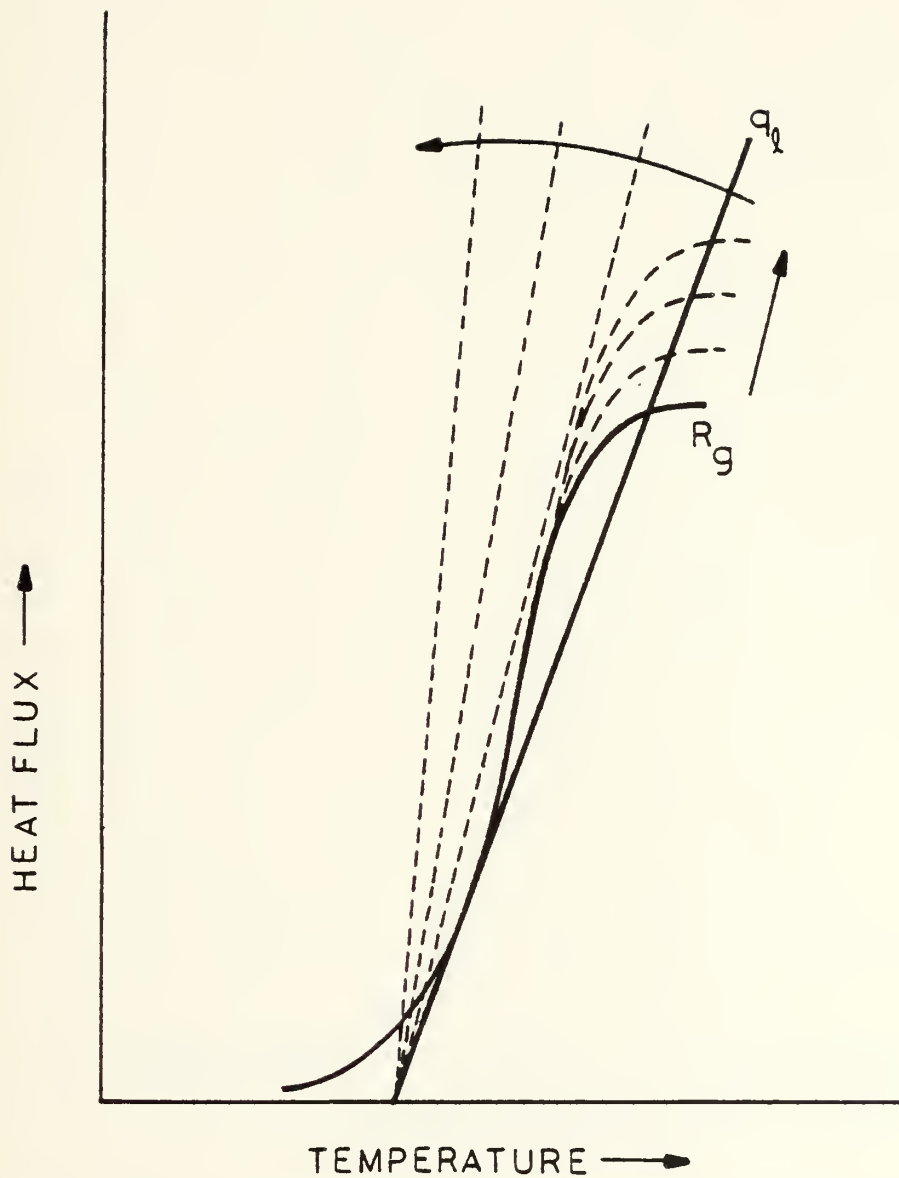
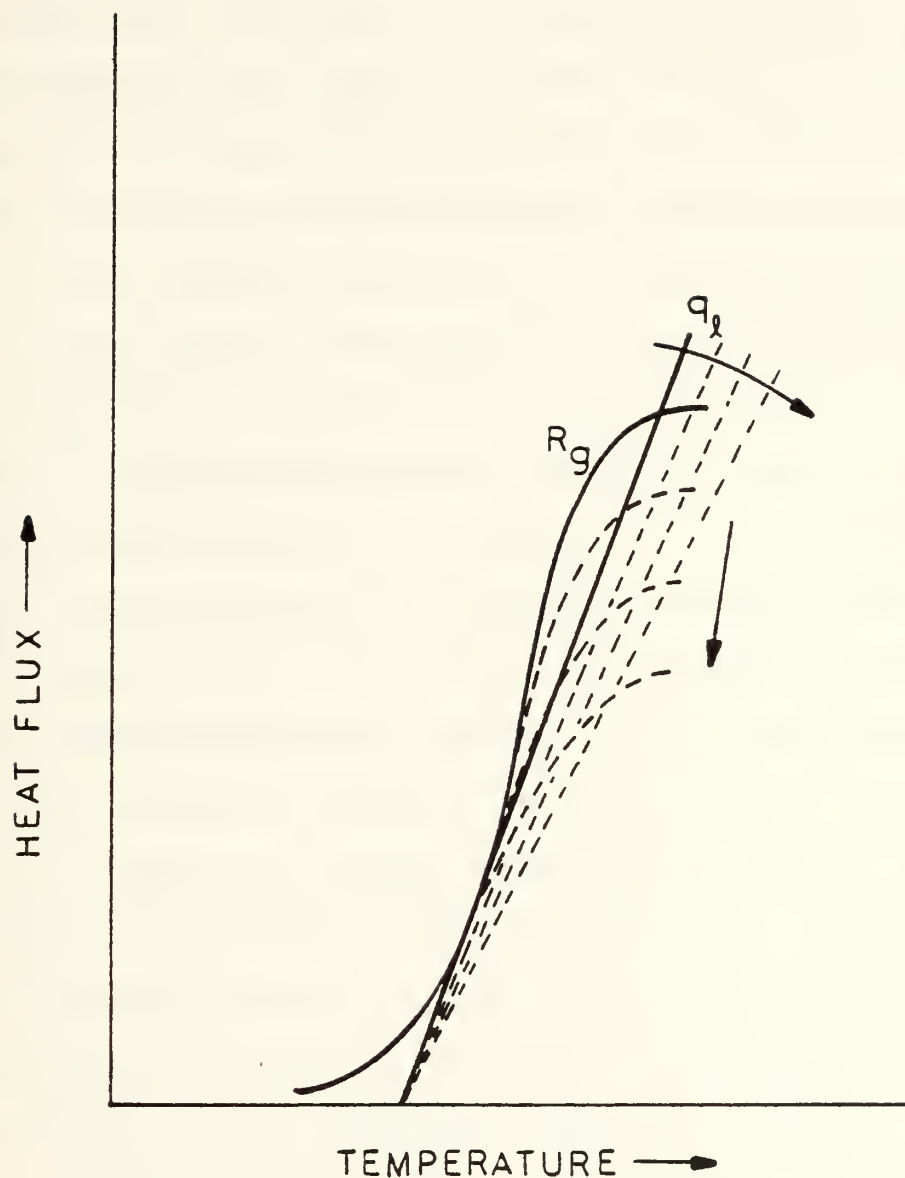FIGURE V.22 --- Effects of increasing pore velocity.

114

FIGURE V.23 --- Effects of decreasing pore velocity.

particular, lower combustion temperatures will occur in the diffusion regime. Unlike the increasing pore velocity case above, there is less certainty in predicting the behavior of combustion when pore velocity is decreased. It appears that conduction and radiation heat transfer become more of a factor at the lower pore velocities. This seems reasonable since the ratio of conduction and radiation heat transfer to convection heat transfer increases with decreasing pore velocity. In addition, the effects of heat transfer from the boundaries at the lower pore velocities must also be considered (shown in Figure V.13 and V.14). The combined effects of all the heat transfer mechanisms, including the boundary conditions, will determine if the porous medium will undergo sustained combustion as the pore velocity is decreased.

Lastly, the effects of the boundary conditions must be considered separately. The results of changing the boundary conditions were presented in Section V.E. It was observed that for heat transfer occurring at the surfaces of the porous solid (e.g., radiation boundary conditions), higher initial temperatures were needed to sustain combustion. Allowing heat transfer from the surfaces of the porous solid (either by convection or by radiation or by both), affects the combustion process in the boundary condition regions as follows. Returning to the Semenov model, there is nothing explicitly associated with the boundary conditions that would change the shape of the heat generation curve. In addition, since pore velocity

determines the magnitude of the internal heat transfer coeffi-
cient, it appears that the slope of the heat transfer line
will also be unaffected. However up to this point, only film
cooling was considered in the heat transfer line of the Semenov
model. Noting that heat transfer from the porous solid boun-
daries results in steeper temperature gradients in regions
near the boundaries, heat transfer by conduction and radiation
must also be considered. With the additional components of
heat transfer, the heat transfer line will curve upward. This
means that the heat transfer changes from a linear function
to a nonlinear function of temperature. The change of the
shape is illustrated in Figure V.24. As can be seen, the
increased heat transfer by conduction and radiation may pre-
vent transition from oxidation to combustion. This, in turn,
will restrict the heat generation to the kinetic regime. It
is reasonable to expect that as the reaction moves towards the
air inlet boundary, the combined effects of greater heat trans-
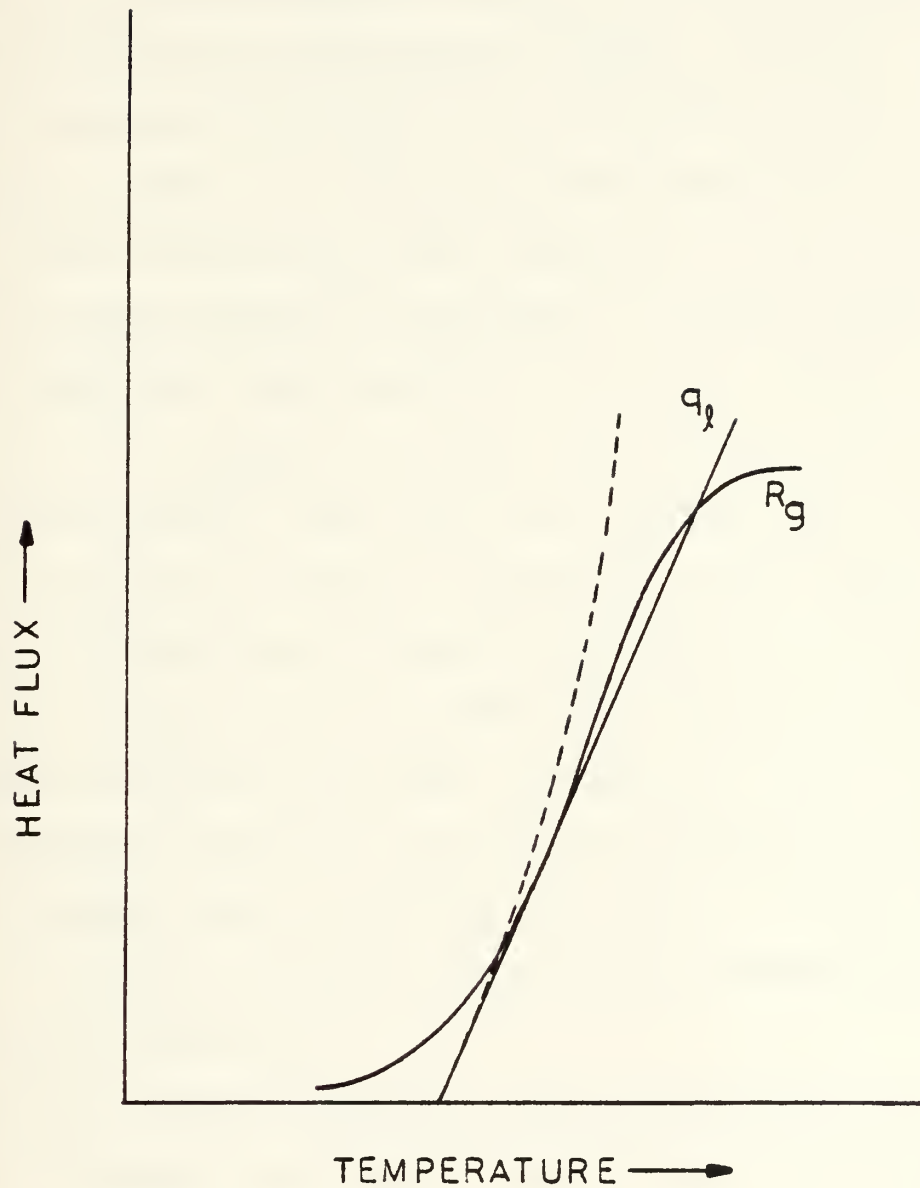fer and lower heat generation will oppose sustained combustion.

FIGURE V.24 --- Effects of boundary conditions on
heat transfer.

VI. CONCLUSIONS

The main objective of developing a model which predicts
the combustion behavior of a porous medium has been achieved.
The results of the mathematical model are in good agreement
with those obtained by experimental methods. Moreover, the
analyses presented have shown that combustion and heat trans-
fer in porous media is a complex process involving the inter-
action of heat transfer and heat generation. This interaction
depends upon the geometric parameters of a porous medium,
boundary conditions, environmental and initial conditions.
The behavior of a system can change radically by altering any
number of parameters. This point was demonstrated by examples
A and B in Section V.C where a difference of one second in
applying a surface heat flux meant combustion or extinguish-
ment. The results have also shown that conduction and radia-
tion between particles may play a significant role in deter-
mining combustion behavior and should be accounted for. The
computer program makes it possible to look at a large number
of cases. Similar analyses by experimental methods would be
economically impractical.

Based on literature surveys performed during this inves-
tigation, it appears that much of the engineering develop-
ment associated with porous media involves a trial and error

process. It seems reasonable that an analytical model would be an essential tool for the engineer to employ in the design process. In this investigation, the model has been assessed for its applicability, and to some extent, its accuracy. It is hoped that in the future the model will be used to determine the effects of the design variables (i.e., the geometric parameters, pressure differential, etc.) on performance. Specifically, the model shows promise for evaluating the combustion efficiency and stability of a system. It is in this capacity that the combustion and heat transfer model will be of greatest value.

APPENDIX A

FORMULATION OF FIELD EQUATIONS

1. PRESSURE DISTRIBUTION EQUATION

   Darcy's law for one dimensional flow, neglecting body forces, is,

$$Q = -\frac{m}{\mu}\left(\frac{dP}{dx}\right) \tag{A.1}$$

Substituting in the Dupuit-Forcheimer relation, and solving for u, equation A.1 becomes,

$$u = -\frac{m}{p\mu}\left(\frac{dP}{dx}\right) \tag{A.2}$$

The continuity equation (derived in Appendix B) is,

$$\frac{\partial(p\rho_a)}{\partial t} + \frac{\partial}{\partial x}(p\,\rho_a\,u) = 0 \tag{A.3}$$

Substituting equation A.2 into equation A.3 yields,

$$\frac{\partial(p\rho_a)}{\partial t} - \frac{\partial}{\partial x}\left(\frac{m\rho_a}{\mu}\frac{dP}{dx}\right) = 0 \tag{A.4}$$

Expanding terms, equation A.4 becomes,

$$\frac{d^2P}{dx^2} + \left(\frac{1}{\rho_a}\frac{\partial\rho_a}{\partial x} + \frac{1}{m}\frac{\partial m}{\partial x} - \frac{1}{\mu}\frac{\partial\mu}{\partial x}\right)\frac{dP}{dx} - \frac{\mu}{m\rho_a}\frac{\partial(p\rho_a)}{\partial t} = 0 \tag{A.5}$$

121

Equation A.5 with associated boundary conditions (presented in Section II.B) is solved for the pressure and pressure gradient distribution. The pressure gradient is then substituted into equation A.2 to obtain the pore velocity.

2. POROUS SOLID HEAT TRANSFER EQUATION

To perform energy balances on both the porous solid and on the air, a differential volume of porous medium was segregated into respective volumes of constituents, that is, $dV_s = (1-p)dV$ for the solid, and $dV_a = pdV$ for the air (shown in Figure A.1). The convention used for the energy balance of an arbitrary differential volume, dV, is,

$$\begin{array}{ccc} \text{Heat into} \\ \text{dV} \end{array} + \begin{array}{c} \text{Heat} \\ \text{Generation} \end{array} = \begin{array}{c} \text{Heat out} \\ \text{of dV} \end{array} + \begin{array}{c} \text{Increase in} \\ \text{Internal Energy} \end{array}$$

The heat transfer mechanisms considered for the carbon particles are conduction, radiation heat transfer between particles, convection heat transfer from the particles to the air, and heat generation. Applying the above convention, the energy balance on a differential volume of porous solid is,

$$(1-p)q_{cond}dA\Big|_x + (1-p)q_{rad}dA\Big|_x + q_{gen}dA' \qquad (A.6)$$

$$= (1-p)q_{cond}dA\Big|_{x+dx} + (1-p)q_{rad}dA\Big|_{x+dx} + q_{conv}dA'$$

$$+ (1-p)\dot{q}_{int}dV$$

POROUS MEDIUM   AIR   SOLID

dV   p·dV   (1-p)·dV

FIGURE A.1 --- Separating a differential volume of
                porous medium into respective volumes
                of solid and air.

Representing terms on the right side of expression A.6 by Taylor series expansions (neglecting higher order terms), the energy balance becomes,

$$(1-p)q_{cond}dA\Big|_x + (1-p)q_{rad}dA\Big|_x + q_{gen}dA' \qquad (A.7)$$

$$= (1-p)q_{cond}dA\Big|_x + \frac{\partial}{\partial x}[(1-p)q_{cond}]dxdA + (1-p)q_{rad}dA\Big|_x$$

$$+ \frac{\partial}{\partial x}[(1-p)q_{rad}]dxdA + q_{conv}dA' + (1-p)\dot{q}_{int}dV$$

Subtracting terms, and rearranging, expression A.7 becomes,

$$- \frac{\partial}{\partial x}[(1-p)q_{cond}]dV - \frac{\partial}{\partial x}[(1-p)q_{rad}]dV - q_{conv}dA'$$

$$+ q_{gen}dA' = (1-p)\dot{q}_{int}dV \qquad (A.8)$$

Substituting the following expressions into equation A.8,

$$q_{cond} = -k_e \frac{\partial T_c}{\partial x} \qquad \text{Fourier's law} \qquad (A.9)$$

$$q_{rad} = -k_r \frac{\partial T_c}{\partial x} \qquad \text{Radiation analogy to} \qquad (A.10)$$
$$\text{Fourier's law}$$

$$q_{conv} = h(T_c - T_a) \qquad \text{Newton's law} \qquad (A.11)$$

$$q_{gen} = R_g \qquad \text{Heat generation} \qquad (A.12)$$

124

$$\dot{q}_{int} = \rho_c \, c_c \, \frac{\partial T_c}{\partial t} \qquad \text{Internal energy} \qquad (A.13)$$

yields,

$$\frac{\partial}{\partial x}[(1-p)(k_e+k_r) \, \frac{\partial T_c}{\partial x}]dV - h(T_c-T_a)dA' + R_g dA' \qquad (A.14)$$

$$= (1-p)\rho_c \, c_c \, \frac{\partial T_c}{\partial t} \, dV$$

Dividing through by dV, and defining dA'/dV as z, the specific internal area (i.e., surface area per unit volume), equation A.14 becomes,

$$\frac{\partial}{\partial x}[(1-p)(k_e+k_r) \, \frac{\partial T_c}{\partial x}] - hz(T_c-T_a) + R_g z \qquad (A.15)$$

$$= (1-p) \, \dot{\rho}_c \, c_c \, \frac{\partial T_c}{\partial t}$$

The expressions used to obtain the values of the properties and parameters in equation A.15 are presented in Section III.E.

3. AIR HEAT TRANSFER EQUATION

The formulation of the air heat transfer equation will begin with the general one dimensional energy equation,

$$p\rho_a \, \frac{D}{Dt}(e + \frac{1}{2}u^2) = \frac{\partial}{\partial x}(p \, k_a \, \frac{\partial T_a}{\partial x}) + hz(T_c-T_a) + uF_x \qquad (A.16)$$

$$- \frac{\partial}{\partial x}(p \, u \, P) - \frac{\partial}{\partial x}(p \, u \, \tau_{xx})$$

125

As in the porous solid heat transfer equation, the time and position dependent porosity appears inside the differential. Expanding terms and neglecting body forces, the air energy equation becomes,

$$p \, \rho_a \frac{De}{Dt} + p \, \rho_a \frac{D(\frac{1}{2}u^2)}{Dt} = \frac{\partial}{\partial x}(p \, k_a \frac{\partial T_a}{\partial x}) + hz(T_c - T_a) \qquad (A.17)$$

$$- \frac{\partial}{\partial x}(p \, u \, P) - \frac{\partial}{\partial x}(p \, u \, \tau_{xx})$$

Consider the momentum equation for the x-direction (neglecting body forces),

$$\frac{\partial}{\partial t}(p \, \rho_a \, u) = - \frac{\partial}{\partial x}(p \, \rho_a \, u^2) - \frac{\partial}{\partial x}(p\tau_{xx}) - \frac{\partial}{\partial x}(pP) \qquad (A.18)$$

and the continuity equation,

$$\frac{\partial}{\partial t}(p\rho_a) = - u \frac{\partial}{\partial x}(p\rho_a) - p \, \rho_a \frac{\partial u}{\partial x} \qquad (A.19)$$

Multiplying the continuity equation through by u, and substituting this into equation A.18, the momentum equation becomes,

$$p \, \rho_a \frac{\partial u}{\partial t} = - p \, \rho_a \, u \frac{\partial u}{\partial x} - \frac{\partial}{\partial x}(pP) - \frac{\partial}{\partial x}(p\tau_{xx}) \qquad (A.20)$$

Multiplying equation A.20 by u and noting that,

$$u \, p \, \rho_a \frac{Du}{Dt} = u \, p \, \rho_a \frac{\partial u}{\partial t} + p \, \rho_a \, u^2 \frac{\partial u}{\partial x} \qquad (A.21)$$

equation A.20 becomes,

$$u \, p \, \rho_a \, \frac{Du}{Dt} = -u \, \frac{\partial}{\partial x}(pP) - u \, \frac{\partial}{\partial x}(p\tau_{xx}) \qquad (A.22)$$

The energy equation A.17, after substituting
$D(\frac{1}{2}u^2)/Dt = uDu/Dt$ and expanding terms, is,

$$p \, \rho_a \, \frac{De}{Dt} + p \, \rho_a \, u \, \frac{Du}{Dt} = \frac{\partial}{\partial x}(p \, k_a \, \frac{\partial T_a}{\partial x}) + hz(T_c - T_a) \qquad (A.23)$$

$$- p \, P \, \frac{\partial u}{\partial x} - u \, \frac{\partial(pP)}{\partial x}$$

$$- u \, \frac{\partial}{\partial x}(p\tau_{xx}) - p \, \tau_{xx} \, \frac{\partial u}{\partial x}$$

Substituting equation A.22 into the above energy equation and
cancelling terms, equation A.23 becomes,

$$p \, \rho_a \, \frac{De}{Dt} = \frac{\partial}{\partial x}(p \, k_a \, \frac{\partial T_a}{\partial x}) + hz(T_c - T_a) - p \, P \, \frac{\partial u}{\partial x} - p \, \tau_{xx} \, \frac{\partial u}{\partial x} \qquad (A.24)$$

The viscous dissipation term, $p\tau_{xx}\partial u/\partial x$, is neglected because
the fluid is a gas flowing at a low velocity. Therefore, the
energy equation for the air in the porous medium is,

$$p \, \rho_a \, \frac{De}{Dt} = \frac{\partial}{\partial x}(p \, k_a \, \frac{\partial T_a}{\partial x}) + hz(T_c - T_a) - p \, P \, \frac{\partial u}{\partial x} \qquad (A.25)$$

With specific enthalpy for a gas defined by,

$$h = e + P/\rho \qquad (A.26)$$

De/Dt can be expressed as,

$$\frac{De}{Dt} = \frac{Dh}{Dt} - \frac{1}{\rho_a} \frac{DP}{Dt} + \frac{P}{\rho_a^2} \frac{D\rho_a}{Dt}$$ (A.27)

Multiplying the continuity equation through by $P/(\rho \rho_a^2)$ gives,

$$\frac{P}{\rho_a^2} \frac{D\rho_a}{Dt} = - \frac{P}{\rho\rho_a} \frac{DP}{Dt} - \frac{P}{\rho_a} \frac{\partial u}{\partial x}$$ (A.28)

Substitution of the above expression into expression A.27,
the substantial derivative of internal energy can be expressed
as,

$$\frac{De}{Dt} = \frac{Dh}{Dt} - \frac{1}{\rho_a} \frac{DP}{Dt} - \frac{P}{\rho_a} \frac{\partial u}{\partial x} - \frac{P}{\rho\rho_a} \frac{DP}{Dt}$$ (A.29)

Substituting expression A.29 into equation A.25, the energy
equation reduces to,

$$\rho \rho_a \frac{Dh}{Dt} - \rho \frac{DP}{Dt} - P \frac{D\rho}{Dt} = \frac{\partial}{\partial x}(\rho k_a \frac{\partial T_a}{\partial x}) + hz(T_c - T_a)$$ (A.30)

The specific enthalpy can be represented in terms of tempera-
ture, as,

$$dh = T \, ds + \frac{1}{\rho} \, dP$$ (A.31)

where s is specific entropy. For a perfect gas, ds may be
expressed by,

128

$$ds = c_p \frac{dT}{T} - \frac{1}{\rho T} dP \tag{A.32}$$

Substituting expression A.32 into expression A.31, and cancelling terms, enthalpy can now be written as,

$$dh = c_p \, dT \tag{A.33}$$

or,

$$\frac{Dh}{Dt} = c_a \frac{DT_a}{Dt} \tag{A.34}$$

Substituting expression A.34 into equation A.30, the air energy equation or heat transfer equation becomes,

$$\frac{\partial}{\partial x}(p \, k_a \frac{\partial T_a}{\partial x}) - p \rho_a u c_a \frac{\partial T_a}{\partial x} + hz(T_c - T_a) \tag{A.35}$$

$$+ \frac{D}{Dt}(pP) = p \rho_a c_a \frac{\partial T_a}{\partial t}$$

Initial results showed that pP changed slowly with time. Therefore, the substantial derivative of pP, as shown here,

$$\frac{D}{Dt}(pP) = \frac{\partial}{\partial t}(pP) + u \frac{\partial}{\partial x}(pP) \tag{A.36}$$

is reduced to $u\partial(pP)/\partial x$. The expressions used to obtain the properties and parameters in the coefficients of equation A.35 are presented in Section III.E.

129

4. OXYGEN MOLECULE DIFFUSION EQUATION

The final consideration in formulating the field equations for the model is the transport of oxygen molecules. The oxygen molecule transport equation is obtained by a conservation of species belance on the differential volume of air, $dV_a = pdV$. The convention used for the species balance is given by,

$$
\begin{array}{c}
O_2 \text{ into} \\ dV
\end{array}
=
\begin{array}{c}
O_2 \text{ out} \\ \text{of } dV
\end{array}
+
\begin{array}{c}
O_2 \\ \text{Consumption}
\end{array}
+
\begin{array}{c}
O_2 \\ \text{Accumulation}
\end{array}
$$

The transport mechanisms considered were diffusion resulting from concentration gradients, convection, and consumption of oxygen by combustion. Applying the above convention, the species balance on the oxygen becomes,

$$
p\,\dot{m}_{diff}\,dA\Big|_{x} + p\,\dot{m}_{conv}\,dA\Big|_{x} = p\,\dot{m}_{diff}\,dA\Big|_{x+dx} \qquad (A.37)
$$

$$
+ p\,\dot{m}_{conv}\,dA\Big|_{x+dx} + \dot{m}_{cons}\,dA' + p\,\dot{m}_{acc}\,dV
$$

Representing the terms on the right side by Taylor series expansions (neglecting higher order terms), the species balance becomes,

$$
p\,\dot{m}_{diff}\,dA\Big|_{x} + p\,\dot{m}_{conv}\,dA\Big|_{x} = p\,\dot{m}_{diff}\,dA\Big|_{x} \qquad (A.38)
$$

$$
+ \frac{\partial}{\partial x}(p\dot{m}_{diff})\,dxdA + p\dot{m}_{conv}dA\Big|_{x} + \frac{\partial}{\partial x}(p\dot{m}_{conv})\,dxdA + \dot{m}_{cons}dA' + p\dot{m}_{acc}dV
$$

130

Cancelling terms and rearranging, equation A.38 becomes,

$$-\frac{\partial}{\partial x}(p\dot{m}_{diff})dV - \frac{\partial}{\partial x}(p\dot{m}_{conv})dV - \dot{m}_{cons}dA' = p\dot{m}_{acc}dV \quad \text{(A.39)}$$

Substituting the following expressions into equation A.39,

$$\dot{m}_{diff} = -\mathcal{D}_e \frac{\partial \phi}{\partial x} \qquad \text{Fick's law} \qquad \text{(A.40)}$$

$$\dot{m}_{conv} = u \phi \qquad \text{Convection transport} \qquad \text{(A.41)}$$

$$\dot{m}_{cons} = R_{O_2} \qquad \begin{array}{l}\text{Consumption by}\\\text{combustion}\end{array} \qquad \text{(A.42)}$$

$$\dot{m}_{acc} = \frac{\partial \phi}{\partial t} \qquad \text{Accumulation} \qquad \text{(A.43)}$$

yields,

$$\frac{\partial}{\partial x}(p\,\mathcal{D}_e \frac{\partial \phi}{\partial x})dV - \frac{\partial}{\partial x}(u\,p\,\phi)dV - R_{O_2}dA' = p\frac{\partial \phi}{\partial t}dV \quad \text{(A.44)}$$

Dividing both sides by dV, and letting dA'/dV equal the specific internal area, z, the oxygen molecule diffusion equation becomes,

$$\frac{\partial}{\partial x}(p\,\mathcal{D}_e \frac{\partial \phi}{\partial x}) - \frac{\partial}{\partial x}(u\,p\,\phi) - R_{O_2}z = p\frac{\partial \phi}{\partial t} \quad \text{(A.45)}$$

The methods and expressions for obtaining the properties and parameters in the coefficients of equation A.45 are presented in Section II.F.

5. TRANSFORMATION OF FIELD EQUATIONS FROM A FIXED COORDINATE TO A MOVING COORDINATE SYSTEM

As discussed previously, the reaction rate at the air inlet surface of the porous medium results in surface recession. To account for this surface recession, the field equations must be transformed from a fixed coordinate to a moving coordinate system. The method of transforming the field equations will be shown for only the porous solid heat transfer equation since the approach for the other field equations (i.e., air heat transfer, and combined Darcy's law and continuity equation) is identical.

The porous solid heat transfer equation with the modified heat generation term is,

$$\frac{\partial}{\partial x}[(1-p)(k_e+k_r)\frac{\partial T_c}{\partial x}] - hz(T_c-T_a) + R_g'\delta^\Delta (x=0) \qquad (A.46)$$

$$= (1-p)\rho_c c_c \frac{\partial T_c}{\partial t}$$

Since the x coordinate is a function of time during surface recession (e.g., $T_c(x(t),t)$), the time derivative term in equation A.46 must be expanded using the chain rule,

$$\frac{\partial}{\partial t}[T_c(x(t),t)]\Big|_i = (\frac{\partial T_c}{\partial x})_t (\frac{dx}{dt})_i + (\frac{\partial T_c}{\partial t})_x$$

$$(A.47)$$

The x coordinate in the field equations is nondimensionalized by $\eta = x/L$. Substituting η for x, expression A.47 becomes,

$$\left(\frac{\partial T_c}{\partial x}\right)_t \left(\frac{dx}{dt}\right)_i + \left(\frac{\partial T_c}{\partial t}\right)_x = \left(\frac{\partial T_c}{\partial \eta}\right)\left(\frac{\partial \eta}{\partial x}\right)_t \left(\frac{dx}{dt}\right)_i + \left(\frac{\partial T_c}{\partial t}\right)_x \qquad (A.48)$$

Noting that,

$$\frac{\partial \eta}{\partial x} = \frac{1}{L} \qquad (A.49)$$

and,

$$\frac{dx}{dt} = L\frac{d\eta}{dt} + \eta\frac{dL}{dt} = \eta\frac{dL}{dt} \qquad (A.50)$$

expression A.48 becomes,

$$\left(\frac{\partial T_c}{\partial x}\right)_t \left(\frac{dx}{dt}\right)_i + \left(\frac{\partial T_c}{\partial t}\right)_x = \frac{\eta}{L}\left(\frac{dL}{dt}\right)\frac{\partial T_c}{\partial \eta} + \frac{\partial T_c}{\partial t} \qquad (A.51)$$

Upon substituting $\eta = x/L$ into the remainder of equation A.46, and substituting expression A.51 for the time derivative term, the porous solid heat transfer equation for the surface recession problem is,

$$L^{-2}\frac{\partial}{\partial \eta}\left[(1-p)(k_e+k_r)\frac{\partial T_c}{\partial \eta}\right] - hz(T_c-T_a) + R_g'\delta^{\Delta}(\eta=0) \qquad (A.52)$$

$$= (1-p)\rho_c c_c\left[\frac{\eta}{L}\dot{L}\frac{\partial T_c}{\partial \eta} + \frac{\partial T_c}{\partial t}\right]$$

As stated in Section III.G, the thickness, L, as a function of time, and $\dot{L}$ can be obtained from expression III.44. The air temperature and combined Darcy's law and continuity

133

equation appear similar to equation A.52 for the surface

recession problem.

APPENDIX B

FORMULATION OF AUXILLIARY EQUATIONS

1. CONTINUITY EQUATION

The law of conservation of mass requires that the substantial derivative of the fluid mass in a differential volume be zero. Therefore, the continuity equation for a fluid in a porous medium is expressed by,

$$\frac{D}{Dt}(p \, \rho_a \, dV) \;=\; 0 \qquad\qquad (B.1)$$

or in an equivalent form,

$$\frac{\partial}{\partial t}(p\rho_a) \;+\; u \, \frac{\partial}{\partial x}(p\rho_a) \;+\; p \, \rho_a \frac{\partial u}{\partial x} \;=\; 0 \qquad (B.2)$$

2. RADIATION HEAT TRANSFER ANALOGY TO FOURIER'S LAW

Radiation heat transfer in the model was represented by an analog to Fourier's law of conduction heat transfer shown by,

$$q_{rad} \;=\; -k_r \, \frac{\partial T_c}{\partial x} \qquad\qquad (B.3)$$

where k_r is an equivalent conductivity of the particles due to radiation. The development is as follows. Assuming air to be transparent to radiation, and treating the idealized geometry of the porous medium (Figure III.1) as a series of

135

closely spaced walls, the net radiation heat flux between adjacent walls is,

$$q_{rad} = \frac{\sigma \, \epsilon}{2-\epsilon} (\hat{T}_x^4 - \hat{T}_{x+dx}^4) \tag{B.4}$$

where $\hat{T}_x$ and $\hat{T}_{x+dx}$ are the respective absolute wall temperatures, ϵ is the emissivity of the carbon, and σ is the Stefan-Boltzman constant. Expanding q_{rad} in a Taylor series about $\hat{T}_{x+dx}$, and neglecting higher order terms, the series expansion may be written as,

$$q_{rad} = \frac{\sigma \, \epsilon}{2-\epsilon}(\hat{T}_x^4 - \hat{T}_x^4) - \frac{4\sigma\epsilon}{2-\epsilon} \hat{T}_{x+dx}^3 \frac{\partial \hat{T}}{\partial x} dx \tag{B.5}$$

Simplifying, the above expression becomes,

$$q_{rad} = - \frac{4\sigma\epsilon}{2-\epsilon} \hat{T}_{x+dx}^3 \frac{\partial T}{\partial x} dx \tag{B.6}$$

Equating expressions B.3 and B.6, and noting that $\partial\hat{T}/\partial x = \partial T/\partial x$, k_r becomes,

$$k_r = \frac{4\sigma\epsilon}{2-\epsilon} dx \, \hat{T}_{x+dx} \tag{B.7}$$

where dx is now equal to δ, the pore diameter. From the close spacing of the particles, the temperature difference will be small as compared to the magnitude of the temperature. Noting this, the average absolute temperature of the carbon particle

may be substituted for T_{x+dx}. The equivalent radiation con-
ductivity expression becomes,

$$k_r = \frac{4\sigma\varepsilon\delta}{2-\varepsilon} \hat{T}_c^3 \qquad (B.8)$$

and the radiation heat transfer from particle to particle
may be represented by,

$$q_{rad} = -\frac{4\sigma\varepsilon\delta}{2-\varepsilon} \hat{T}_c^3 \frac{\partial T_c}{\partial x} \qquad (B.9)$$

For small pore diameters equation B.9 will be a good approxi-
mation of the radiation heat transfer between particles.

3. POLYNOMIAL APPROXIMATIONS OF THERMAL PROPERTIES

Relations giving the dynamic viscosity, thermal conduc-
tivity, and specific heat at constant pressure of air at
different temperatures were required. A simple method to
obtain values for these properties is to fit empirical data
with 2nd order Lagrange polynomials.

The general form of the 2nd order Lagrange plynomial is,

$$k_i = \frac{(T_i-T_2)(T_i-T_3)}{(T_1-T_2)(T_1-T_3)} k_1 + \frac{(T_i-T_3)(T_i-T_1)}{(T_2-T_3)(T_2-T_1)} k_2 \qquad (B.10)$$

$$+ \frac{(T_i-T_1)(T_i-T_2)}{(T_3-T_1)(T_3-T_2)} k_3$$

where k_i is the property value at the ith temperature, T_i.

Choosing three temperatures that are representative of those observed during the analysis, the corresponding values of the properties are,

(subscript)	Temp. deg-F	μ lbm/ft-hr	k_a Btu/ft-hr-F	c_a Btu/lbm-F
1	80	4.7973×10^{-2}	1.5161×10^{-2}	.24020
2	1340	1.0045×10^{-1}	3.9013×10^{-2}	.27268
3	3140	1.5725×10^{-1}	7.1647×10^{-2}	.31196

Applying expression B.10 to each set of properties results in the following set of polynomials,

$$\mu = -3.308 \times 10^{-9} \; T_a^2 + 4.633 \times 10^{-5} T_a + 4.427 \times 10^{-2} \qquad (B.11)$$

$$k_a = -2.608 \times 10^{-10} \; T_a^2 + 1.930 \times 10^{-5} T_a + 1.361 \times 10^{-2} \qquad (B.12)$$

$$c_a = -1.293 \times 10^{-9} \; T_a^2 + 2.758 \times 10^{-5} T_a + .238 \qquad (B.13)$$

Each expression gives property values within two percent of the data for temperatures to 3000 degrees Fahrenheit.

4. JUSTIFICATION OF THE DANCKWERT'S BOUNDARY CONDITIONS

    The Danckwerts' boundary conditions for the air heat transfer are,

$$k_a \frac{\partial T_a}{\partial x} = \rho_a \, u \, c_a (T_a - T_\infty) \qquad (B.14)$$

$$\frac{\partial T_a}{\partial x} = 0 \qquad\qquad (B.15)$$

Bischoff [41] presents a discussion of these boundary conditions applied to mass diffusion equations in porous media. An analogous discussion is made here for the Danckwerts' boundary conditions applied to the air heat transfer equation.

The porous medium with entrance and exit regions is shown in Figure B.1. The air temperature, T_a, for each section of the region is distinguished by subscripts, as are the properties. The air heat transfer equations for each of the regions are as follows,

$$k_a \frac{d^2 T_{a_1}}{dx^2} - \rho_a u_1 c_a \frac{dT_{a_1}}{dx} = 0 \qquad x \le 0 \qquad (B.16)$$

$$\frac{d}{dx}(p\, k_a \frac{dT_a}{dx}) - \rho_a u c_a \frac{dT_a}{dx} + hz(T_c - T_a) = 0 \quad 0 \le x \le L \qquad (B.17)$$

$$k_a \frac{d^2 T_{a_2}}{dx^2} - \rho_a u_2 c_a \frac{dT_{a_2}}{dx} = 0 \qquad x \ge L \qquad (B.18)$$

with the boundary conditions,

$$T_{a_1}(-\infty) = T_\infty \qquad\qquad (B.19)$$
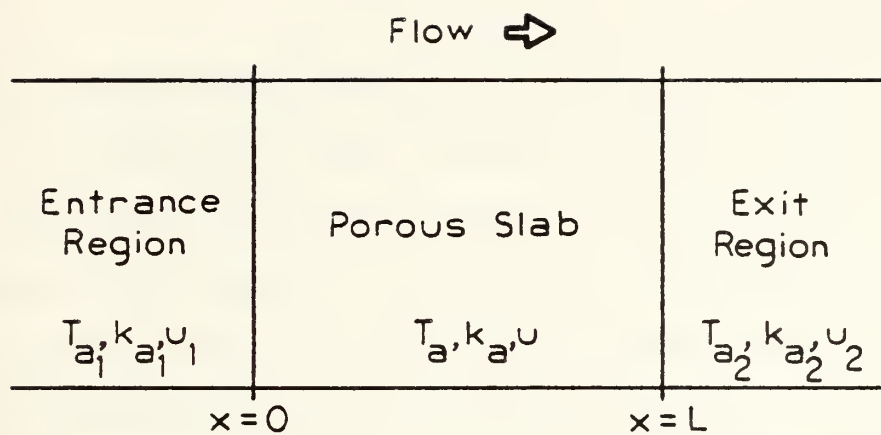
$$T_{a_1}(0) = T_a(0) \qquad\qquad (B.20)$$

FIGURE B.1 --- Justification of the Dankwerts boundary conditions.

$$\rho_a u_1 c_a T_{a_1}(0) - k_a \frac{d}{dx}[T_{a_1}(0)] = p\rho_a u c_a T_a(0) - pk_a \frac{d}{dx}[T_a(0)]$$

(B.21)

$$T_{a_2}(L) = T_a(L)$$

(B.22)

$$\rho_a u_2 c_a T_{a_2}(1) - k_a \frac{d}{dx}[T_{a_2}(L)] = p\rho_a u c_a T_a(0) - pk_a \frac{d}{dx}[T_a(L)]$$

(B.23)

$$T_{a_2}(\infty) = \text{finite}$$

(B.24)

The above boundary conditions impose the restriction that there is no convection heat transfer from the porous solid to the air at the boundary surfaces. The difficulty of mixing Danckwerts' and convection heat transfer boundary conditions is discussed in Section III.H. For convenience, the thermo-physical properties will be treated as constant in the entrance and exit regions.

An analytical closed-form solution of this set of equations is unknown because of the nonlinearity of the temperature dependent properties in equation B.17. However, the solutions of equations B.16 and B.18 are,

$$T_{a_1} = K_1 + K_2 \exp\left(\frac{\rho_a u_1 c_a}{k_a} x\right) \qquad x \leq 0 \qquad \text{(B.25)}$$

$$T_{a_2} = K_3 + K_4 \exp\left(\frac{\rho_a u_2 c_a}{k_a} x\right) \qquad x \geq L \qquad \text{(B.26)}$$

Applying boundary conditions B.19 and B.24, the following
results are obtained,

$$K_1 = T_\infty \qquad (B.27)$$

$$K_4 = 0 \qquad (B.28)$$

The solutions, B.25 and B.26, become,

$$T_{a_1} = T_\infty + K_2 \exp\left(\frac{\rho_a u_1 c_a}{k_a} x\right) \qquad x \leq 0 \qquad (B.29)$$

$$T_{a_2} = K_3 \qquad x \geq L \qquad (B.30)$$

It would be necessary to have the solution for the nonlinear
equation B.17 to solve for K_2 and K_3. However, the constants
need not be known to continue with the analysis.

From equation B.29,

$$T_{a_1}(0) = T_\infty + K_2 \qquad (B.31)$$

and,

$$\frac{d}{dx}[T_{a_1}(0)] = \frac{\rho_a u_1 c_a}{k_a} K_2 \qquad (B.32)$$

Substituting these into equation B.21 gives,

142

$$\rho_a u_1 c_a T_\infty + \rho_a u_1 c_a K_2 - \rho_a u_1 c_a K_2 = p\rho_a uc_a T_a(0) - pk_a\frac{d}{dx}[T_a(0)]$$

(B.33)

Cancelling terms and noting $u_1 = up$ (i.e., $u_1 p_1 = u_2 p_2$)
yields,

$$p\,\rho_a\,u\,c_a\,T_\infty = p\,\rho_a\,u\,c_a\,T_a(0) - p\,k_a\frac{d}{dx}[T_a(0)]$$

(B.34)

Rearranging, the Danckwerts' boundary condition at $x = 0$ is,

$$k_a\frac{d}{dx}[T_a(0)] = \rho_a\,u\,c_a(T_a - T_\infty)$$

(B.35)

Noting that K_3 is a constant, the derivative of equation B.30
is,

$$\frac{d}{dx}\,T_{a_2} = 0$$

(B.36)

and,

$$\frac{d}{dx}[T_{a_2}(L)] = 0$$

(B.37)

Sbustituting these expressions and equation B.22 into equa-
tion B.23, and noting $u_2 = up$ (i.e., $u_1 p_1 = u_2 p_2$) gives,

$$p\,\rho_a\,u\,c_a\,T_a(L) - k_a\frac{d}{dx}[T_a(L)] = p\,\rho_a\,u\,c_a\,T_a(L)$$

(B.38)

Upon cancelling terms, the second Danckwerts' boundary
condition becomes,

143

$$\frac{d}{dx}[T_a(L)] = 0 \qquad (B.39)$$

An important consideration for using the Danckwerts' boundary conditions is that it simplifies the analysis since equations similar to B.17 may be solved independently without having to consider entrance and exit regions.

5. PRESSURE DIFFERENTIAL CALCULATION RESULTING FROM EXTERNAL FLOW AT SURFACE X = L

To obtain the pressure differential, ΔP, for simulating the conditions of Fontenot's experiments [1] (discussed in Section III.H), Bernoulli's equation was used. The following observations showed this to be a valid assumption. Schlichting [54] points out that for the ratio of u/U_∞ in the range of .0001 to .01, the effects of "blowing" or "suction" on the potential flow over the external surface of the porous medium may be neglected. A typical value of u/U_∞ for the model at which U_∞ = 25 knots was .0028. For steady flow over a flat plate, the flow field outside the boundary layer may be described by Bernoulli's equation. This is a direct result of the Navier-Stokes equation. In addition, the pressure gradient across the boundary layer may be taken as zero. Therefore, Bernoulli's equation,

$$\int \frac{dP}{\rho_a} + \frac{U^2}{2} = \text{constant} \qquad (B.40)$$

may be used to obtain the pressure differential across the plate. The parameters in equation B.40 are defined as follows:

144

P, pressure; ρ_a, density of air; U, free stream velocity of the air over an external surface of the porous medium. For the model, the density of the air was approximated by the ideal gas law as,

$$\rho_a = P/R_a \hat{T}_a \qquad (B.41)$$

where R_a is the gas constant of air, $\hat{T}_a$ is the absolute temperature of the air, and P is the pressure. Substituting equation B.41 into equation B.40 gives,

$$\int \frac{R_a \hat{T}_a}{P} \, dP + \frac{U^2}{2} = \text{constant} \qquad (B.42)$$

Upon integrating, equation B.42 becomes,

$$R_a \hat{T}_a \ln(P) + \frac{U^2}{2} = \text{constant} \qquad (B.43)$$

or,

$$R_a \hat{T}_{a_1} \ln(P_1) + \frac{U_1^2}{2} = R_a \hat{T}_{a_2} \ln(P_2) + \frac{U_2^2}{2} \qquad (B.44)$$

Letting,

$$P_1 = P_\infty, \quad U_1 = 0, \quad T_{a_1} = T_{a_2} = T_\infty, \quad P_2 = P_L, \quad U_2 = U_\infty$$

and substituting these into equation B.44, yields,

145

$$R_a \; \hat{T}_\infty \; \ln(P_\infty) \;\; = \;\; R_a \; \hat{T}_\infty \; \ln(P_L) + \frac{U_\infty^2}{2} \tag{B.45}$$

Rearranging, equation B.45 becomes,

$$R_a \; \hat{T}_\infty \; \ln(P_\infty/P_L) \;\; = \;\; \frac{U_\infty^2}{2} \tag{B.46}$$

Taking the exponential of both sides, and solving for P_L, results in,

$$P_L \;\; = \;\; P_\infty \; \exp(-U_\infty^2/2R_a \; \hat{T}_\infty) \tag{B.47}$$

From the above expression, and noting that $\Delta P = P_L - P_\infty$, ΔP may be expressed as,

$$\Delta P \;\; = \;\; P_\infty [\exp(-U_\infty^2/2 \; R_a \; \hat{T}_\infty) - 1] \tag{B.48}$$

Expression B.48 was used to approximate the pressure differential across the porous medium when simulating the conditions of Fontenot's experiments [1].

APPENDIX C

NUMERICAL FORMULATION

1. FINITE ELEMENT METHOD

The solution of the system of nonlinear, coupled, partial differential equations given by equations III.32, III.38, and III.39, subject to boundary and initial conditions, was obtained by a Galerkin formulation of the finite element method. The solution of equation III.12 was obtained using a shooting method.

a. Galerkin Formulation

A Galerkin formulation of the Finite Element Method was used to obtain solutions of the porous solid and air energy equations, and the oxygen diffusion equation. A convenient form of equations III.32, III.38, and III.39 was used in the formulation as shown by,

$$L^{-2} \frac{\partial}{\partial \eta}[(1-p)(k_e+k_r)\frac{\partial T_c}{\partial \eta}] - hz(T_c-T_a) + R_g z = (1-p)\rho_c c_c \frac{\partial T_c}{\partial t}$$

(C.1)

$$L^{-2} \frac{\partial}{\partial \eta}(p\, k_a \frac{\partial T_a}{\partial \eta}) - p\, \rho_a\, c_a\, u\, L^{-1} \frac{\partial T_a}{\partial \eta} + hz(T_c-T_a)$$

(C.2)

$$+ u\, L^{-1} \frac{\partial}{\partial \eta}(pP) = p\, \rho_a\, c_a\, \frac{\partial T_a}{\partial t}$$

$$L^{-2} \frac{\partial}{\partial \eta}(p\, \mathcal{D}_e \frac{\partial \phi}{\partial \eta}) - L^{-1} \frac{\partial}{\partial \eta}(p\, u\, \phi) - R_{O_2} z = p\, \frac{\partial \phi}{\partial t}$$

(C.3)

where the spatial coordinate, x, was nondimensionalized by $\eta = x/L$.

The closed domain $(0,1)$ was partitioned into $(n-1)$ contiguous elements of variable length ℓ_i, $i = 1,\ldots,n-1$. This defines an n nodal point model. The three field variables, T_c, T_a, ϕ were approximated by,

$$T_c(\eta,t) \cong \psi_1(\eta,t) = \sum G(\eta)\theta_1(t) \tag{C.4}$$

$$T_a(\eta,t) = \psi_2(\eta,t) = \sum G(\eta)\theta_2(t) \tag{C.5}$$

$$\phi(\eta,t) = \psi_3(\eta,t) = \sum G(\eta)\theta_3(t) \tag{C.6}$$

where G_i, for $i = 1,\ldots,n$ is a set of specified basis functions with local support, and the sets $\{\theta_1, \theta_2, \theta_3; i = 1,\ldots,n\}$ are the solution coefficients to be determined. The G_i were selected to satisfy the condition $G_i(\eta_j) = \delta_{ij}^k$, where the Kronecker delta, δ_{ij}^k, is defined by $\delta_{ij}^k = 1$ for $i = j$, and $\delta_{ij}^k = 0$ for $i \neq j$. As a result, θ_1, θ_2, and θ_3 are the values ψ_1, ψ_2, ψ_3 at the nodal points (i.e., $\theta_{1_i}(t) = \psi_1(\eta_i,t)$).

Linear interpolation functions (shown in Figure C.1) were used as the basis functions. These are the lowest polynomial functions which provide the necessary function continuity.

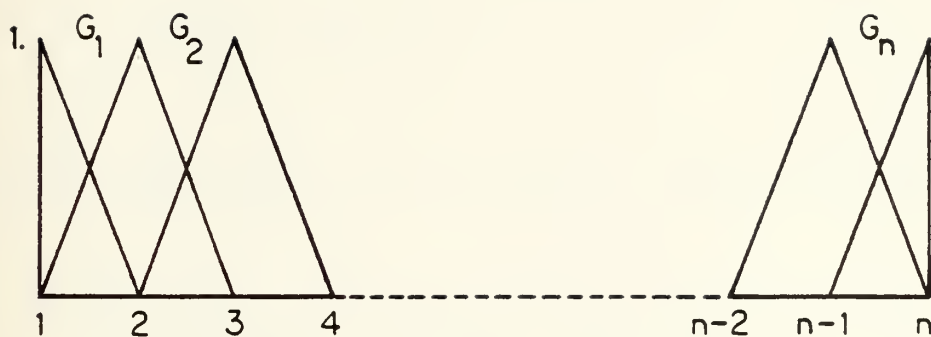As a measure of error, a residual function, r_i, is defined for each field equation by,

FIGURE C.1 --- Linear shape functions used in the
Galerkin formulation of the FEM.

$$r_i(\eta, t) = \Lambda_i(\psi) - \dot{\psi}_i \qquad i = 1, 2, 3 \qquad (C.7)$$

where Λ_i denotes the spatial operator of the ith equation. For convenience, the following convention for differentiation is adopted,

$$\frac{\partial}{\partial \eta}(\ ) = (\ )' \qquad (C.8)$$

$$\frac{\partial^2}{\partial \eta^2}(\ ) = (\ )'' \qquad (C.9)$$

$$\frac{\partial}{\partial t}(\ ) = (\dot{\ }) \qquad (C.10)$$

For field equations C.1, C.2, and C.3, the residuals are,

$$r_1 = L^{-2}[(1-p)(k_e+k_r) \sum_{i=1}^{n} G_i' \theta_{1_i}]' - hz \sum_{i=1}^{n} G_i(\theta_{1_i} - \theta_{2_i}) \qquad (C.11)$$

$$+ R_g \theta_{3_i}^{-1} z \sum_{i=1}^{n} G_i \theta_{3_i} - (1-p)\rho_c c_c \sum_{i=1}^{n} G_i \dot{\theta}_{1_i}$$

$$r_2 = L^{-2}(p k_a \sum_{i=1}^{n} G_i' \theta_{2_i})' - p \rho_a c_a u L^{-1} \sum_{i=1}^{n} G_i' \theta_{2_i} \qquad (C.12)$$

$$+ hz \sum_{i=1}^{n} G_i(\theta_{1_i} - \theta_{2_i}) + uL^{-1}(pP)' - p \rho_a c_a \sum_{i=1}^{n} G_i \dot{\theta}_{2_i}$$

$$r_3 - L^{-2}\left(p\,\mathcal{D}_e \sum_{i=1}^{n} G_i'\theta_{3_i}\right)' - L^{-1}\left(p\,u \sum_{i=1}^{n} G_i\theta_{3_i}\right)' \qquad (C.13)$$

$$- R_{O_2}\,\theta_{3_i}^{-1}\, z \sum_{i=1}^{n} G_i\theta_{3_i} - p \sum_{i=1}^{n} G_i\dot{\theta}_{3_i}$$

where the coefficients multiplying the response variables are themselves functions of the response variables, and thus, the equations are nonlinear. In accordance with the Galerkin method, the final system of ordinary differential equations was obtained by setting each residual, r_j, orthogonal to each basis function, G_i, that is,

$$\int_0^1 G_i\, r_j\, d\eta = 0 \qquad \begin{array}{l} i = 1,2,\ldots,n \\[4pt] j = 1,2,3 \end{array} \qquad (C.14)$$

The 3n ordinary differential equations given by equations C.14 retain the character of the original set of partial differential equations. Thus, linear field operators transform to matrix operators and nonlinear, coupled field operators become nonlinear, coupled algebraic operators. Incorporation of the boundary conditions resulted in 3n nonlinear coupled ordinary differential equations,

$$\underset{\approx}{A}(t)\,\underset{\sim}{\psi}(\theta_1,\theta_2,\theta_3) + \underset{\sim}{F}(t) = \underset{\approx}{B}(t)\,\underset{\sim}{\dot{\psi}} \qquad (C.15)$$

subject to initial conditions, where $\underset{\approx}{B}$ is a 3n × 3n matrix,

151

$\underset{\sim}{A}$ is the operator associated with the field operator Λ_i in expression C.7, and $\underset{\sim}{F}$ is an excitation vector.

Adopting the convention,

$$<G_i> \{\theta_i\} = \sum_{i=1}^{n} G_i \theta_i \qquad (C.16)$$

and applying the operation of expression C.14 with an integration by parts on the second order derivatives gives,

$$\{G_i\} L^{-2} (1-p)(k_e+k_r)<G_i>'\{\theta_1\}\Big|_0^1 - L^{-2}(1-p)(k_e+k_r) \int_0^1 \{G_i\}'<G_j>' d\eta$$

$$-hz \int_0^1 \{G_i\}<G_j> d\eta \{\theta_1\} + hz \int_0^1 \{G_i\}<G_j> d\eta \{\theta_2\} \qquad (C.17)$$

$$+ R_g z \theta_3^{-1} \int_0^1 \{G_i\}<G_j> d\eta \{\theta_3\} = (1-p)\rho_c c_c \int_0^1 \{G_i\}<G_j> d\eta \{\dot{\theta}_1\}$$

$$\{G_i\} L^{-2} p k_a <G_i>'\{\theta_2\}\Big|_0^1 - L^{-2} p k_a \int_0^1 \{G_i\}'<G_j>' d\eta \{\theta_2\} \qquad (C.18)$$

$$- p\rho_a c_a u L^{-1} \int_0^1 \{G_i\}<G_j>' d\eta \{\theta_2\} + hz \int \{G_i\}<G_j> d\eta \{\theta_1\}$$

$$-hz \int_0^1 \{G_i\}<G_j> d\eta \{\theta_2\} + u L^{-1}(pP)' \int_0^1 \{G_i\} d\eta$$

$$= p \rho_a c_a \int_0^1 \{G_i\}<G_j> d\eta \{\dot{\theta}_2\}$$

152

$$\{G_i\}L^{-2}p\nu_e<G_i>'\{\theta_3\}\big|_0^1 - L^{-2}p\nu_e \int_0^1 \{G_i\}'<G_j>'d\eta\{\theta_3\} \qquad (C.19)$$

$$- puL^{-1}\int_0^1 \{G_i\}<G_j>'d\eta\{\theta_3\} - L^{-1}(pu)'\int_0^1 \{G_i\}<G_j>d\eta\{\theta_3\}$$

$$- R_{O_2}z\theta_3^{-1}\int_0^1\{G_i\}<G_j>d\eta\{\theta_3\} \;=\; p\int_0^1\{G_i\}<G_j>d\eta\{\dot{\theta}_3\}$$

The first term in each of the above expressions is a boundary term which permits incorporation of natural boundary conditions. Implementation of the boundary conditions is presented in Section C.1.b. The coefficients in equations C.17, C.18, and C.19 are comprised of variable dependent properties, and were taken as the average value of the properties over an element. In the limit, as the elements get smaller (i.e., $n \to \infty$), the average values of the coefficients converge to the exact values.

Inspection of expressions C.17, C.18 and C.19 shows the four operators,

$$\int \{G_i\}'<G_j>'d\eta \qquad (C.20)$$

$$\int \{G_i\}<G_j>'d\eta \qquad (C.21)$$

$$\int \{G_i\}<G_j>d\eta \qquad (C.22)$$

$$\int \{G_i\}d\eta \qquad (C.23)$$

To formulate these operators, the global shape function, G_i, was defined on the local level by,

$$G_i = g_1^{(i-1)} \oplus g_2^{(i)} \tag{C.24}$$

where g_1 and g_2 were defined by,

$$g_1^{(e)} = \begin{cases} (1 - \dfrac{\xi}{\ell_e}) & \text{for } \xi \text{ in element (e)} \\ \\ 0 & \text{for } \xi \text{ not in element (e)} \end{cases} \tag{C.25}$$

$$g_2^{(e)} = \begin{cases} \dfrac{\xi}{\ell_e} & \text{for } \xi \text{ in element (e)} \\ \\ 0 & \text{for } \xi \text{ not in element (e)} \end{cases} \tag{C.26}$$

and ℓ_e is the length of the eth element. The $\oplus$ notation in expression C.24 means that G_i is the union of $g_1^{(i-1)}$ and $g_2^{(i)}$. The local shape functions (i.e., the elements) have the following properties,

(i) $$\int_0^{\ell_e} g_i^{(j)} g_k^{(m)} = 0 \quad \text{if } j \neq m \tag{C.27}$$

(ii) $$g_i^{(e)}(\eta_j) = \delta_{ij}^k = \begin{cases} 1 & \text{if } i = j \\ \\ 0 & \text{if } i \neq j \end{cases} \tag{C.28}$$

Having defined the local shape functions, the elemental matrix operators contributing to the global matrix operators C.20 through C.23 are,

$$\int_0^1 \{G_i\}'<G_j>'d\eta \;\rightarrow\; \frac{1}{\ell_e} \begin{bmatrix} 1 & -1 \\ -1 & 1 \end{bmatrix} \tag{C.29}$$

$$\int_0^1 \{G_i\}<G_j>' \;\rightarrow\; \frac{1}{2} \begin{bmatrix} -1 & 1 \\ -1 & 1 \end{bmatrix} \tag{C.30}$$

$$\int_0^1 \{G_i\}<G_j> \;\rightarrow\; \frac{\ell_e}{6} \begin{bmatrix} 2 & 1 \\ 1 & 2 \end{bmatrix} \tag{C.31}$$

$$\int_0^1 \{G_i\} \;\rightarrow\; \frac{\ell_e}{2} \begin{Bmatrix} 1 \\ 1 \end{Bmatrix} \tag{C.32}$$

The derivations of these operators are presented in Section C.1.d of this appendix.

b.   Implementation of Boundary Conditions

Having formulated the system matrices for the field equations, treatment of the boundary conditions will now be discussed. Each field equation is considered individually.

1.   Porous Solid Transfer Equation

The third set of porous solid heat transfer boundary conditions (i.e., expressions III.57 and III.58) will only be considered since the first and second sets are subsets of the third. The third set of boundary conditions for

the porous solid are,

$$L^{-1}(k_e+k_r)\frac{\partial\theta_1}{\partial\eta} = h_1(T_c-T_\infty) + \sigma\varepsilon(\hat{T}_c^4-\hat{T}_\infty^4) \qquad \eta = 0 \qquad (C.33)$$

$$L^{-1}(k_e+k_r)\frac{\partial\theta_1}{\partial\eta} = -h_2(T_c-T_\infty) - \sigma\varepsilon(\hat{T}_c^4-\hat{T}_\infty^4) \qquad \eta = 1 \qquad (C.34)$$

Since the first term in expression C.17 is,

$$\{G_i\}L^{-2}(1-p)(k_e+k_r)<G_i>'\{\theta_1\}\Big|_0^1 \qquad (C.35)$$

or in analogous form,

$$L^{-2}(1-p)(k_e+k_r)\frac{\partial\theta_1}{\partial\eta} \qquad (C.36)$$

Natural boundary conditions, C.33 and C.34, may be directly
substituted into equation C.36. The response dependent
parameters, h_1, h_2, and T_c, changing with time, are evaluated
continuously within the integration routine. Thus, the boun-
dary conditions are incorporated in the system matrices as
follows.

(1) $-L^{-1}(1-p)h_1$: added to the stiffness matrix $\underset{\sim}{A}(t)$ at location $A_{1,1}$

(2) $L^{-1}(1-p)[h_1T_\infty-\sigma\varepsilon(\hat{T}_c^4-\hat{T}_\infty^4)]$: added to the excitation vector $\underset{\sim}{F}(t)$ at location F_1

(3) $-L^{-1}(1-p)h_2$: added to the stiffness matrix $\underset{\sim}{A}(t)$
at location $A_{3n-2,3n-2}$

(4) $L^{-1}(1-p)[h_2 T_\infty - \sigma \varepsilon (\hat{T}_c^4 - \hat{T}_\infty^4)]$: added to the excitation
vector $\underset{\sim}{F}(t)$ at location
F_{3n-2}

2. Air Heat Transfer Equation

The first and second set of boundary conditions

for the air heat transfer equation are,

$$L^{-1} k_a \frac{\partial T_a}{\partial \eta} = \rho_a c_a u(T_a - T_\infty) \qquad \eta = 0 \qquad (C.37)$$

$$\frac{\partial T_a}{\partial \eta} = 0 \qquad \eta = 1 \qquad (C.38)$$

Since these are both natural boundary conditions, they are

substututed for the first term of expression C.18 at $\eta = 0$

and $\eta = 1$, respectively. The time dependent properties and

parameters in the coefficient are evaluated continuously

within the integration routine. The boundary conditions are

implemented by adding,

(1) $-p \rho_a c_a u L^{-1}$: to the stiffness matrix $\underset{\sim}{A}(t)$ at location
$A_{2,2}$

(2) $p \rho_a c_a u L^{-1} T_\infty$: to the excitation vector $\underset{\sim}{F}(t)$ at
location F_2

The third set of air heat transfer boundary conditions are,

$$T_a = T_\infty \qquad \eta = 0 \qquad (C.39)$$

157

$$\frac{\partial T_a}{\partial \eta} = 0 \qquad\qquad \eta = 1 \qquad (C.40)$$

The essential boundary condition at $\eta = 0$ is imposed in the Galerkin equation as follows. The $A_{2,i}$ row of the $\underset{\sim}{A}(t)$ matrix, the $B_{2,i}$ row and the $B_{i,2}$ column of the $\underset{\sim}{B}(t)$ matrix, and the F_2 location of the excitation vector, $\underset{\sim}{F}(t)$, are all set equal to zero. The $B_{2,2}$ location of the $\underset{\sim}{B}(t)$ matrix is then set equal to one.

3. Oxygen Transport Equation

For the oxygen diffusion equation, the first and second set of boundary conditions are,

$$L^{-1} \mathcal{D}_e \frac{\partial \phi}{\partial \eta} = u(\phi - \phi_\infty) \qquad\qquad \eta = 0 \qquad (C.41)$$

$$\frac{\partial \phi}{\partial \eta} = 0 \qquad\qquad \eta = 1 \qquad (C.42)$$

Since these are natural boundary conditions, they were sub-stituted for the first term in expression C.19. The proper-ties are evaluated continuously within the integration routine. The boundary conditions are implemented by adding,

(1) $-p\,u\,L^{-1}$: to the stiffness matrix $\underset{\sim}{A}(t)$ at location $A_{3,3}$

(2) $p\,u\,L^{-1}\,\phi_\infty$: to the excitation vector $\underset{\sim}{F}(t)$ at location F_3

The third set of boundary conditions for the oxygen diffusion equation are,

$$\phi = \phi_\infty \qquad\qquad \eta = 0 \qquad (C.43)$$

$$\frac{\partial \phi}{\partial \eta} = 0 \qquad\qquad \eta = 1 \qquad (C.44)$$

The essential boundary condition at $\eta = 0$ is imposed in the Galerkin equation as follows. The $A_{3,i}$ row of the $\underset{\approx}{A}(t)$ matrix, the $B_{3,i}$ row and the $B_{i,3}$ column of the $\underset{\sim}{B}(t)$ matrix, and the F_3 location of the excitation vector, $\underset{\sim}{F}(t)$, are all set equal to zero. The $B_{3,3}$ location of the $\underset{\approx}{B}(t)$ matrix is then set equal to one.

4.   Surface Recession Problem

As discussed previously, the oxygen diffusion equation is eliminated during the surface recession phase of a problem. By doing this, a reordering of the system matrices must take place, including the locations for applying the boundary conditions. The boundary conditions of the particle and air temperature equations are implemented the same as above except the indices identifying the matrix locations of the form, $3n-i$, are changed to $2n-(i-1)$.

c.   Treatment of the Reaction Rate Term

An exponential reaction rate term appears in both the porous solid heat transfer and the oxygen diffusion equation. The modified Gear integration routine requires calculating or approximating the Jacobian matrix from the system matrices,

159

$A(t)$ and $B(t)$, In order to include the reaction rate term in the Jacobian matrix, thus improving the efficiency of the integration routine, the exponential terms were treated as follows. The reaction rate terms were multiplied and divided by the oxygen concentration (only the heat generation term is shown, oxygen consumption is treated identically),

$$R_g z \theta_{3_i}^{-1} \sum_{i=1}^{n} G_i \theta_{3_i} \tag{C.45}$$

Applying the operation of expression C.14, and moving the reaction rate term divided by the oxygen concentration outside the integral, the Galerkin operator for the heat generation becomes,

$$R_g z \theta_3^{-1} \int_0^1 \{G_i\} <G_j> d\eta \{\theta_3\} \tag{C.46}$$

The coefficient of expression C.46 is treated as a time dependent parameter. The Galerkin operators are distributed into the stiffness matrix at locations, $3n-2, 3n$ for heat generation, and $3n, 3n$ for oxygen consumption. During the surface recession phase, reaction rate is treated in a different manner as discussed in Section III.G.

d. Derivation of the FEM Operators

In the section on the finite element formulation, the following four differential operators were identified,

$$\int_0^1 \{G_i'\}<G_j'>d\eta \qquad\qquad (C.47)$$

$$\int_0^1 \{G_i\}<G_j'>d\eta \qquad\qquad (C.48)$$

$$\int_0^1 \{G_i\}<G_j>d\eta \qquad\qquad (C.49)$$

$$\int_0^1 \{G_i\}d\eta \qquad\qquad (C.50)$$

where the G_i are the global basis functions. These operators are constructed on the element level by introducing the corresponding element basis functions, g_i. The global and element basis functions are related by,

$$G_i = g_1^{(i-1)} \oplus g_2^{(i)} \qquad\qquad (C.51)$$

where g_1 and g_2 are defined by

$$g_1^{(e)} = \begin{cases} (1 - \dfrac{\xi}{\ell_e}) & \text{for } \xi \text{ in element (e)} \\[2ex] 0 & \text{for } \xi \text{ not in element (e)} \end{cases} \qquad (C.52)$$

161

$$g_2^{(e)} = \begin{cases} \dfrac{\xi}{\ell_e} & \text{for } \xi \text{ in element (e)} \\[2mm] 0 & \text{for } \xi \text{ not in element (e)} \end{cases} \qquad \text{(C.53)}$$

and ℓ_e is the length of the (e)th element.

The derivation of the local elemental matrices according to the Galerkin method for the global operations proceeds as follows:

For operator C.47,

global	local

$$\int_0^1 \{G_i'\}\langle G_j'\rangle d\eta \qquad\qquad U[\int_0^{\ell_e} \begin{Bmatrix} g_1' \\ g_2' \end{Bmatrix} \langle g_1' \ \ g_2' \rangle d\xi] \qquad \text{(C.54)}$$

Noting that,

$$g_1' = -\frac{1}{\ell_e} \qquad\qquad\qquad\qquad \text{(C.55)}$$

$$g_2' = \frac{1}{\ell_e} \qquad\qquad\qquad\qquad \text{(C.56)}$$

the elemental matrix becomes

$$\int_0^{\ell_e} \begin{bmatrix} (\frac{1}{\ell_e})^2 & -(\frac{1}{\ell_e})^2 \\ -(\frac{1}{\ell_e})^2 & (\frac{1}{\ell_e})^2 \end{bmatrix} d\xi \ \to \ \frac{1}{\ell_e} \begin{bmatrix} 1 & -1 \\ -1 & 1 \end{bmatrix} \qquad \text{(C.57)}$$

For operator C.48,

<div align="center">

global   local

</div>

$$\int_0^1 \{G_i\} <G_j'> d\eta \qquad\qquad U[\int_0^{\ell_e} \begin{Bmatrix} g_1 \\ g_2 \end{Bmatrix} <g_1' \ g_2'> d\xi] \quad (C.58)$$

Substituting in the local shape functions gives,

$$\int_0^{\ell_e} \begin{Bmatrix} (1 - \frac{\xi}{\ell_e}) \\[2mm] (\frac{\xi}{\ell_e}) \end{Bmatrix} <(-\frac{1}{\ell_e}) \ (\frac{1}{\ell_e})> d\xi \qquad\qquad (C.59)$$

Carrying out the operations gives

$$\int_0^{\ell_e} \begin{bmatrix} (-\frac{1}{\ell_e} + \frac{\xi}{\ell_e}) & (\frac{1}{\ell_e} - \frac{\xi}{\ell_e^2}) \\[3mm] -(\frac{\xi^2}{2\ell_e^2}) & (\frac{\xi^2}{2\ell_e^2}) \end{bmatrix} d\xi \ \rightarrow \ \frac{1}{2} \begin{bmatrix} -1 & 1 \\ -1 & 1 \end{bmatrix} \quad (C.60)$$

For operator C.49,

<div align="center">

global   local

</div>

$$\int_0^1 \{G_i\} <G_j> d\eta \qquad\qquad U[\int_0^{\ell_e} \begin{Bmatrix} g_1 \\ g_2 \end{Bmatrix} <g_1 \ g_2> d\xi] \quad (C.61)$$

Substituting in for the local shape functions

$$\int_0^{\ell_e} \left\{ \begin{array}{c} (1 - \frac{\xi}{\ell_e}) \\ \\ (\frac{\xi}{\ell_e}\cdot) \end{array} \right\} <(1 - \frac{\xi}{\ell_e})\ (\frac{\xi}{\ell_e})>d\xi \qquad (C.62)$$

the elemental matrix becomes

$$\int_0^{\ell_e} \left[\begin{array}{cc} (1 - 2\frac{\xi}{\ell_e} + \frac{\xi^2}{\ell_e^2}) & (\frac{\xi}{\ell_e} - \frac{\xi^2}{\ell_e^2}) \\ \\ (\frac{\xi}{\ell_e} - \frac{\xi^2}{\ell_e^2}) & (1 - 2\frac{\xi}{\ell_e} + \frac{\xi^2}{\ell_e^2}) \end{array} \right] d\xi \rightarrow \frac{\ell_e}{3} \left[\begin{array}{cc} 1 & \frac{1}{2} \\ \\ \frac{1}{2} & 1 \end{array} \right] \qquad (C.63)$$

For operator C.50,

$$\begin{array}{ccc} \underline{\text{global}} & & \underline{\text{local}} \\ \\ \int_0^1 \{G_i\} d\eta & & U[\int_0^{\ell_e} \left\{ \begin{array}{c} g_1 \\ \\ g_2 \end{array} \right\} d\xi] \qquad (C.64) \end{array}$$

Substituting in the local shape function, and integrating, the expression becomes

$$\int_0^{\ell_e} \left\{ \begin{array}{c} (1 - \frac{\xi}{\ell_e}) \\ \\ \frac{\xi}{\ell_e} \end{array} \right\} d\xi \rightarrow \frac{\ell_e}{2} \left\{ \begin{array}{c} 1 \\ \\ 1 \end{array} \right\} \qquad (C.65)$$

164

This last operator is used for the excitation vector as described in the FEM formulation.

2. SHOOTING METHOD

The solution of equation III.12 is obtained by the shooting method. A general discussion of the shooting method with examples is presented by Gerald [55]. The method is based on iterative solutions of equation III.12 until a solution is reached which also satisfies the boundary conditions, $P(0) = P_\infty$ and $P(1) = P_L$. Along with the boundary condition at $\eta = 0$, an initial estimate to $dP/d\eta$ is specified, and equation III.12 is integrated from $\eta = 0$ to $\eta = 1$ using Euler's method. An approximate Newton's method is then used as follows,

$$\left.\frac{dP}{d\eta}\right|_i = \left.\frac{dP}{d\eta}\right|_{i-1} - P(1)_{i-1} \frac{\left.\frac{dP}{d\eta}\right|_i - \left.\frac{dP}{d\eta}\right|_{i-2}}{P(1)_i - P(1)_{i-2}} \qquad (C.66)$$

to provide a better approximation of $dP/d\eta$. The procedure is repeated until the solution has converged. A solution satisfying equation III.12 and its associated boundary conditions is calculated at each time step. The current values of the properties are used and $\partial\rho_a/\partial t$ is approximated by linear interpolation using the current and past values of ρ_a. The $\partial\rho_a/\partial t$ term was neglected for the first two integrations of a problem. The reason for this is associated with the difficulty of specifying a reasonable set of initial conditions for the

165

temperature and oxygen diffusion equations. When equation III.12 was treated as an initial condition problem, the pressure gradient in a small region of the porous medium would approach zero for some initial conditions of temperature and oxygen concentration (the starting heat generation rate for those initial conditions was large at time, $t = 0$). The pressure gradient approaching zero resulted in numerical instabilities for the temperature and oxygen diffusion equations.

LIST OF REFERENCES

1. Fontenot, J. S., <u>Graphite-Epoxy Composite Material Response to Carrier Deck Fire</u>, Naval Weapons Center, NWC Technical Memorandum 3351, November, 1979.

2. Vatikiotis, C. S., <u>Analysis of Combustion and Heat Transfer in a Porous Graphite Medium</u>, M. E. Thesis, Naval Postgraduate School, Monterey, 1980.

3. Kordylewski, W., "Influence of Aerodynamics on the Critical Parameters of Thermal Ignition," International Journal for Numerical Methods in Engineering, Vol. 17, p. 1081-1091, 1981.

4. Sahota, M. S. and Pagni, P. J., "Heat and Mass Transfer in Porous Media Subject to Fires," International Journal of Heat Transfer, Vol. 22, p. 1069-1081, 1981.

5. Mehta, P. S. and Sams, W. N. and Luss, D., "Wrong Way Behavior of Packed-Bed Reactors," AIChE Journal, Vol. 27, p. 234-246, March, 1981.

6. Slattery, J. C., <u>A Fundamental Approach to Mass Transfer in Porous Media</u>, Workshop on Heat and Mass Transfer in Porous Media, Case Western Reserve University, 1975.

7. Yaron, I., <u>Cell Model Approach to Transport Phenomena in Porous Media</u>, Workshop on Heat and Mass Transfer in Porous Media, Case Western Reserve Univeristy, 1975.

8. Kassoy, D. R., <u>Some Remarks on the Continuum Derivation of the Equations for Flow in Thermally Active Porous Media</u>, Workshop on Heat and Mass Transfer in Porous Media, Case Western Reserve University, 1975.

9. Scheidegger, A. E., <u>The Physics of Flow Through Porous Media</u>, University of Toronto Press, Toronto, 1974.

10. Carman, P. C., <u>Flow of Gases Through Porous Media</u>, Academic Press, London, 1956.

11. Boffa, C. C., <u>Experimental Gas Flow Characteristics in Transpiration Cooled Porous Matrices</u>, 5th Int'l Heat Transfer Conf., Tokyo, Japan. Proceedings, 5, September, 1974.

12. Frank-Kamenetskii, D. A., <u>Diffusion and Heat Transfer in Chemical Kinetics</u>, Plenum Press, New York, 1969.

167

13. Vulis, L. A., *Thermal Regimes of Combustion*, McGraw-Hill Book Co., New York, 1961.

14. Semenov, N. N., *Chemical Kinetics and Chain Reactions*, Clarendon Press, Oxford, 1935.

15. Thomas, G. R., and Stevenson, A. J., and Evans, D. G., "Ignition of Coal Particles without Temperature Jump," Combustion and Flame, 21, 1973, p. 133-136.

16. Parker, A. S., and Hottel, H. C., "Combustion Rate of Carbon," Ind. and Eng. Chem., 28, November, 1936, p. 1334-1341.

17. Arthur, J. A., "Reactions between Carbon and Oxygen," Trans. Faraday Soc., 47, 1951, p. 164-178.

18. JANAF Thermochemical Tables, 2nd Edition, Dow Chemical Company, 1970.

19. Smoot, D. L., and Pratt, D. T., *Pulverized-Coal Combustion and Gasification*, Plenum Press, New York, 1979.

20. Green, D. W., and Perry, R. H., *Heat Transfer with a Flowing Fluid Through Porous Media*, Chem. Eng. Prog. Symp., Series No. 32, 57, 1961, p. 61-68.

21. Sundaresan, S. and Amundson, N. R. and Rutherford, A., "Observations on Fixed-Bed Dispersion Models: The Role of the Interstitial Fluid," AIChE Journal, 26, July, 1980, p. 529-536.

22. Riaz, M., "Analytical Solutions for Single- and Two-Phase Models of Packed-Bed Thermal Storage Systems," J. of Heat Transfer, 99, August, 1977, p. 489-492.

23. Mendelsohn, A. R., "Transient Temperature of a Porous-Cooled Wall," AIAA Journal, 1, June, 1963, p. 1449-1451.

24. Schneider, P. J., and Brogan, J. J., "Temperature Response of a Transpiration-Cooled Plate," ARS Journal, February, 1962, p. 233-236.

25. Russel, H. W., "Principles of Heat Flow in Porous Insulators," Am. Ceramic Soc. J., 18, 1935, p. 1-5.

26. Rohsenow, W. M., and Hartnett, J. P., *Handbook of Heat Transfer*, McGraw-Hill Book Co., New York, 1973.

27. Whitaker, S., "Radiant Energy Transport in Porous Media," Joint ASME/AIChE 18th National Heat Conference, San Diego, August, 1979.

28. Yoshida, F. and Ramaswami, D., and Hougen, D. A., "Temperature and Partial Pressures at the Surfaces of Catalyst Particles," AIChE Journal, 8, 1962.

29. Mason, E. A. and Saxena, S. C., The Physics of Fluids, Vol. 1, p. 360-369, 1958.

30. Reynolds, W. C. and Perkins, H. C., Engineering Thermodynamics, McGraw-Hill Book Company, 1977.

31. Bird, R. B. and Stewart, W. E. and Lightfoot, E. N., Transport Phenomena, John Wiley and Sons Inc., 1960.

32. Bennet, C. O. and Myers, J. E., Momentum, Heat, and Mass Transfer, McGraw-Hill Book Company, 1974.

33. Treybal, R. E., Mass Transfer Operations, McGraw-Hill Book Co., New York, 1968.

34. Gilliland, E. R., "Diffusion Coefficients in Gaseous Systems," Ind. Eng. Chem., 26, 1934, p. 681.

35. Holman, J. P., Heat Transfer, McGraw-Hill Book Co., New York, 1976.

36. Denbigh, K. G., and Turner, J. C. R., Chemical Reactor Theory, Cambridge Press, London, 1971.

37. Koizumi, M., The Combustion of Solid Fuels in Fixed Beds, 6th Int'l Symposium on Combustion, New Haven, Ct., Proceedings, p. 577-583, August, 1956.

38. Crank, J., The Mathematics of Diffusion, Clarendon Press, Oxford, 1975.

39. Murray, W. D. and Landis, F., J. Heat Transfer, Vol. 81, 106, 1959.

40. Ozisik, M. N., Heat Conduction, Wiley and Sons, New York, 1980.

41. Bischoff, K. B., "A Note on Boundary Conditions for Flow Reactors," Chem. Eng. Sci., 16, December, 1961, p. 131-133.

42. Merkin, J. H., "Free Convection with Blowing and Suction," Journal of Heat Transfer, Vol. 15, p. 989-999, 1972.

43. Kays, W. M., Convective Heat and Mass Transfer, McGraw-Hill Book Company, 1966.

44. Franke, R., _A Program for the Numerical Solution of Large Sparse Systems of Algebraic and Implicitly Defined Stiff Differential Equations_, Naval Postgraduate School Report NPS-53Fe76051, 1976.

45. Gear, C. W., _Numerical Initial Value Problems in Ordinary Differential Equations_, Prentice-Hall Inc., 1971.

46. Brown, R. L. and Gear, C. W., _Documentation for DFASUB: A Program for the Solution of Simultaneous Implicit Differential and Nonlinear Equations_, Dept. of Computer Science, Illinois University, July, 1973.

47. Bui, T. D., "Solving Stiff Differential Equations in the Simulation of Physical Systems," Simulation, p. 37-46, August, 1980.

48. Burka, M. K., "Solution of Stiff Ordinary Differential Equations by Decomposition and Orthogonal Collocation," AIChE Journal, Vol. 28, No. 1, p. 11-20, January, 1982.

49. Gelinas, R. J. and Doss, S. K. and Miller, K., _The Moving Finite Element Method: Applications to General Partial Differential Equations With Multiple Large Gradients_, Report No. SAI/PL/180, Science Applications Inc., June, 1980.

50. Schiesser, W. E. and Stein, F. P., _Dynamic Simulation of Coal Conversion Plants_, Proceedings of a Conference on Mathematical Modeling of Coal Conversion Processes, p. 95-125, Washington D. C., November, 1976.

51. Fontenot, J. S., Private Communication.

52. Spalding, D. B., _Some Fundamentals in Combustion_, Academic Press Inc., 1955.

53. Kolodstev, Kh. I., "Dynamics of Gas Formation in a Carbon Layer," Moscow ZHURNAL FIZICHESKOY KHIMII, Vol. XIX, No. 9, p. 417-428, 1945.

54. Schlichting, H., _Boundary Layer Theory_, McGraw-Hill Book Company, 1956.

55. Gerald, C. F., _Applied Numerical Analysis_, Addison-Wesley Publishing Company, 1978.

INITIAL DISTRIBUTION LIST

11. Mr. J. Fontenot, Code 3274   1
     Naval Weapons Center
     China Lake, California   93555

12. Mr. K. Farmer, Code 3383   1
     Naval Weapons Center
     China Lake, California   93555

13. Mr. J. Mansfield, Code 223-6   1
     Chemical Research Project Office
     NASA Aimes Research Center
     Moffett Field, California   94035

14. Mr. R. Murphy, AIR-03PA   1
     Naval Air Systems Command
     Washington, D. C.   20361

15. Professor A. Kanury   1
     Department of Aerospace and
       Mechanical Engineering
     University of Notre Dame
     Notre Dame, Indiana   46556

16. Professor P. Pagni   1
     Department of Mechanical Engineering
     University of California at Berkeley
     Berkeley, California   94720

17. Professor Ivo Babuska   1
     Department of Mathematics
     University of Maryland
     College Park, Maryland   20740